DISSERTATION

Endothelial heterogeneity in response to autophagy activation prompts distal vascular muscularization in pulmonary hypertension

Endothelheterogenität als Reaktion auf Autophagie-Aktivierung führt zu distaler vaskulärer Muskularisierung bei pulmonaler Hypertension

zur Erlangung des akademischen Grades
Doctor medicinae (Dr. med.)

vorgelegt der Medizinischen Fakultät

Charité – Universitätsmedizin Berlin

von

Qi, Zhang

Erstbetreuung: Professor Dr.med. Wolfgang M., Kuebler

Datum der Promotion: 30.06.2024

Table of Contents

List of Figures

List of Abbreviations

ACD	Autophagic cell death
ATG	Autophagy-related gene
BafA1	Bafilomycin A1
BCA	Bicinchoninic acid
BSA	Bovine serum albumin
CA4	Carbonic Anhydrase 4
Cl-Cas3	Cleaved caspase 3
CM	Conditioned medium
DMEM	Dulbecco's Modified Eagle Medium
EC	Endothelial cell
ECGM	Endothelial Cell Growth Medium
ECGM·MV	Endothelial Cell Growth Medium MV
FBS	Fetal bovine serum
GS-IB4	*Griffonia simplicifolia* IB4
gCap	general capillary endothelial cell
HBSS	Hank’s balanced salt solution
IPAH	Idiopathic pulmonary arterial hypertension
LC3B	Microtubule-associated protein-1 light chain-3B
mPAP	Mean pulmonary arterial pressure
mTOR	Mammalian target of rapamycin
MVEC	Microvascular endothelial cells
NO	Nitric oxide
Nx/Hx	Normoxia/Hypoxia
PAEC	Pulmonary artery endothelial cells
PASMC	Pulmonary arterial smooth muscle cells
PCA	Principal component analysis
PCLS	Precision cut lung slices
PDGF-BB	Platelet-derived growth factor-BB
PFA	Paraformaldehyde
PH	Pulmonary hypertension
PVDF	Polyvinylidene difluoride
RIPA	Radioimmunoprecipitation assay buffer
RT	Room temperature
RVSP	Right ventricular systolic pressure
scRNA-seq	Single-cell RNA sequencing
SDS-PAGE	Sodium dodecyl sulfate polyacrylamide gel electrophoresis
siRNA	Small interfering RNA
SOX17	SRY-Box Transcription Factor 17

TEM	Transmission electron microscopy
TGF-β1	Transforming growth factor beta 1
TP53INP1	Tumor protein 53-induced nuclear protein 1
TMB	Tetra-methylbenzidine
TPM	Transcripts per million
ULK1	Uncoordinated-51-like protein kinase 1
WB	Western blot
WHRIL	Window for High-Resolution Imaging of the Lung
WPb	Weibel-Palade body
WT	Wild-type
α-SMA	α-smooth muscle actin

Abstract

Background: Accumulating evidence points to an ambiguous role of autophagy activation in the development of pulmonary hypertension (PH). Here, we speculate that autophagy activation may induce differential responses in macro- and micro-vascular endothelial cells, resulting in the proliferation of pulmonary artery endothelial cells (PAEC) and autophagic cell death of microvascular endothelial cells (MVEC). Thus, proliferating PAEC may replace MVEC in pulmonary precapillary arterioles, driving small vessel muscularization and the development of PH.

Methods: Proliferative and apoptotic states were evaluated by ki67 and cleaved caspase 3 (Cl-Cas3) immunostaining, respectively, in human and rat PAEC and MVEC, and in precision cut lung slices (PCLS) of wild-type (WT) mice or mice with an endothelial-specific autophagy related gene 7 deletion (*Atg7*$^{EN-KO}$). To probe for replacement of MVEC by PAEC, we discriminated between PAEC as Weibel-Palade body positive (WPbs^{+}) endothelial cells (ECs) by transmission electron microscopy (TEM) and *Griffonia simplicifolia* positive (GS^{+}) MVEC by immunofluorescence. Right heart hemodynamics and hypertrophy were quantified by right ventricular systolic pressure (RVSP) and Fulton index measurements, respectively. Vascular muscularization was quantified by immunohistostaining of α-actin.

Results: Immunostaining results, both *in vitro* and *in vivo*, revealed an increased proliferation of PAEC and apoptosis of MVEC under hypoxia as compared to normoxia. These distinct responses were prevented in hypoxic *Atg7*$^{EN-KO}$ mice, with reduced proliferation in PAEC and inhibited apoptosis of MVEC compared to hypoxic WT mice. Chronic hypoxia increased the abundance of WPbs^{+} PAEC and decreased *GS*$^{+}$ MVEC in precapillary arterioles, suggesting that MVEC were replaced by PAEC, while this phenomenon was reversed in hypoxic *Atg7*$^{EN-KO}$ mice. Conditioned medium from hypoxic PAEC, not MVEC, stimulated smooth muscle cell (SMC) proliferation and migration. Chronic hypoxia resulted in elevated RVSP, Fulton index, and distal vessel muscularization in WT mice that was attenuated in *Atg7*$^{EN-KO}$ mice.

Conclusion: Hypoxia-induced autophagy activation in parallel promotes PAEC proliferation and MVEC apoptosis. These antithetical responses to autophagy cause proliferative PAEC to replace MVEC in small pulmonary arterioles, promoting SMC proliferation and migration, ultimately driving distal vessel muscularization and the development of PH.

Zusammenfassung

Hintergrund: Zahlreiche Hinweise deuten auf eine relevante Autophagie-Aktivierung bei der Entwicklung der pulmonalen Hypertonie (PH) hin; deren Rolle ist bislang aber unklar. Hier spekulieren wir, dass die Autophagie-Aktivierung unterschiedliche Reaktionen in makro- und mikrovaskulären Endothelzellen auslösen könnte, was zur Proliferation von Lungenarterien-Endothelzellen (PAEC) und zum autophagischen Zelltod von mikrovaskulären Endothelzellen (MVEC) führt. Somit könnten proliferierende PAEC die MVEC in den pulmonalen präkapillären Arteriolen ersetzen und so die Muskularisierung der kleinen Gefäße und die Entwicklung der PH befördern.

Methoden: Zellproliferation und -apoptose wurden durch ki67- bzw. Cl-Cas3-Immunfärbung in PAEC und MVEC von Mensch und Ratte sowie in präzisionsgeschnittenen Lungenschnitten (PCLS) von Wildtyp-Mäusen (WT) oder Mäusen mit einer endothelspezifischen Deletion des Autophagie-Gens *Atg7* (*Atg7*$^{EN\text{-}KO}$) untersucht. Um den Ersatz von MVEC durch PAEC zu untersuchen, identifizierten wir PAEC mittels Transmissionselektronenmikroskopie (TEM) als Weibel-Palade Körperchen positive (WPbs^{+}) Endothelzellen (ECs) und MVEC mittels Immunfluoreszenz als *Griffonia simplicifolia* positive (*GS*$^{+}$) EC. Hämodynamik und Hypertrophie des rechten Herzens wurden durch Messung des systolischen Drucks der rechten Herzkammer (RVSP) bzw. des Fulton-Index quantifiziert. Die vaskuläre Muskularisierung der Lunge wurde durch Immunhistologische Färbung von α-Actin quantifiziert.

Ergebnisse: Die Ergebnisse der Immunfärbungen *in vitro* als auch *in vivo* zeigten eine erhöhte Proliferation von PAEC und die Apoptose von MVEC unter Hypoxie im Vergleich zu Normoxie. Diese Reaktionen waren bei hypoxischen *Atg7*$^{EN\text{-}KO}$-Mäusen vermindert, insofern dass die Proliferation von PAEC reduziert und die Apoptose von MVEC im Vergleich zu hypoxischen WT-Mäusen gehemmt waren. Chronische Hypoxie erhöhte das Vorkommen von WPbs^{+} PAEC und verringerte die Zahl *GS*$^{+}$ MVEC in präkapillären Arteriolen. Dies weist darauf hin, dass MVEC durch PAEC ersetzt wurden. Hingegen war dieses Phänomen bei hypoxischen *Atg7*$^{EN\text{-}KO}$-Mäusen umgekehrt. Konditioniertes Medium von hypoxischen PAEC, nicht aber solches von MVEC, stimulierte die Proliferation und Migration von glatten Muskelzellen (SMC). Chronische Hypoxie führte bei WT-Mäusen zu einem erhöhtem RVSP, einem Anstieg des Fulton-Index und distaler

Gefäßmuskularisierung, diese Veränderungen waren bei *Atg7*$^{EN-KO}$-Mäusen abgeschwächt.

Schlussfolgerung: Hypoxie-induzierte Autophagie-Aktivierung fördert parallel die Proliferation von PAEC und die Apoptose von MVEC. Diese gegensätzlichen Reaktionen auf Autophagie führen dazu, dass proliferative PAEC die MVEC in den kleinen Lungenarteriolen ersetzen, wodurch die SMC-Proliferation und -Migration gefördert wird, was letztlich zur Muskularisierung der distalen Gefäße und zur Entwicklung einer PH führt.

1. Introduction

Pulmonary hypertension is a general term encompassing a heterogeneous group of life-threatening cardiopulmonary diseases, defined by a mean pulmonary arterial pressure (mPAP) exceeding 20 mmHg at rest[1]. The 2022 ESC/ERS Guidelines for the diagnosis and treatment of PH classify PH as follows: 1) pulmonary arterial hypertension (PAH); 2) PH associated with left heart disease; 3) PH associated with lung diseases and/or hypoxia; 4) PH associated with pulmonary artery obstructions; 5) PH with unclear and/or multifactorial mechanisms[1]. PH commonly presents with a series of symptoms, e.g., dyspnea, fatigue, and chest pain, at a rather late stage of the disease when detrimental remodeling in the lung and of the RV has already progressed extensively. This can ultimately lead to advanced right ventricular failure and death, with an estimated mean 5-year mortality between 33.3% and 46% depending on PH subtype[2]. Current existing therapies for PH, such as prostacyclin analogues or endothelin receptor antagonists, target specific molecular pathways involved in regulating vascular tone and pulmonary vascular resistance. Although these medications can help improve symptoms and slow down disease progression, they do not specifically address or reverse pulmonary vascular remodeling in PH, and as such, are not able to reverse the disease process. As a result, there is still a dire need for novel therapies that directly target and modulate the remodeling process to further improve outcomes in patients with PH.

1.1 Pulmonary hypertension

1.1.1 Vascular remodeling in PH

Pulmonary vascular remodeling constitutes a pivotal structural alteration in the pathogenesis of pulmonary hypertension (PH) and encompasses a complex array of maladaptive processes. These processes include the hypertrophy of the vascular media and intima, muscularization of small vessels, and the formation of plexiform lesions, specifically observed in idiopathic pulmonary arterial hypertension (IPAH)[3]. Consequently, these changes culminate in the narrowing or complete occlusion of the effective vascular lumen, primarily affecting the small precapillary arterioles. In healthy lungs, fully-muscularized pulmonary arteries and arterioles are predominantly confined to pulmonary arteries larger than 40 µm in diameter, while smaller arterioles are not or only partially muscularized[4]. In

PH, however, distal pulmonary arterioles with < 50 µm in diameter become progressively muscularized with a thickened media, a process considered critical for the characteristic alteration in pulmonary hemodynamics in PH[5,6]. Studies aimed at understanding the process of small vessel muscularization have mainly focused on pulmonary arterial smooth muscle cells (PASMC). In contrast, the role of the vascular endothelium in this process has been sparsely addressed, although endothelial dysfunction constitutes an important initial trigger of structural changes in the vasculature [7].

1.1.2 Endothelial dysfunction in PH

Endothelial cell (EC) dysfunction is a critical pathophysiological characteristic in pulmonary hypertension (PH). EC form a monolayer along the inner surface of blood vessels and play a crucial role in regulating vascular tone, coagulation and immune cell trafficking, in maintaining vascular barrier function, and in the control of blood flow. However, in PH, various environmental stressors, including hypoxia, inflammation, and shear stress, can lead to damage and dysfunction of EC, serving as early triggers for lung vascular remodeling. Dysfunctional EC in PH are characterized by an inability to balance vasodilation and contraction, by dysregulated growth factor production, and by impaired homeostasis of EC apoptosis and proliferation. In particular, the latter has been proposed as a driver of lung vascular remodeling in PH[8].

Over the past decade, multiple lines of evidence from various animal models of PH and IPAH patients have consistently shown an increase in apoptosis of pulmonary EC in PH[9-11]. Notably, the occurrence of EC apoptosis is detected as early as the third day following monocrotaline (MCT) injection in rats[9], while peak levels of apoptotic EC are observed on the seventh day after initiating the exposure of mice to hypoxia or a combination of the VEGF receptor antagonist Sugen5416 with hypoxia (SuHx)[12]. These findings strongly suggest that EC apoptosis is predominantly an early event in PH pathogenesis.

In line with this notion, apoptosis has been considered an initial trigger event in PH. As reported by Taraseviciene-Stewart and colleagues, the use of a pan-caspase inhibitor, Z-Asp-CH2-DCB, decreased caspase 3 activity and alleviated right ventricular systolic pressure (RVSP) as well as distal arteriolar muscularization in the SuHx rat model[11]. This

indicates that inhibiting apoptosis can effectively prevent the development of PH. Conversely, transgenic mice expressing a Fas-induced apoptosis construct under the regulation of the EC-specific Tie2 promoter develop EC apoptosis, which in turn results in the subsequent development of pulmonary hypertension (PH)[13]. Hence, EC apoptosis is not only required but sufficient to drive PH development.

Alongside endothelial apoptosis, however, PH is also characterized by both intimal thickening and excessive EC proliferation[12]. Plexiform lesions in lung samples from IPAH patients have been reported to exhibit monoclonal growth of ECs[14]. Disordered endothelial proliferation is also thought to underlie the formation of plexiform lesions, which are a pathognomonic morphological feature of severe idiopathic PAH[15]. In accordance with this view, cultured pulmonary ECs isolated from IPAH patients showed augmented proliferation as compared to ECs isolated from healthy donors[16], and lung biopsies from PH patients expressed high levels of the anti-apoptotic protein Bcl-2[17]. In the SuHx rat model, inhibition of Notch signaling, which promotes pulmonary artery endothelial cell (PAEC) proliferation through downregulation of P21 expression, significantly ameliorated right ventricular dysfunction[18], further consolidating the functional relevance of endothelial proliferation in PH.

Interestingly, in chronic hypoxic and SuHx murine models, EC apoptosis reaches its peak on the seventh day, while EC proliferation gradually increases over the subsequent three weeks[12]. The paradoxical coexistence of EC apoptosis and proliferation in PH has been attributed to the notion that early EC apoptosis is followed by the subsequent emergence of anti-apoptotic and over-proliferative EC, which then propagate pulmonary vascular remodeling[19]. However, there is still no direct evidence to validate the sequential or causal relationship between EC apoptosis and proliferation in PH, due to the lack of reporter mice allowing the monitoring of apoptotic and proliferative EC in real time as well as due to the lack of non-invasive techniques for long-term dynamic observation of ECs *in vivo*. More notably, the mechanisms underlying the differential fate of EC, with some cells undergoing apoptosis and others becoming apoptosis-resistant and hyperproliferative, remain largely unclear. Recently, a series of single cell sequencing (scRNA-seq) studies have unveiled a remarkable heterogeneity of transcriptome changes among different pulmonary EC subtypes in response to PH[20-22]. These findings raise an intriguing possibility,

namely that the parallel presence of apoptotic and proliferative ECs in PH could be attributable to distinct EC subtypes.

1.1.3 Lung EC heterogeneity in PH

EC line the inner surface of blood vessels and lymphatic vessels in all organs. Although EC share some common functions, such as the maintenance of vascular barrier function as well as the balance between coagulation and anticoagulation, EC exhibit remarkable heterogeneity in terms of cell morphology, function, and molecular profiles[23,24]. For instance, brain capillaries exhibit a highly selective barrier property, while glomerular ECs are characterized by a high level of filtration[23,25,26]. EC in the linear segments of arteries, but not in veins, are aligned in the direction of blood flow[24]. EC are heterogeneous between different organs, different vascular segments in the identical organ, and even among adjacent ECs. A recent scRNA-seq study revealed two distinct subtypes of lung MVEC, namely aerocyte and general capillary EC (gCap)[27]. Although both subtypes are distributed within the pulmonary microvasculature, aerocytes play a primary role in gas exchange and leukocyte trafficking, whereas gCaps proliferate and can differentiate into aerocytes to replenish the loss of aerocytes in cases of injury.

In this study, we mainly focused on EC subtypes lining the distal pulmonary arterioles and the pulmonary microvasculature. This focus was motivated by the fact that the primary pulmonary vascular lesions in PH are distal arteriole muscularization and microvascular rarefaction[28]. There are two distinct EC subtypes in this region: pulmonary arteries with inner diameters of > 60 µm are covered primarily by PAEC, while vessels less than 20 µm in diameter are predominantly covered by MVEC, with vessel diameters between 60 and 20 µm exhibiting a mixed endothelial phenotype. This region is accordingly referred to as the “transition zone” [29]. It was previously recognized that PAEC and MVEC differ remarkably not only in terms of their localization, but also in their origin, structure, function, and specific markers[25]. PAEC are derived from the pulmonary trunk through angiogenesis, while MVEC originate from blood islands by vasculogenesis. In terms of their functional characteristics, PAEC and MVEC differ in terms of their barrier function (with MVEC being more restrictive to protein and water flux as compared to PAEC), nitric oxide production (MVEC < PAEC), responses to mechanical stress, and their Ca^{2+} response to different stimuli[30-33]. Rat PAEC and MVEC can be differentiated based on lectin staining of the

sugar residues expressed on their plasma membrane surface, in that rat PAEC stain positively with *Helix pomatia* lectin but not *Griffonia simplicifolia*, whereas rat MVEC show the opposite staining pattern[29,30]. Furthermore, the cytosolic organelles of PAEC and MVEC differ, with PAEC containing Weibel-Palade bodies (WPbs) while they are lacking in MVEC[34]. At the transcriptome level, recent scRNA-seq studies have revealed a remarkable difference in up- and down-regulated genes and gene ontology (GO) terms between PAEC and MVEC in PH animal models and IPAH patients[20-22]. However, the specific roles and fate of these distinct phenotypes within the context of PH, as well as the cellular signaling pathways that underlie differential responses of EC subsets in PH, have yet to be investigated.

1.2 Autophagy in PH

A potential underlying pathway that may contribute to the differential responses of EC in PH is autophagy. This hypothesis is primarily supported by two rationales: first, numerous studies have demonstrated an upregulation of autophagic flux in lung tissues of individuals with pulmonary hypertension; and second, autophagy plays a crucial regulatory role in determining cell survival versus cell death. In the following sections, I will provide a detailed introduction to autophagy and its potential role in PH.

1.2.1 Autophagy as a regulator of cell death and survival

Over the past decade, autophagy has garnered significant attention as a fundamental process in the regulation of cellular homeostasis and in the pathogenesis of numerous human diseases. Autophagy is a physiological cellular process by which unused cytoplasmic proteins and damaged organelles are degraded and recycled through a lysosome-dependent degradation pathway[35]. In brief, redundant or defective proteins and organelles are gradually encapsulated by the initiation and elongation of a bilayer membrane (the so called “phagophore”), eventually leading to vesiculation (the “autophagosome”) and subsequent fusion with lysosomes for degradation (the “autophagolysosome”) (Figure 1). Autophagy is primarily regulated by a group of autophagy-related genes (*ATGs*) and their corresponding gene products, of which 27 have been identified thus far[35]. These ATGs participate in the formation of two ubiquitin-like conjugate systems, namely the ATG5-12 system and the ATG8 system (known as LC3-I in mammals) (Figure 1). The ATG5-12 conjugate system facilitates autophagosome formation, while

the ATG8 system is responsible for autophagosome expansion, closure, and cargo degradation[36]. Of importance, both conjugation systems are critically reliant on ATG7. Under physiological conditions, starvation or energy depletion upregulates autophagy by inhibiting the mammalian target of rapamycin (mTOR) pathway and the consequent disinhibition of the mammalian uncoordinated-51-like protein kinase (ULK1/2) complex[37]. Activation of the ULK1/2 complex triggers the activation of Beclin-1, which, in turn, promotes phagosome formation.

Autophagy serves as a cell survival mechanism in response to environmental stress by recycling unused proteins and organelles, providing energy resources, and inhibiting apoptosis and necrosis[37]. However, it is important to note that excessive activation of autophagy can also lead to autophagic cell death (ACD) or necrosis[38,39]. The specific outcome of autophagy, namely whether it is cytoprotective[40] or lethal[39], depends on various factors such as the specific stimulus, cell type, intracellular metabolic activity, and extracellular nutrient supply. Consequently, autophagy acts as a double-edged sword in the regulation of cell death versus survival[41].

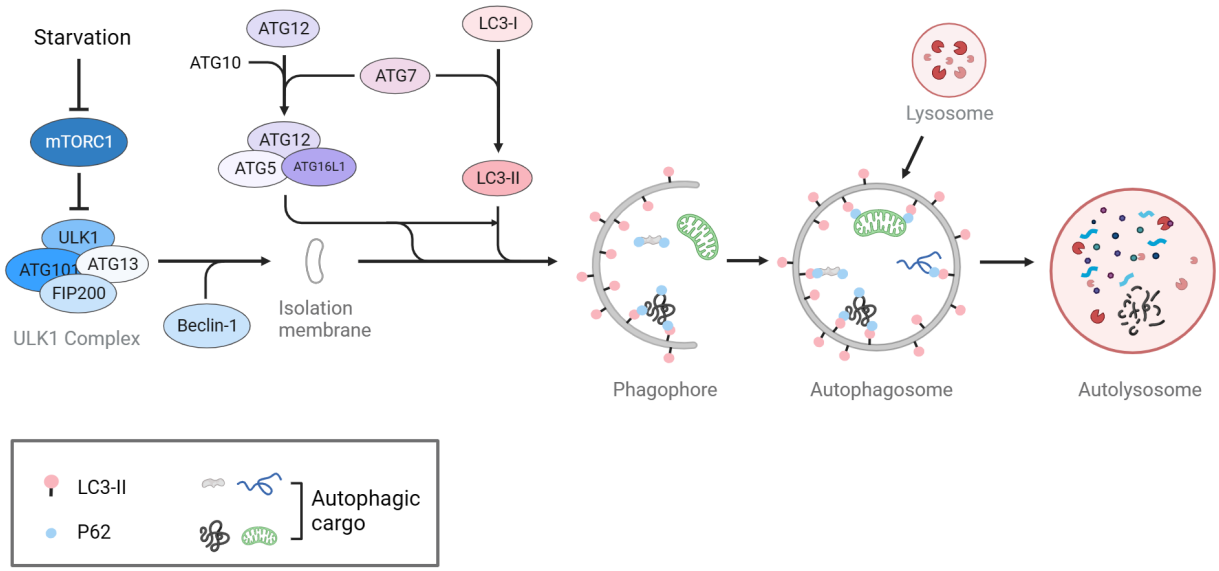

Figure 1. Diagram of autophagy pathway. Autophagy is upregulated by starvation or energy depletion via inhibition of the mammalian target of rapamycin complex 1 (mTORC1) and consequential disinhibition of the mammalian uncoordinated-51-like protein kinase (ULK1/2) complex. The ULK1/2 complex, in turn, activates Beclin-1, which drives the formation of the isolation membrane. Autophagy is regulated by a set of so far 27 identified autophagy-related genes (*ATGs*) and gene products forming 2 sequential conjugate systems, named ATG5-12 and ATG8 (known as LC3-I in mammals), respectively. Both systems are reliant on ATG7. The cargo adaptor protein p62 binds to ubiquitinated substrates and interfaces with LC3-II on the

autophagosome membrane, facilitating the fusion of the autophagosome with the lysosome, culminating in substrate degradation within the autolysosome.

1.2.2 Autophagy in PH

Recent studies have provided emerging insights into the activation of autophagy in EC and SMC in patients with PH and in corresponding animal models[42-45]. Elevated expression of microtubule-associated protein-1 light chain-3B (LC3B) and an increased ratio of LC3B-II over LC3B-I have been detected by Western blot in the lungs of PH patients and chronic hypoxic PH mice, indicating autophagy activation. However, seemingly contradictory findings have been reported regarding the role of autophagy in PH. For instance, inhibition of autophagy by chloroquine has been shown to attenuate monocrotaline-induced PH in rats[42]. Similarly, inhibition of the autophagy pathway by activation of mTOR has been demonstrated to attenuate hypoxia-induced proliferation of PAEC and the progression of PH[46]. Conversely, however, chronic hypoxic LC3B knockout mice have been found to exhibit more severe PH compared to wild-type mice, suggesting a protective role of autophagy[43]. Such seemingly paradoxical results may be attributable to cell-specific roles of autophagy and the previous inability of pharmacological interventions or global knockout models to target autophagy activation or inhibition in a cell type-specific manner, particularly in EC and PASMC. As such, the mechanisms by which autophagy determines the fate of different cell types and how autophagy activation in individual cell subtypes affects the progression of PH remain unclear.

1.3 Central hypothesis

In this study, we hypothesize that hypoxia induces the activation of autophagy in both PAEC and MVEC. However, activation of autophagy may stimulate pro-survival and proliferative responses in PAEC, while MVEC undergo autophagic cell death. As a result, hyperproliferative PAEC would gradually replace apoptotic MVEC in the precapillary transition zone of the pulmonary vasculature, i.e., in the distal arterioles which, in the healthy lung, contain both PAEC and MVEC. Additionally, autophagy-activated PAEC may release growth factors that stimulate SMC migration and proliferation. Consequently, SMC would migrate and progressively populate the small microvessels, which would be now predominantly lined by PAEC instead of MVEC. This process eventually leads to small vessel muscularization and the development of PH.

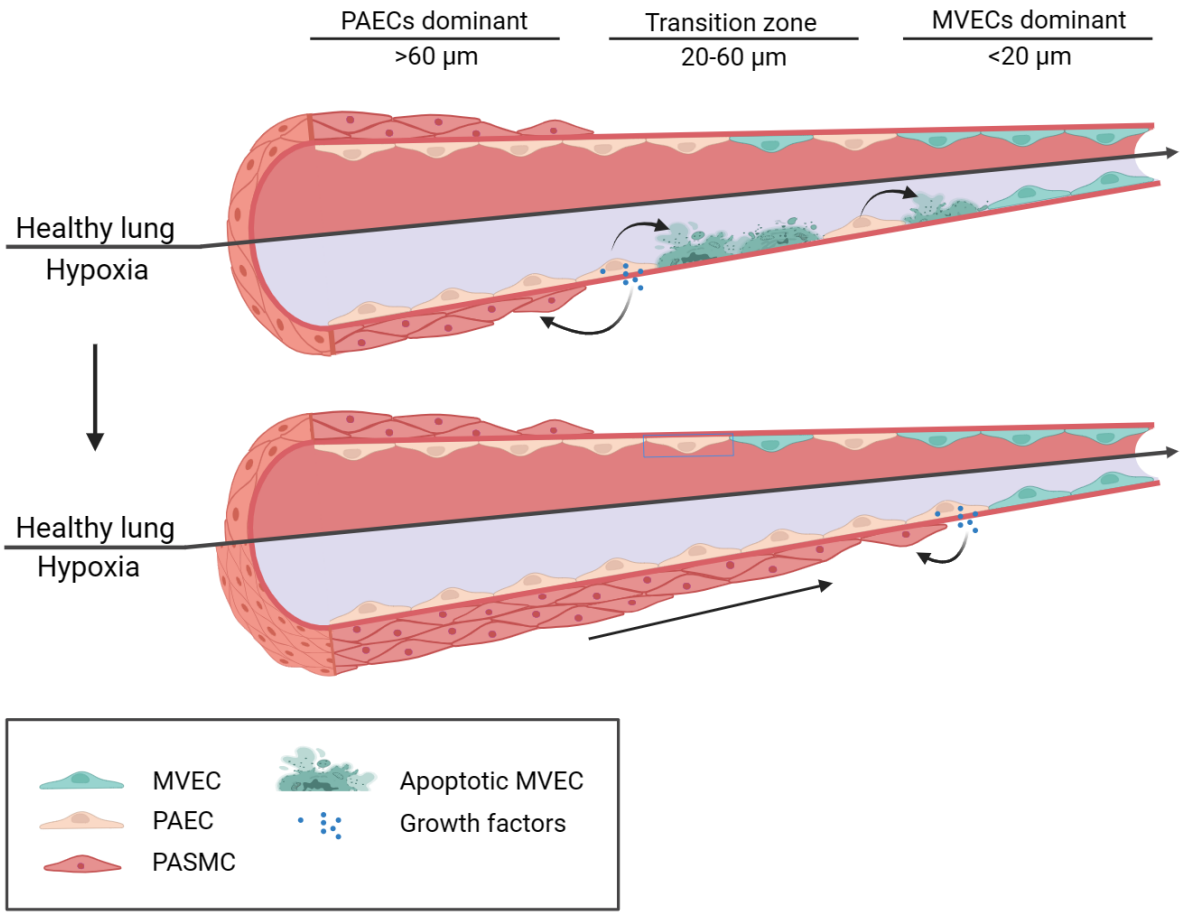

Figure 2. Schematic illustration of the novel concept of distal vessel muscularization in PH. In healthy lungs, PAEC cover larger (> 60 µm diameter) pulmonary arteries and arterioles, while microvessels and precapillaries <20 µm are populated by MVEC, and vessels with diameters between 20-60 µm show mixed EC subtypes. Following stimulation with PH triggers such as hypoxia, autophagy is induced in both endothelial cell subtypes, yet while PAEC begin to hyperproliferate in response to autophagic stress, MVEC undergo autophagic cell death. This differential response results in the invasion of PAEC into distal pulmonary microvessels where they replace MVEC. Secretion of growth factors by PAEC stimulates SMC proliferation and guides their migration into precapillary arterioles, resulting in distal vessel muscularization and the development of PH.

2. Methods

2.1 Animals

All animal experiments were performed at the Charité-Universitätsmedizin Berlin and approved by the local government authorities (LAGeSo Berlin) under animal protocol number G0066/19. All animal experiments conformed to the Guide for the Care and Use of Laboratory Animals published in 1996 by the US National Institutes of Health (NIH Publication No. 85-23) as well as Directive 2010/63/EU of the European Parliament on the protection of animals used for scientific purposes. In all experiments, 8-10-week-old male mice of a C57BL/6 background were used. Mice were housed in enriched cages, limited to 4 mice each, on ventilated racks under a controlled 12 hr/12 hr light-dark cycle.

To evaluate the role of autophagy in EC and SMC for the development of PH, we generated mice with an EC-specific or SMC-specific knockout of the core autophagy gene *Atg7* by crossing *Atg7*$^{flox/-}$ mice[47,48] with mice expressing the Cre recombinase under control of either the VE-cadherin promoter (*Cdh5*-Cre$^{tg/+}$)[49] or the Sm22α promoter (*Sm22α*-Cre$^{tg/+}$)[50], respectively. *Atg7*$^{flox/flox}$; *Cdh5*-Cre$^{tg/+}$ and *Atg7*$^{flox/flox}$; *Sm22α*-Cre$^{tg/+}$ mice were used as EC-(*Atg7*$^{EN\text{-}KO}$) and SMC-(*Atg7*$^{SMC\text{-}KO}$) specific *Atg7* knockout mice, with *Atg7*$^{flox/flox}$; *Cdh5*-Cre$^{-/-}$ (*Atg7*$^{EN\text{-}WT}$) and *Atg7*$^{flox/flox}$; *Sm22α*-Cre$^{-/-}$ (*Atg7*$^{SMC\text{-}WT}$) mice serving as corresponding controls. Homozygous GFP-LC3 transgenic mice[51] were utilized to evaluate autophagic flux in EC, as measured by counting GFP^{+} punctate signals by fluorescence microscopy. Ear biopsies were collected for genotyping by PCR.

All mouse strains were either exposed to 10% oxygen for 5 weeks to induce chronic hypoxic PH, or to 21% oxygen as normoxic controls.

2.2 Pulmonary hemodynamics and right ventricular hypertrophy

The measurements of right ventricular hemodynamics and hypertrophy in chronic hypoxic mice have been described previously[52]. Briefly, mice were anesthetized by intraperitoneal injection of ketamine (200mg/kg) and xylazine (10mg/kg). Adequate depth of anesthesia was confirmed by checking the absence of the inter-toe reflex. To measure right ventricular systolic pressure (RVSP), a 1F Millar Micro-Tip Catheter (SPR-1000; Millar, Houston, TX) linked to a PowerLab data acquisition system was introduced into the right ventricle (RV) via the jugular vein, and a steady RV pressure signal was recorded for at least 2

minutes with LabChart 8 software (ADInstruments, Australia). Immediately after the haemodynamic measurements, mice were sacrificed by exsanguination using a cardiac puncture. The heart was removed and dissected into the RV and the left ventricle including the septum (LV+S) to determine the Fulton index, a weight ratio of RV/(LV+S) as a measure of RV hypertrophy.

2.3 Immunofluorescence and histology of lung sections

2.3.1 Precision cut lung slices

Precision cut lung slices (PCLS) present an effective *ex vivo* tool for maintaining cellular viability and lung structural integrity in lung sections of 100-500 µm thickness[53]. Here, PCLS was used for differentiating EC subtypes by lectin staining and evaluating autophagic flux in the lungs of GFP-LC3 transgenic mice. PCLS was generated from lungs perfused *in situ*, as described before[54,55]. In short, Hank's balanced salt solution (HBSS; Gibco, REF14025; Waltham, MA) containing 4% bovine serum albumin (BSA, Roth, Karlsruhe, Germany) was perfused *in situ* into murine lungs through a cannula introduced into the main pulmonary artery (PA) and eventually exited through a catheter inserted into the apex of the left ventricle. Subsequently, the perfusion was changed to pre-warmed 6% gelatin (AppliChem, Darmstadt, Germany) for 5 min, and lungs were inflated by slow injection of 1.5 mL of pre-warmed 2% low-melting-point agarose (Roth, Karlsruhe, Germany) in HBSS via the tracheal cannula. Lungs were excised and cooled at 4°C for 15 min. The left lung lobe was isolated and temporarily stored in ice-cold 10% fetal bovine serum (FBS, PAN-Biotech, Germany) diluted by Dulbecco's Modified Eagle Medium (DMEM; Gibco, REF31053; USA) and subsequently sectioned into 120 µm thick PCLS using a vibratome system (Leica VT1200, Wetzlar, Germany). The collected PCLS were either directly immunostained or cultured in 10% FBS/DMEM at 37°C and 5% CO_2 in 24-well plates for three days with a daily medium change.

2.3.2 Fluorescence imaging of PCLS

To distinguish PAEC from MVEC, PCLS were stained with von Willebrand factor (vWF) as a pan-EC marker and Alexa Fluor 647-conjugated isolectin *Griffonia simplicifolia* IB4 (GS-IB4), which specifically labels MVEC but not PAEC[56]. In brief, PCLS were incubated with GS-IB4 (0.5 µg/mL; Invitrogen™, Carlsbad, CA) at 37°C for 15 min, then rinsed three times with DMEM. PCLS were sequentially fixed with 4% paraformaldehyde (PFA; Roth,

Karlsruhe, Germany) for 20 min, washed three times with PBS, then incubated with PBTB solution (0.2% Triton X-100, 5% normal goat serum, 0.2% BSA in PBS) for 1 h for permeabilization and blocking, and eventually incubated with primary antibody at 4°C overnight. The primary antibodies and respective dilutions applied for immunostaining of PCLS as well as lung histological sections were as follows: anti-PECAM-1 (1:400; mouse monoclonal; #sc-376764, Santa Cruz, CA), anti-Ki67 (1:1000; rabbit polyclonal; #ab15580, Abcam, Cambridge, UK), anti-cleaved-caspase 3 (Cl-Cas3; 1:400; rabbit polyclonal; #9661, Cell Signaling, Danvers, MA), anti-von Willebrand factor (vWF; 1:400; rabbit polyclonal; Sigma-Aldrich, #F3520, Burlington, MA). After incubation with primary antibodies, PCLS were washed 3x with PBS, followed by incubation with fluorescent dye-conjugated secondary antibodies at room temperature (RT) for 1 h and again 3x washing in PBS. The secondary antibodies were: Alexa Fluor™ 488 goat anti-rabbit antibody (1:800; A11034); Alexa Fluor™ 568 goat anti-rabbit antibody (1:800; A11011); Alexa Fluor™ 488 goat anti-mouse antibody (1:800; #A11001); Alexa Fluor™ 568 goat anti-mouse antibody (1:800; #A-11004; all Invitrogen™, Carlsbad, CA). Stained PCLS were placed and gently flattened on glass slides and mounted using Fluoromount-G™ with DAPI (Invitrogen™, Carlsbad, CA). PCLS were imaged by confocal microscopy (upright spinning disk CSU-X on a Nikon Ti2 base; Nikon Instruments, Tokyo, Japan), and Z-stacks were recorded for 3-dimensional vascular reconstruction.

To assess cell type-specific changes in autophagic flux in response to hypoxia, PCLS from GFP-LC3 transgenic mice were incubated under hypoxia (1% O_2) or normoxia (21% O_2) for 24 h in the presence of 20 nMol/L bafilomycin A1 (BafA1, AdipoGen, San Diego, CA) to preserve autophagosomes for subsequent imaging of GFP fluorescence with EC counterstained for vWF.

In a subset of experiments, PCLS were imaged continuously over 48 h. After washing with pre-warmed PBS, PCLS were stained with GS-IB4 (1:1000), Alexa Fluor™ 488-anti-CD31 (1:200; Invitrogen™, # MA5-18135, Carlsbad, CA), and Hoechst 33342 (1:1000; Invitrogen™, # 62249, Carlsbad, CA) in ECGMMV for 1.5 hours at 37°C. Following another round of washing, PCLS were placed in a 10 mm^2 dish and gently covered with a 40 µm cell strainer (BD #352340, NJ). PCLS were cultured in 3 ml ECGMMV containing 3x penicillin/streptomycin, and were kept in an incubator (37 degrees, 1% O_2, 5% CO_2) on an EVOS fluorescence microscope. Images were captured every 5 min for 2 days. Time-series images were analyzed using ImageJ software.

2.3.3 Histological assessment of lung sections

Pulmonary arteriolar muscularization was assessed as described before[57,58]. In brief, lungs were harvested from euthanized mice, gently inflated with 1.6 ml room air, and fixed in 4% PFA for 24 h. Lung lobes were embedded in paraffin and sectioned at a thickness of 5 µm. Paraffin-embedded slices were dewaxed with xylene and then successively immersed in 100%, 95%, 70%, and 50% ethanol for 3 min each. Samples were boiled in Tris-EDTA buffer for 10 min in a microwave oven at 600 W, followed by cooling for 20 min. After rinsing in PBS for 5 min, slices were blocked with PBTB solution at RT for 1 h, and subsequently incubated with primary anti-α-smooth muscle actin (α-SMA) antibody (1: 400; mouse monoclonal; Sigma-Aldrich, Burlington, MA) in PBTB at 4°C overnight. After washing three times with PBS for 5 min each, samples were incubated with a horse radish peroxidase-conjugated goat anti-mouse IgG secondary antibody (#ab97023; Abcam, Cambridge, UK) in PBTB at RT for 1.5 h, then washed again as in the previous step. The whole slices were covered with DAB solution and then rinsed with double-distilled H_2O (ddH_2O) to stop the reaction. Sections were mounted with resin and stored at RT for further visualization. Vascular muscularization was assessed based on the pattern of α-SMA staining, and the proportion of non- (i.e., no apparent smooth muscle attached), partially- (i.e., with only a crescent of muscle), or fully- (i.e., with a complete medial coat of muscle) muscularized pulmonary arterioles of <50 µm diameter was calculated in a blinded manner as previously described[58]. In parallel, paraffin-embedded lung sections were stained with hematoxylin and eosin (H&E), and the absolute vessel wall thickness of pulmonary arteri(ol)es was measured in a blinded manner with vessels categorized in 10 µm intervals of inner diameter.

2.4 *In vitro* experiments

2.4.1 Cell culture

All human primary cells and their respective adapted media were ordered from Promocell (Heidelberg, Germany). Human PAEC (hPAEC) were cultured in Endothelial Cell Growth Medium (ECGM) containing supplementMix (C-22010), human pulmonary MVEC (hMVEC) in Endothelial Cell Growth Medium MV (ECGM·MV) with supplementMix (C-22020), and human PASMC (hPASMC) in Smooth Muscle Cell Growth Medium 2 with supplementMix (C-22062), with all media supplemented with 1x penicillin/streptomycin solution (Gibco, Waltham, Massachusetts). Cells were used at passage numbers of 4-10.

Rat PAEC (rPAEC) and MVEC (rMVEC) were kindly provided by Drs. Troy Stevens and Diego Alvarez, University of South Alabama, AL, and cultured in the same way as human cells. To generate conditioned media (CM), media were exchanged after EC reached subconfluence; subsequently, CM was harvested from flasks after EC had been exposed to hypoxia (1% O_2) or normoxia (21% O_2) for 24 h and CM was stored at -80°C.

2.4.2 Reagents

Tat-Beclin1 D11 autophagy-inducing Peptide (#NBP2-49888) was used to induce autophagy activation in hPAEC and hMVEC according to the official user manual, while the scrambled control peptide Tat-Beclin1 L11S Peptide (#NBP2-49887; both Novus Biologicals, Englewood, CO) was used as negative control. Briefly, cells were treated with 20 µMol/L Beclin11 D11 or L11s in acidified OptiMEM (Gibco, Waltham, MA) with 0.15 % 6 N HCl for 24 h at 37°C. BafA1 was applied to inhibit the late stage of autophagy by preventing the fusion of lysosome s with autophagosomes. BafA1 was dissolved in DMSO to generate a stock solution of 8 mMol/L, and cells were treated with 20 nMol/L BafA1 diluted in culture medium for 24 h, or medium containing equal amounts of DMSO as negative control.

2.4.3 siRNA transfection

ATG7 small interfering RNA (siRNA) transfection was used to inhibit autophagy by preventing *ATG7* translation in hPAEC and hMVEC. ON-TARGETplus human *ATG7* siRNA (si*ATG7*) and the corresponding non-targeting control siRNAs (siCtrl) were purchased from Horizon Discovery (Cambridge, UK). Following the manufacturer's instructions, ECs were seeded on 12-well plates and cultured in antibiotic-free medium until cells reached 70% confluence. In brief, DharmaFECT Transfection Reagents (Horizon Discovery, Cambridge, UK) were either added with si*ATG7* or siCtrl working solution and incubated at RT for 20 min, then diluted in antibiotic-free complete medium to a final siRNA concentration of 100 nMol/L. After 24 h of siRNA treatment of the cells, the medium was changed back to the regular complete medium. After another 24 h, cells were collected for WB to verify the efficiency of *ATG7* knockdown or transferred to the hypoxic incubator (1% O_2) at 37°C for 24 h, followed by cell proliferation or apoptosis assays as described below.

2.4.4 Autophagy imaging in cultured ECs

A CYTO-ID® autophagy detection kit was used to assess autophagic flux in cells. In brief, 15,000 hPAEC or hMVEC were seeded on ibidi µ-slide 8-well plates (ibidi, Cat.No:80826, Gräfelfing, Germany). When 50-70% confluence was reached, cells were exposed to hypoxia (1% O_2) or normoxia (21%) for 24 h, then stained with CYTO-ID® green dye (1:500) for autophagic vacuoles and Hoechst 33342 for nuclei (1:1,000, both from Enzo Biochem, USA) for 30 min at 37°C. Green fluorescent punctae located in the cytoplasm were detected by confocal microscopy (*vide supra*) and counted in 50 random cells from three independent replicates of each group for quantitative analysis.

2.4.5 Endothelial cell co-culture

To investigate whether PAEC would replace MVEC under hypoxic conditions, both EC subtypes were respectively labeled with PKH26 Red Fluorescent Cell Linker® (for rPAEC) and PKH67 Green Fluorescent Cell Linker® (for rMVEC, both from Sigma-Aldrich, Burlington, MA), then mixed 1:1 and co-seeded in 24-well plates in hypoxia or normoxia for up to 7 days. The ratio of the area covered by rPAEC (red) at day 1, 3, or 7 was quantified relative to day 0 as a measure of rPAEC expansion.

As the staining with the lipophilic membrane dyes PKH26 and PKH67 is not retained after fixation and permeabilization for immunostaining, a different strategy had to be applied to concurrently assess cell proliferation by Ki67 immunostaining. To this end, hPAEC were stained with CellTrace™ Oregon Green® 488 (C34555; Thermo Fisher, Waltham, Massachusetts) and hMVEC with CellTracker™ Blue CMAC Dye (C2110; Thermo Fisher, Waltham, Massachusetts), then mixed 1:1 and co-seeded in an ibidi 8-well plate. EC were serum starved overnight in basal medium with 0.2% FBS, followed by exposure to hypoxia or normoxia for 24 h, and staining for Ki67 to assess cell proliferation.

2.4.6 BrdU assay

Besides Ki67 staining, EC proliferation was also evaluated by BrdU assay (Abcam, #ab126556, Cambridge, UK). To this end, fifteen thousand cells were seeded in a 96-well plate. Twenty µL of 1×BrdU was loaded into each well 12 hours before the endpoint of the experiment. After fixation and DNA denaturation, cells were incubated with the ready-made anti-BrdU antibody for 1 h at RT, rinsed three times with PBS, subsequently incubated with peroxidase-conjugated secondary antibody for 30 min at RT, and rinsed 3x

again. Tetra-methylbenzidine (TMB) peroxidase substrate was added and incubated for 30 min at RT, and the reaction was stopped by adding 2N HCl. Absorbance at λ=450 nm was measured with a spectrometer.

2.4.7 Wound healing assay

Culture-insert 2 well 24 plates (ibidi, Gräfelfing, Germany) were used for the wound healing assay. In brief, twenty thousand hPAEC and hMVEC were seeded in the left or right silicon wells of the plate, respectively. The plates were exposed to hypoxia or normoxia for 24 h, and serum starved in medium with 0.2% FBS for the last 12 h, then the silicone inserts were removed to generate a 500 µm cell-free gap ("wound"). Brightfield microscopic images of the original gap area were captured at 0 and 12 h. To study the effect of autophagy on cell motility, EC were treated with the autophagy inhibitor BafA1 (20 nMol/L) or DMSO (vehicle) after the silicon inserts were removed. To record an accurate migration distance, specific landmarks were marked on the plate. To assess the effect of hypoxic PAEC or MVEC on PASMC motility, CM from hypoxic hPAEC or hMVEC was harvested and added to a confluent monolayer of hPASMC after scratching a gap with a 200 µl pipette tip. In some experiments, hPASMC were cultured in CM from hPAEC or hMVEC with or without the platelet-derived growth factor receptor (PDGFR) inhibitor imatinib (100 nMol/L; Sigma-Aldrich, #SML-1207, Burlington, MA), followed by staining with Ki67 antibody to detect proliferation.

2.5 Transmission electron microscopy

TEM was performed to detect WPbs in PAEC. In detail, murine lungs were gently perfused with 4% FBS/HBSS as described above to flush out blood, followed by 2.5% glutaraldehyde (Serva, Heidelberg, Germany) in 0.1 M sodium cacodylate buffer (Serva, Heidelberg, Germany) for 10 min. Left lung lobes were cut into small pieces and preserved in fixative at 4°C. After washing with cacodylate buffer, the samples were post-fixed with 1% osmium tetroxide (Electron Microscopy Sciences, Hatfield, USA) and 0.8% potassium ferrocyanide II (Roth, Karlsruhe, Germany) in 0.1 M cacodylate buffer for 1.5 h followed by another washing step. The samples were dehydrated in a graded ethanol series, transferred to a mixture of propylene oxide (Serva, Heidelberg, Germany) and Epon resin, and eventually embedded in Epon resin (Roth, Karlsruhe, Germany).

Ultrathin sections of 70 nm were gently sliced by a diamond knife on an ultramicrotome (Leica, Wetzlar, Germany), collected on pioloform-coated copper grids, and stained with uranyl acetate and lead citrate[59]. Images were obtained with a Zeiss EM 906 electron microscope at 80 kV acceleration voltage (Carl Zeiss, Oberkochen, Germany), equipped with a 2K CCD camera (TRS, Moorenweis, Germany). The samples used for imaging were randomly selected, and the operator was blinded to the individual sample group during the imaging process.

To distinguish PAEC from MVEC by TEM, we screened for WPbs, a vesicular organelle of arterial EC that is absent in lung capillaries[29,60]. In PAEC, WPbs are visible as rod-shaped, dense organelles with numerous parallel stripes along the long axis of the organelle, wrapped by a smooth and tight bounding mono-membrane[60,61]. In highly mature WPbs, it may occasionally be challenging to identify the characteristic parallel stripes as the electron density of the WPbs matrix may vary from moderate to high based on the maturity of the organelle[62,63].

To evaluate autophagic processes in EC, we detected autophagosomes by TEM, which have a double membrane structure containing undigested cellular components such as endoplasmic reticulum membranes, mitochondria, or ribosomes[64].

2.6 Western blotting

Cells were cultured on 6-well plates until confluence, washed with ice-cold PBS, then treated with 100 µL radioimmunoprecipitation assay buffer (RIPA) containing 1X protease inhibitor (Roche, REF 04693124001; Switzerland) and 1X phosphatase inhibitor (Thermo Fisher, #A32957; Waltham, MA). Cells were scraped off with a cell scraper, and the suspension was harvested and incubated on ice for 30 min, subsequently vortexed and centrifuged for 10 min at 14 rpm at 4°C. Protein concentration was quantified by Pierce bicinchoninic acid (BCA) assay (Thermo Fisher, #23227, Waltham, MA). Proteins (20 µg) were loaded on a gel, with an appropriate gel concentration depending on the molecular size of the target protein. Sodium dodecyl sulfate polyacrylamide gel electrophoresis (SDS-PAGE) and electrophoretic transfer were performed sequentially. Polyvinylidene difluoride (PVDF) membranes (Roth, T830.1; Karlsruhe, Germany) were blocked with 4% BSA in TBST (Tris-buffered saline with 0.1% Tween 20) for 1 h at RT, then incubated with primary antibody in blocking buffer at 4°C overnight, and rinsed 3 times with TBST, followed by incubation with secondary antibody for 1.5 h at RT, then washed again 3x with

TBST, immersed in Clarify ECL substrate working solution (Bio-Rad, #1705061, Hercules, CA) for 2 min, and finally exposed in a Biostep Chemiluminescence-Imager CELVIN S 420 (Burkhardtsdorf, Germany). The primary antibodies used for immunoblotting included: anti-LC3B (1:1000; Cell Signaling, #2775, Danvers, MA), anti-α-tubulin (1:1000, Sigma-Aldrich, #T6199, Burlington, MA), anti-ATG7 (1:1000; Cell Signaling, #8558, Danvers, MA), and anti-β-actin (1:1000; Cell Signaling, #3700, Danvers, MA). The secondary antibodies included goat anti-rabbit antibody (1:10000; Abcam, #ab97051, Cambridge, UK) and sheep anti-mouse antibody (1:10000; GE Healthcare, #NA931V, Chicago, IL).

2.7 Bulk RNA sequencing

To explore whether hypoxia induces a phenotypic switch from MVEC to PAEC, we performed bulk RNA sequencing (RNA-seq) of hypoxic (1% O_2, 24 h) and normoxic hPAEC and hMVEC in three biological replicates. Total RNA was purified from cell pellets using a QIAGEN RNeasy kit (QIAGEN, Germantown, MD). A TruSeq® Stranded mRNA Library Prep Kit (Illumina, San Diego, CA) was used for library preparation. After the RNA quality was confirmed by a Bioanalyzer system, the RNA was loaded on a NovaSeq 6000 sequencer for RNA-seq. Sequencing datasets were uploaded to Dr. Tom, a web-based bioinformatics platform provided by the Beijing Genomics Institute, for downstream RNA-seq analysis. RNA-seq Data were normalized and are shown as transcripts per million (TPM). Differentially expressed genes between normoxic hPAEC versus hMVEC were filtered based on a q-value <0.05 and log2 fold-change ≥3 or ≤-3, respectively.

2.8 Statistical analysis

Statistical analyses were performed using GraphPad Prism 8 software or IBM SPSS Statistics 20. Normal distribution and equality of variance were assessed by Shapiro-Wilk test and Levene's test, respectively. Data were analyzed by unpaired two-sided t-test or one-way analysis of variance (ANOVA) with post-hoc Tukey HSD for multiple comparisons. Results are presented as means ± SD, and differences with $p<0.05$ are considered significant.

3. Results

3.1 PAEC and MVEC differ in their response to PH triggers *in vitro*

3.1.1 Hypoxia

To probe for potential differential responses of PAEC and MVEC to PH stimuli, we measured proliferation and apoptosis of both EC subtypes after 24 h and 48 h exposure to hypoxia (1% O_2) or normoxia (21% O_2). Ki67 staining revealed that proliferation was increased in hypoxic hPAEC yet decreased in hypoxic hMVEC as compared to normoxia (Fig. 3A,B). On the other hand, Cl-Cas3 staining showed a significant increase in the proportion of apoptotic cells in hypoxic vs. normoxic hMVEC, yet hPAEC remained unchanged (Fig. 3C,D).

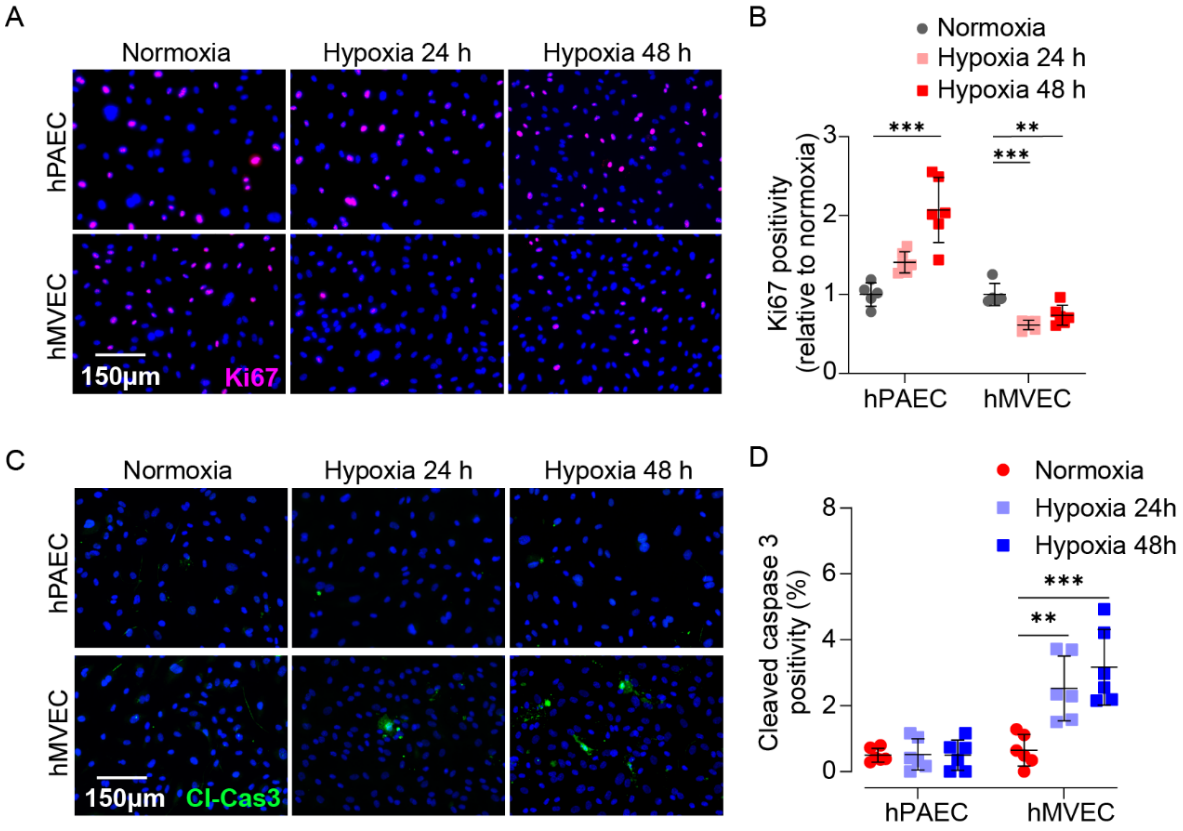

Figure 3. Differential responses of PAEC and MVEC to hypoxia *in vitro*. Representative images (**A,C**) and quantitative analysis (**B,D**) of Ki67 (red) (**A,B**) and cleaved caspase 3 (Cl-Cas3, green) (**C,D**) staining in human PAEC (hPAEC) and human MVEC (hMVEC) in response to 24 h and 48 h of hypoxia (1% O_2). Data are given as percentage of $Ki67^+$ cells relative to normoxia (**B**), and percentage of Cl-Cas3 positive cells (**D**), respectively. **A-B**: n=5-6 replicates each, **C-D**: n=6 replicates each; ** P ≤0.01, *** P ≤0.001.

3.1.2 TGF-β1

To validate the findings in Section 3.1.1, hPAEC and hMVEC were subjected to another PH trigger, transforming growth factor beta 1 (TGF-β1), for 72 hours. Consistent with the response to hypoxia, ki67 staining revealed an increase in proliferation in hPAEC in response to TGF-β1, while hMVEC showed reduced proliferation (Fig. 4A,B). Furthermore, Cl-cas3 staining indicated a higher percentage of apoptosis in TGF-β1 treated hMVEC compared to control, whereas apoptosis was still sparse in hPAEC (Fig. 4C,D). These findings provide further support that hPAEC and hMVEC respond differentially to PH triggers.

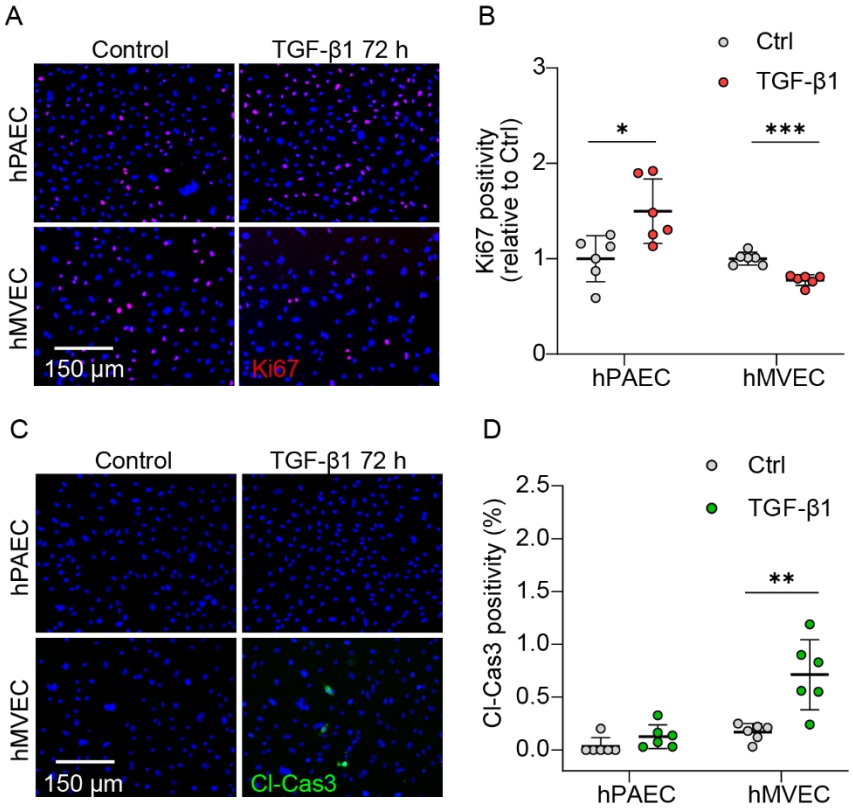

Figure 4. Differential responses of PAEC and MVEC to TGF-β1 *in vitro.* Representative images (**A,C**) and quantitative analysis (**B,D**) of Ki67 (red) (**A,B**) and cleaved caspase 3 (Cl-Cas3, green) (**C,D**) staining in human PAEC (hPAEC) and human MVEC (hMVEC) in response to 72 h of TGF-β1 (10 ng/mL). Data are given as percentage of $Ki67^+$ cells relative to vehicle control (**B**), and percentage of Cl-Cas3 positive cells (**D**), respectively. **A-D**: n=6 replicates each; * P ≤0.05, ** P ≤0.01, *** P ≤0.001.

3.2 PAEC and MVEC differ in their response to hypoxia *in vivo*

3.2.1 Validation of GS-IB4 as a reliable marker for MVEC *in vivo*

Before testing for a similar differential response of the two EC subsets *in vivo*, we tested the validity of *Griffonia simplicfolia* IB4 (GS-IB4)[25] as a marker for MVEC in PCLS from mice. GS-IB4 lectin is commonly used to stain MVEC as it recognizes the terminal α-D-galactose residues on MVEC-specific glycoproteins. To assess the specificity of GS-IB4 in intact lung tissue, we treated PCLS with α-galactosidase, an enzyme that catalyzes the removal of the terminal α-galactose from oligosaccharides, followed by GS-IB4 staining. As shown in Fig. 5A, capillaries and precapillaries can be positively labeled by GS-IB4, but this staining is no longer detectable after α-galactosidase treatment, confirming the specificity of GS-IB4 for MVEC. As endothelial glycocalyx may be shed in response to stressors such as hyperglycemia or hemorrhagic shock[65], we next tested whether α-D-galactose expression on MVEC is preserved under hypoxia. To this end, both rat EC subsets were subjected to hypoxic or normoxic conditions for 24 hours, followed by GS-IB4 staining. As shown in Fig. 5B-C, the mean intensity of GS-IB4 in hypoxic MVEC remained significantly higher than that in hypoxic PAEC. These findings demonstrate that GS-IB4 can be utilized as a reliable marker for MVEC both *in vitro* and in PCLS.

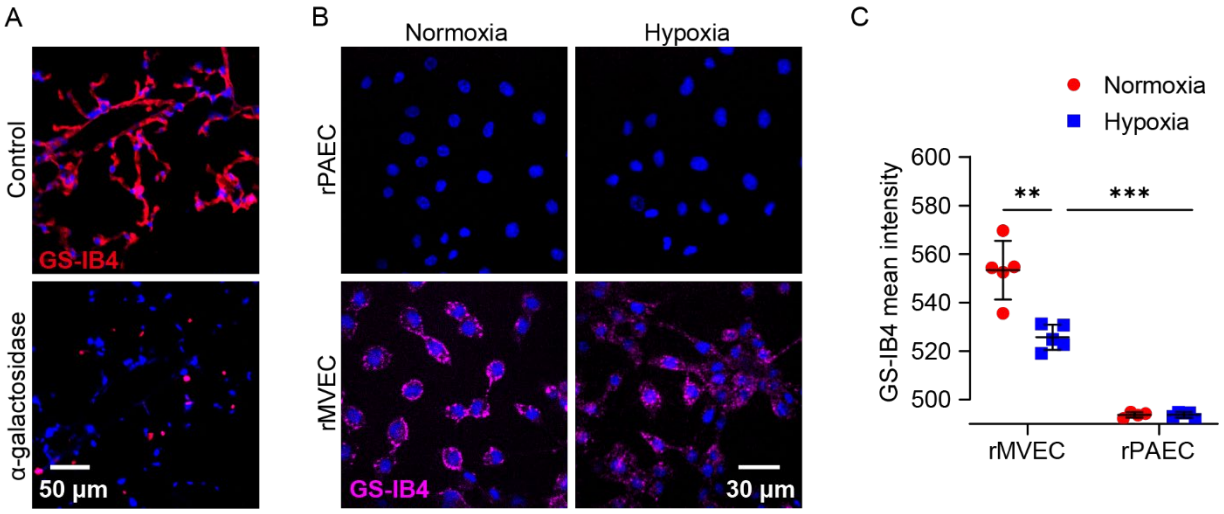

Figure 5. GS-IB4 stains MVEC in murine lungs. (A, top) GS-IB4 (red) positively stains α-galactose residues on capillaries and precapillaries. (A, bottom) GS-IB4 positivity is largely lost following PCLS treatment with α-galactosidase (1.2 U/mL at 37°C for 40 min). Representative images (B) and quantitative data (C) show GS-IB4 staining only in MVEC that is maintained in hypoxia. A: n=5 replicates each, B-C: n=4-5 replicates each. ** P ≤0.01, *** P ≤0.001.

3.2.2 PAEC and MVEC differ in their response to hypoxia *in vivo*

To investigate whether the differential responses observed *in vitro* are consistent with *in vivo* effects, we performed Ki67 and Cl-Cas3 staining on PCLS from mice exposed to chronic hypoxia or normoxia to assess proliferation and apoptosis in both EC subsets, respectively. MVEC were defined as GS-IB4^{+}CD31^{+} cells, and PAEC as GS-IB4^{-}CD31^{+} cells. By analyzing the stained PCLS, we observed that the proportion of vessels containing at least one proliferating (Ki67^{+}) PAEC was approximately four times higher in the PCLS of chronically hypoxic mice compared to normoxic mice. However, the ratio of vessels with Ki67^{+} MVEC remained unchanged (Fig. 6A,B). Conversely, we found that the proportion of vessels with at least one apoptotic (Cl-Cas3^{+}) MVEC increased in PCLS from hypoxic mice, while apoptotic PAEC were rarely observed (Fig. 6C,D). These findings provide further evidence for the differential behavior of PAEC and MVEC in response to hypoxia both *in vitro* and *in vivo*.

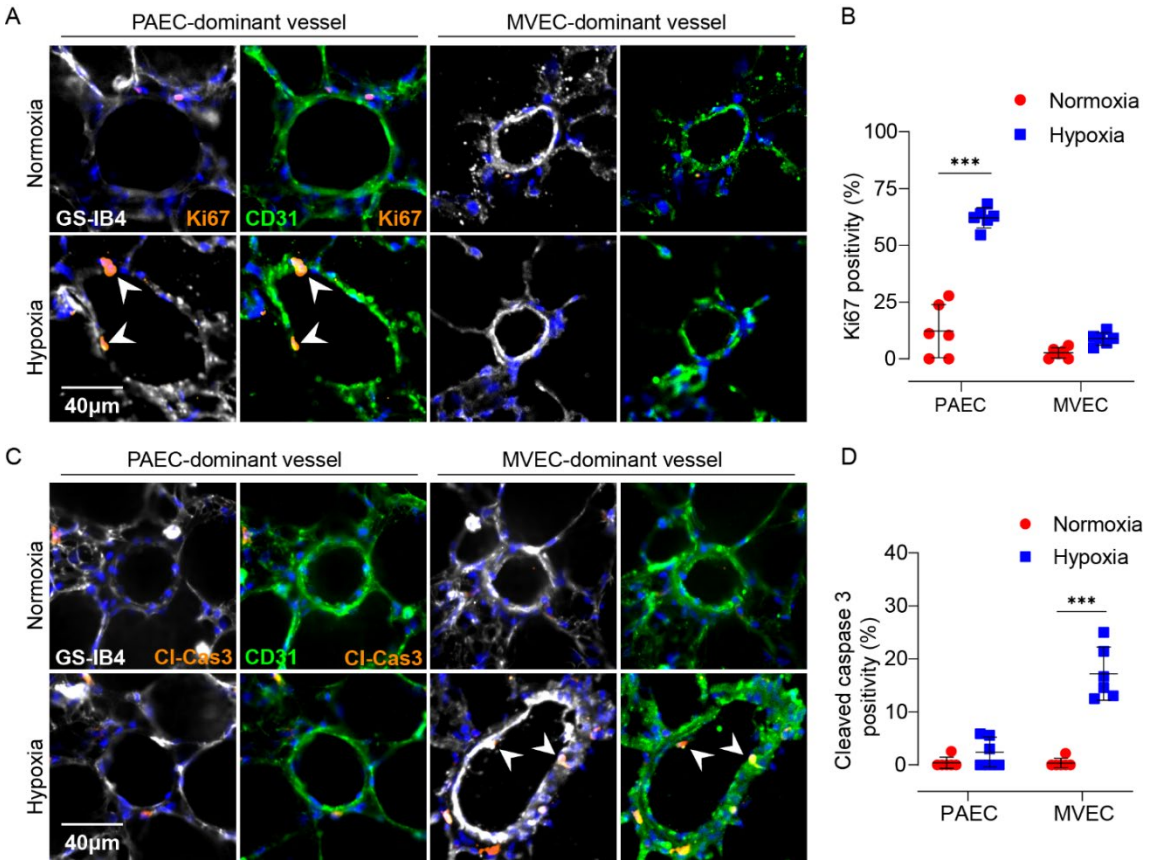

Figure 6. Differential responses of PAEC and MVEC to hypoxia *in vivo*. Representative images (**A,C**) and quantitative analysis (**B,D**) of Ki67 (orange) (**A,B**) and cleaved caspase 3 (Cl-Cas3, orange) (**C,D**)

staining in PAEC- and MVEC-dominant vessels in precision-cut lung slices (PCLS) from chronic (5 weeks) normoxic or hypoxic (10% O_2) mice. MVEC are identified by double positivity for the pan-endothelial marker CD31 (green) and *Griffonia simplicifolia* IB4 lectin (GS-IB4; white), while PAEC are defined by CD31 positivity but GS-IB4 negativity. Proliferating GS-IB4$^-$CD31$^+$ PAEC and apoptotic GS-IB4$^+$CD31$^+$ MVEC in chronic hypoxic lungs are marked by arrowheads. Data are shown as percentage of vessels containing at least one Ki67 (**B**) or Cl-Cas3 (**D**) positive PAEC or MVEC, respectively. n=6 replicates each; *** P ≤0.001.

3.3 PAEC replace MVEC in chronic hypoxia

3.3.1 PAEC replace MVEC in chronic hypoxia *in vitro*

Based on the observed differential responses described in Sections 3.1 and 3.2, we hypothesized that simultaneous PAEC proliferation and MVEC apoptosis may result in the progressive replacement of MVEC by PAEC. To test this *in vitro*, rat PAEC (rPAEC) and rat MVEC (rMVEC) labeled with different fluorophores were co-cultured under normoxic or hypoxic conditions for up to 7 days. Under hypoxic conditions, the proportion of the surface occupied by rPAEC gradually increased, whereas it remained relatively unchanged under normoxia, demonstrating rPAEC expansion at the expense of rMVEC (Fig. 7A,B). Additionally, a wound healing assay showed higher migration rates of hPAEC compared to hMVEC that were further accelerated by hypoxia (Fig. 7C,D), suggesting that hypoxic PAEC could migrate rapidly and occupy the vacant spaces opened by apoptotic MVEC.

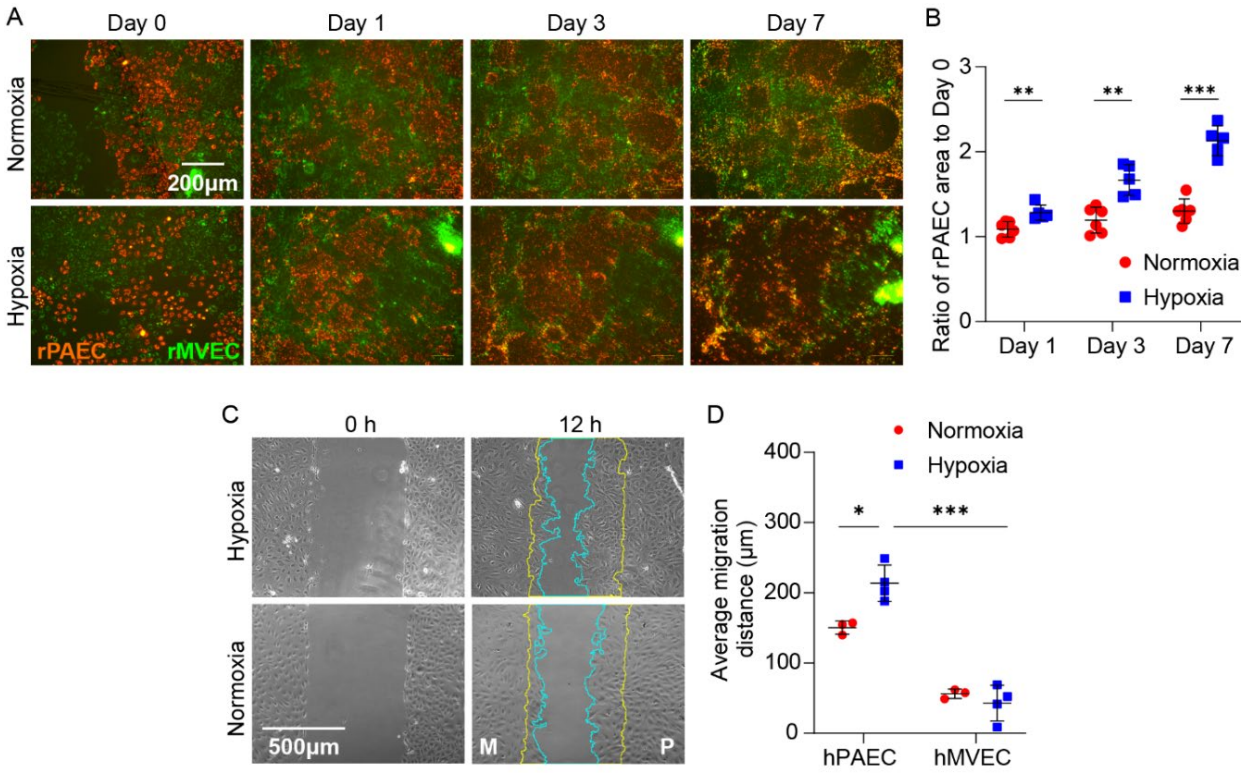

Figure 7. PAEC replace MVEC under hypoxia *in vitro*. Representative images (**A**) and quantitative analysis (**B**) depict the co-culture of PKH26 red-labeled rat PAEC (rPAEC) with PKH67 green-labeled rat MVEC (rMVEC) under hypoxia (1% O_2) or normoxia at day 0, 1, 3, and 7. The progressive coverage by rPAEC is presented as the ratio of the total red (rPAEC) area at each specific day relative to day 0. Representative images (**C**) and quantitative analysis (**D**) demonstrate a wound healing assay with hMVEC (M) and hPAEC (P) cultured on the left and right side of the wound, respectively. The outlines of the wound gap captured at 0 and 12 hours under normoxia or hypoxia are marked by yellow and cyan lines, respectively. Data give the average migration distance. **A,B**: n=5-6 replicates each, **C,D**: n=3-4 replicates each; * P ≤0.05, ** P ≤0.01, *** P ≤0.001.

3.3.2 Differentiation between PAEC and MVEC *in vivo*.

Next, we aimed to validate this concept in an *in vivo* setting. Prior to this, it was essential to determine the respective distribution of the two EC subsets based on vessel size in the normal mouse lung. The prevailing consensus is that pulmonary macrovascular segments (arteries and veins) and microvascular segments (capillaries) develop independently and subsequently merge during the later stages of the pseudo-glandular phase of pulmonary development[66,67]. This concept suggests the existence of a transition zone between capillaries predominantly composed of MVEC and arterioles predominantly composed of PAEC. In Fig. 8A, a small vessel is depicted with positive staining for GS-IB4, whereas a large vessel shows negative staining for GS-IB4. In addition, Fig. 8B displays a 3D-rendered vessel containing yellow line enclosed GS-IB4$^-$ PAEC as opposed to GS-IB4$^+$ MVEC. To facilitate quantitative analysis of PAEC/MVEC coverage in the transition zone, we determined a GS-IB4 mean intensity of 2500 in EC (identified as CD31 or vWF positive) as the threshold to distinguish between PAEC- (< 2500) and MVEC- (≥ 2500) dominant vessels (Fig. 8C). In line with a previous study[29], we found vessels larger than 60 µm in diameter to be outlined by PAEC, while vessels with a diameter < 20 µm were predominantly covered by MVEC, with vessels in between forming a transition zone (Fig. 8D).

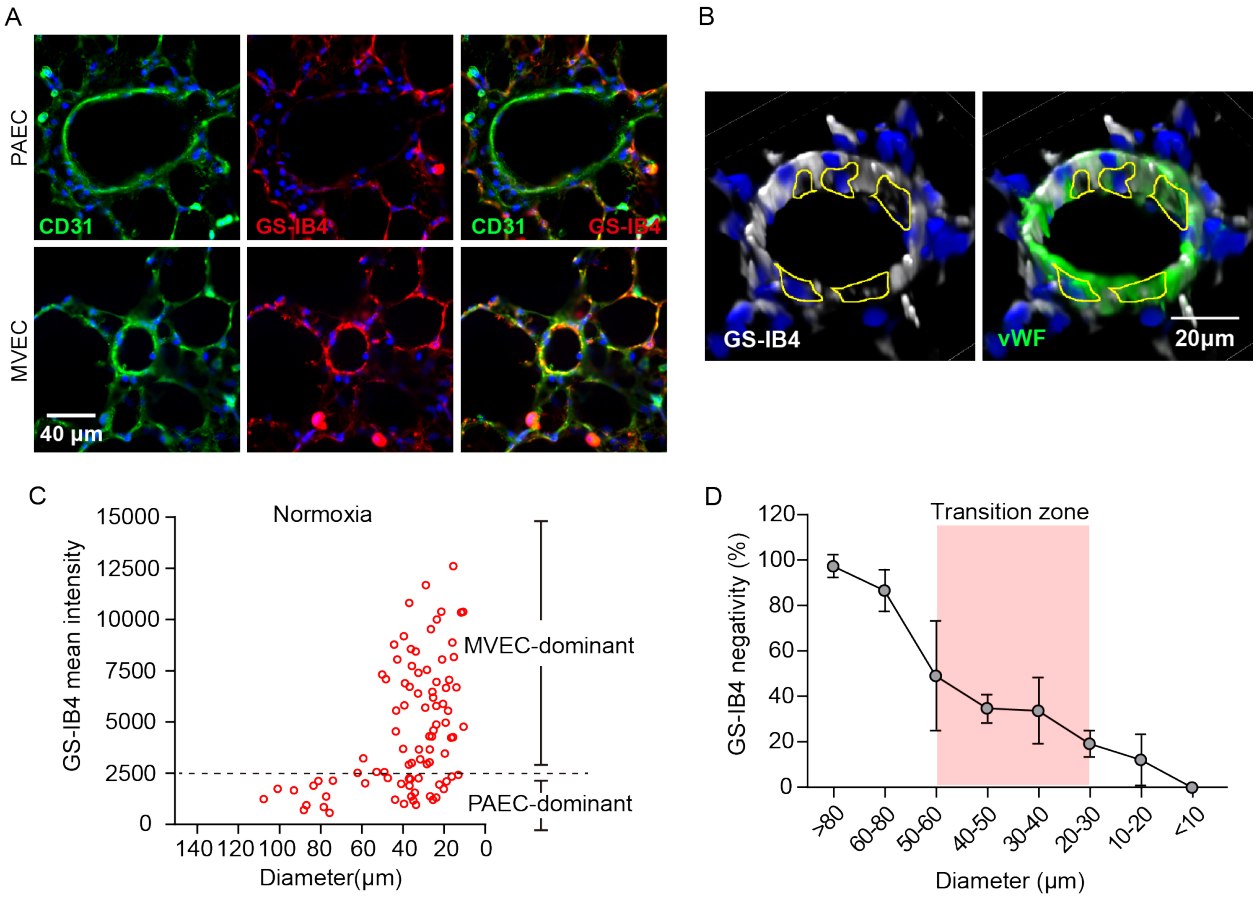

Figure 8. Definition of PAEC- and MVEC-dominant vessels. (**A**) Representative images of CD31 (green) and *Griffonia simplicifolia* IB4 (GS-IB4; white) staining in a PAEC- (upper) and MVEC- (lower) dominant vessel. (**B**) Representative 3D rendered image of a vessel containing $GS^{+}vWF^{+}$MVEC and $GS^{-}vWF^{+}$ PAEC (yellow lines). **(C)** Scatter plot showing the relationship between vessel diameter and GS-IB4 mean intensity. A mean intensity of 2500 was defined as the threshold to distinguish PAEC- ($GS\text{-}IB4^{-}$) and MVEC- ($GS\text{-}IB4^{+}$) dominant vessels. (**D**) Quantitative analysis shows the level of GS-IB4 negativity in different sizes of vessels in normoxic mice. The area above the curve indicates MVEC coverage, while the area below the curve denotes PAEC coverage. The red area highlights vessels with a diameter ranging from 20 to 60 µm which showed a mixed coverage by PAEC and MVEC and were accordingly designated as the transition zone. **A-D**: n=6 replicates.

3.3.3 PAEC replace MVEC in chronic hypoxia *in vivo*

Based on the technique we developed in the previous section, we next assessed MVEC replacement by PAEC in hypoxia *in vivo*. To this end, GS-IB4 negativity of subgroups with different vessel diameters was quantified in normoxic and chronic hypoxic mice. Within the transition zone, there was a notable increase in the proportion of vessels dominated by PAEC in PCLS obtained from chronically hypoxic mice compared to normoxic mice

(Fig. 9A,B). In contrast, the abundance of vessels dominated by either PAEC or MVEC remained relatively constant in both larger and smaller vessels, respectively (Fig. 9B). To further consolidate this concept of PAEC replacing MVEC within the transition zone, we employed electron microscopy to examine the presence of WPb, an organelle that is typically found in PAEC but absent in MVEC[34]. Consistent with our hypothesis, TEM analysis showed a significantly increased percentage of PAEC-containing vessels in the transition zone in hypoxia when compared to normoxia (Fig. 9C,D), while WPb remained abundant or absent in larger and smaller vessels, respectively (Fig. 9D). These data suggest that in hypoxia, proliferative PAEC replace apoptotic MVEC in the transition zone.

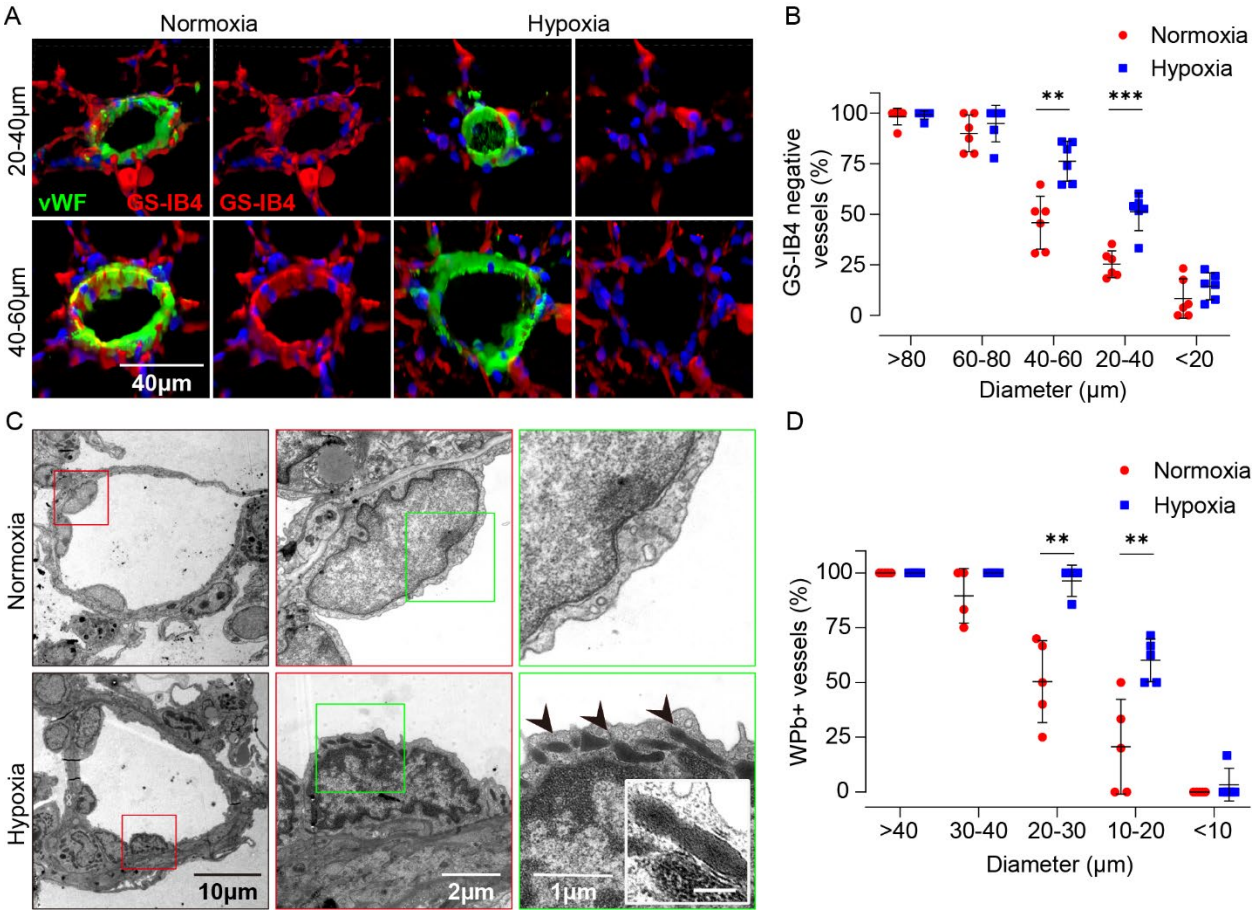

Figure 9. PAEC replace MVEC in hypoxia *in vivo*. Representative micrographs (**A**) and quantitative analysis (**B**) show abundance of MVEC (double positive with von Willebrand factor (vWF; green) and *Griffonia simplicifolia* IB4 (GS-IB4; red) and GS-IB4$^-$ vWF$^+$ PAEC in precapillary arterioles of 20-60 µm diameter in precision cut lung slices (PCLS) from chronic (5 weeks) normoxic or hypoxic (10% O_2) mice. Data give percentage of GS-IB4 negative (i.e., PAEC-dominant) vessels as a function of vessel diameter. **C**: Representative transmission electron micrographs of pulmonary precapillary arterioles (diameters approximately 20 µm) from chronic hypoxic or normoxic mice at (from left to right) increasing levels of magnification show Weibel-Palade bodies (WPb), a PAEC-specific organelle (marked by arrowheads and shown enlarged as

inserts (scalebar: 200 nm)). **D:** Corresponding quantitative analysis shows the percentage of WPb^+ (i.e., PAEC-containing) vessels, defined as vessels with at least one WPb detected in the endothelium, as a function of vessel diameter. **A,B:** n=6 replicates each, **C,D:** n=5 replicates each, ** P ≤0.01, *** P ≤0.001.

3.3.4 Live imaging of MVEC loss in chronic hypoxia

The results of the previous section confirm that PAEC progressively invade the transition zone to replace MVEC, causing a progressive functional arterialization of lung precapillary microvessels in hypoxia. However, this notion is based on static end-point analyses rather than time-resolved monitoring. To address this issue at least in part, we developed an *ex vivo* imaging system to visualize the dynamic changes in PAEC and MVEC under hypoxia. PCLS with a thickness of 150 µm were stained with GS-IB4, Alexa 488-labeled anti-CD31 antibody, and Hoechst 33342 to mark MVEC, pan-endothelial cells, and nuclei, respectively. The pre-stained PCLS were placed in a 10 mm² dish and gently pressed using a 45 mm filter, ensuring that the PCLS remained in a stable position (Fig. 10A). This device was then placed on an EVOS fluorescence microscope equipped with an incubating chamber containing an O_2, CO_2, and temperature controller system to maintain the viability of the PCLS. As shown in exemplary images in Fig 10B, we observed several GS-$IB4^+$ MVEC detaching from the vessel wall over a 48 h period of hypoxia. Over time, this process led to the transition of the respective vessel from a vessel containing both GS-$IB4^-CD31^+$ PAEC and GS-$IB4^+CD31^+$ MVEC to a vessel outlined by GS-$IB4^-CD31^+$ PAEC only. In PCLS exposed to 48 h of normoxia, no such detachment of MVEC and subsequent replacement by PAEC was detected (Fig 10B).

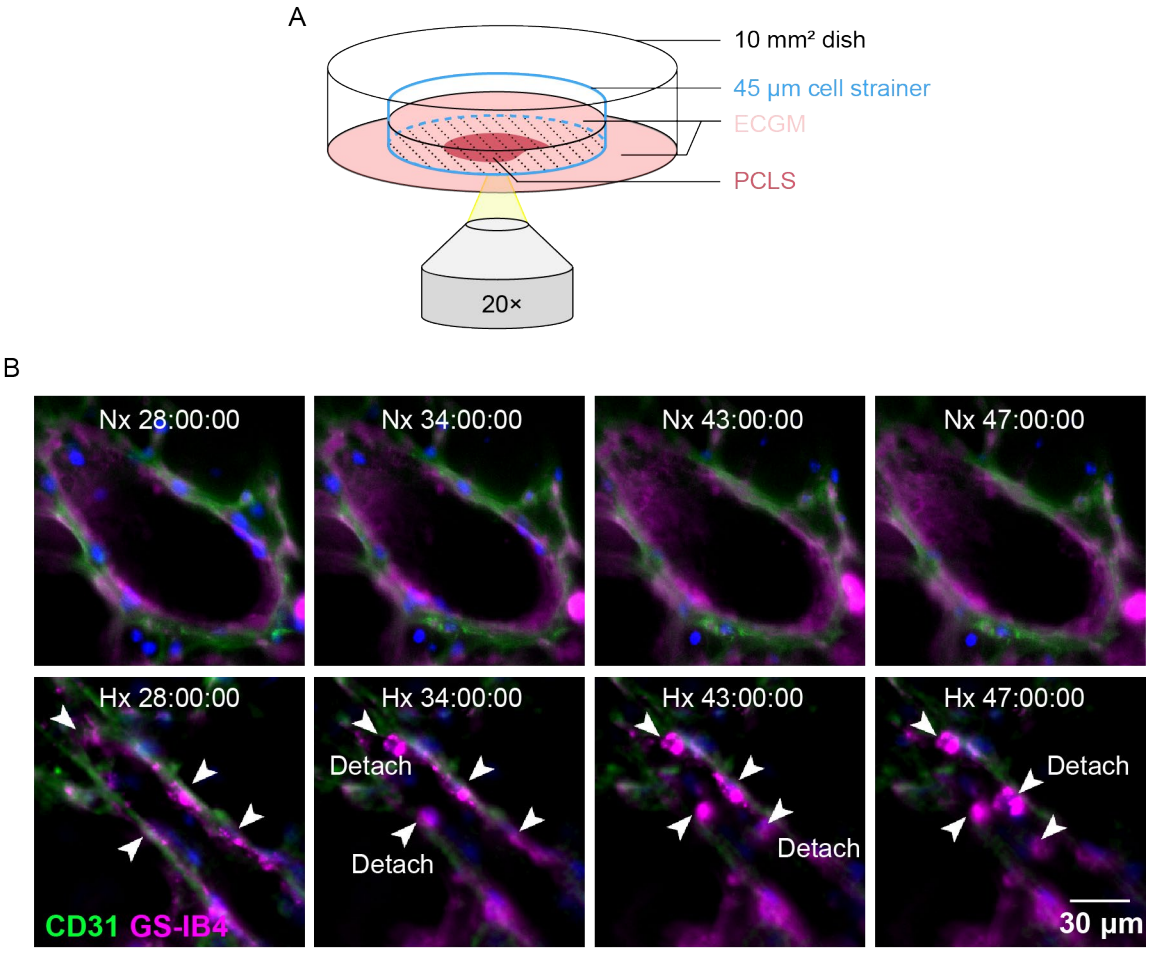

Figure 10. Live imaging of PCLS under hypoxia shows MVEC detachment and replacement by PAEC. (**A**) Schematic representation of the *ex vivo* setup for live imaging of PCLS; (**B**) Representative images show detachment of MVEC (GS-IB4$^+$CD31$^+$) between 24-48 hours after onset of hypoxia (1% O_2, lower panel). This is not detected in normoxic PCLS (upper panel). Detached MVEC are indicated by white arrowheads. Time is displayed as hr:min:sec. **A,B**: n=6 replicates.

3.3.5 Phenotypic switch of PAEC to MVEC

In our current discourse, we primarily focused on the concept of PAEC replacing MVEC in hypoxic lung precapillary microvessels. As an alternative mechanism, however, we also took into consideration the possibility that the increased prevalence of PAEC in the transition zone may not solely result from the proliferation and migration of PAEC into distal lung vessels, but could potentially be attributed to a phenotypic conversion of MVEC into PAEC under hypoxia. To address and investigate this hypothesis, we performed next-generation mRNA sequencing analyses of cultured hPAEC and hMVEC exposed to either hypoxia or normoxia for 24 h and 7 d. Principal component analysis (PCA) revealed no evidence of transdifferentiation of hMVEC into a hPAEC-like phenotype under hypoxic

conditions after exposure to hypoxia for either 24 h or after 7 d. Specifically, the cluster of hypoxic hMVEC did not overlap with either the normoxic or hypoxic hPAEC clusters (Fig. 11A). Additionally, the expression levels of specific hMVEC marker genes recently identified by single-cell RNA-seq[68] such as *CA4*, *AFF3*, and *NCALD* remained high, while the expression of hPAEC marker genes including *DKK2*, *FBLN5*, and *MCTP1* remained low in hypoxic hMVEC (Fig. 11B). Similarly, the expression levels of the top 15 ranked genes specific to normoxic hPAEC did not show a significant increase in hypoxic hMVEC compared to normoxic hMVEC (Fig. 11C).

In a parallel approach, we utilized WPb, a characteristic organelle of PAEC, to probe for a potential phenotypic switch of MVEC to PAEC. As depicted in Figure 11D-F, TEM analysis revealed the absence of WPb in rat MVEC exposed to both normoxia and hypoxia for 7 days. Similarly, vessels smaller than 5 µm in chronic hypoxic mice exhibited no detectable WPb either in normoxia or in hypoxia. These findings collectively suggest that the observed increase in PAEC coverage in the transition zone is not due to a phenotypic transition of MVEC into PAEC in response to hypoxia, but due to a progressive invasion of PAEC where they replace MVEC.

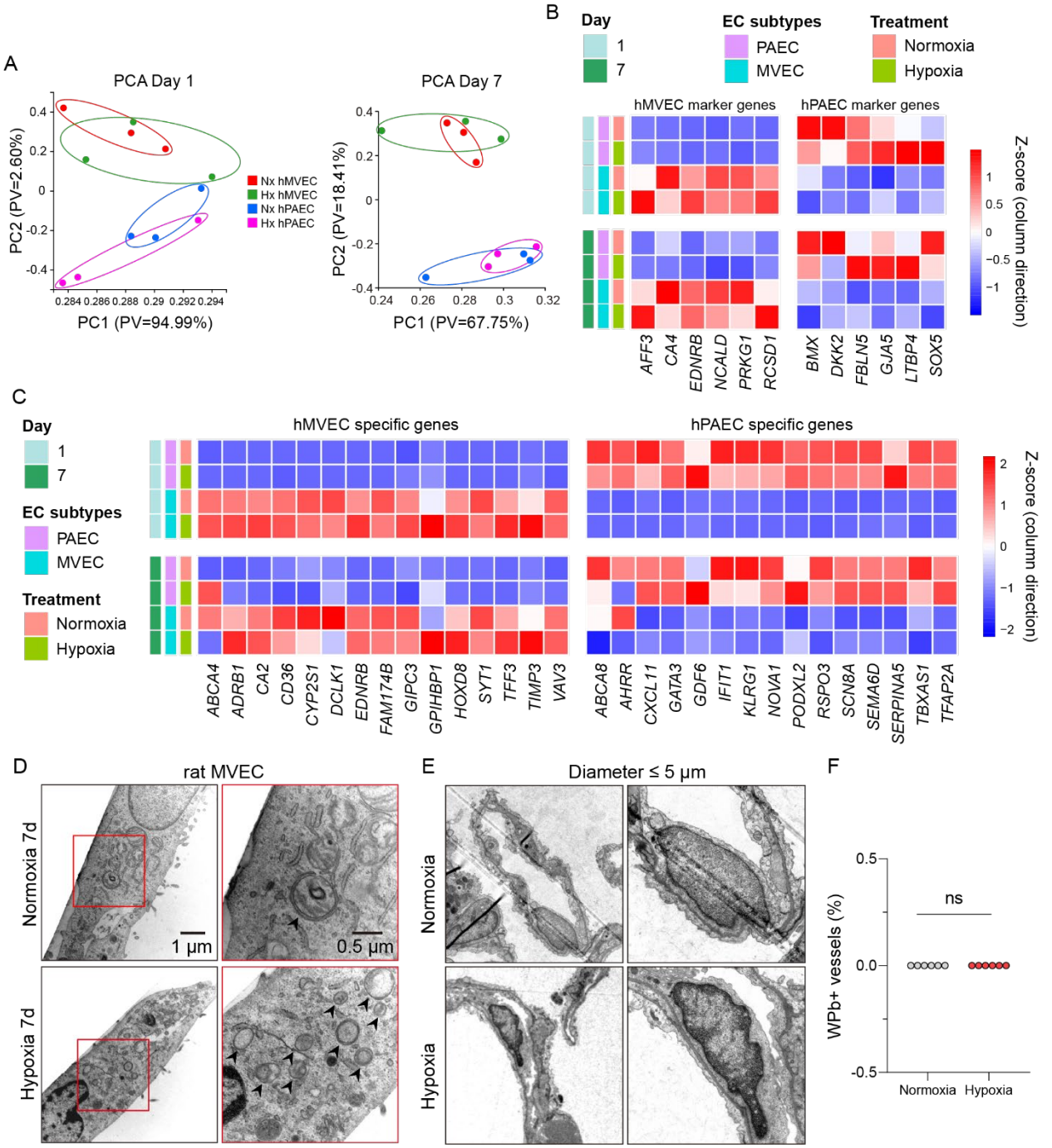

Figure 11. MVEC retain their microvascular transcriptomic signature in hypoxia. (**A**) Principal component analysis (PCA) of the mRNA expression profile in normoxic or hypoxic (1%O_2 for 24 h and 7d) hPAEC and hMVEC reveals no overlap between the hypoxic hMVEC cluster and any of the hPAEC clusters. PV: Proportion of variance. (**B**) Heatmap of representative hMVEC marker genes and hPAEC marker genes in normoxic and hypoxic hPAEC and hMVEC. hPAEC and hMVEC marker genes were selected from published single-cell RNA sequencing analyses[69]. (**C**) Heatmap of the top 15 ranked differentially expressed genes (sorted by log2 fold difference of ≥ 3 or ≤ -3 between normoxic human PAEC (hPAEC) and MVEC (hMVEC)) in normoxic and hypoxic (1%O_2, for 24 h and 7d) hPAEC and hMVEC. Note that expression profiles between hPAEC and hMVEC remain distinct in hypoxia. (**D**) Representative transmission electron (TEM) micrographs of rat MVEC exposed to normoxia and hypoxia for 7 d. Autophagosomes are marked

by black arrowheads. (**E**) Representative TEM micrographs of two capillaries (diameters < 5 µm) from chronic hypoxic or normoxic mice and (**F**) corresponding quantitative analysis show no Weibel-Palade body (WPb) positive endothelial cells in capillaries of chronic hypoxic or normoxic mice. **A-F**: n=6 replicates; * P ≤0.05, ** P ≤0.01, *** P ≤0.001.

3.4 Differential responses of PAEC and MVEC to PH triggers are mediated by autophagy

So far, we have demonstrated that PH triggers lead to differential responses in two EC subsets, namely PAEC proliferation and MVEC apoptosis, which in turn cause progressive endothelial arterialization of precapillary lung microvessels, with the replacement of MVEC by PAEC in the transition zone. As a putative mechanism underlying these distinct changes, we propose the central hypothesis that the differential responses of PAEC and MVEC may be attributed to the activation of autophagy in PH.

3.4.1 Activation of endothelial autophagy *in vitro*

To investigate this hypothesis, we first assessed the autophagic flux in PAEC and MVEC in hypoxia *in vitro*. As depicted in Figure 12A, using Western blot analysis, we detected an increased ratio of LC3BII/I, a well-established marker of autophagy activation, in both hypoxic PAEC and MVEC compared to their normoxic counterparts. To quantitatively assess the accumulation of autophagosomes in both cell subsets in response to hypoxia, we next treated cells with BafA1 to inhibit the fusion of autophagosomes with lysosomes. When either PAEC or MVEC were exposed to hypoxia in conjunction with BafA1, a more pronounced reduction in the level of LC3B-I was detected, indicating a higher conversion of LC3B-I to LC3B-II (Fig. 12A,B). Additionally, we performed Cyto-ID staining to label autophagic vacuoles and found an elevated number of autophagic vacuoles in both PAEC and MVEC following exposure to hypoxia relative to normoxic controls (Fig. 12C-D). Interestingly, MVEC exhibited a higher baseline level of autophagic vacuoles compared to PAEC under normoxia, which increased further in response to hypoxia. Similarly, MVEC consistently exhibited a relatively higher level of autophagic vacuoles at each time point during TGF-β1 treatment when compared to PAEC (Fig. 12E,F). These findings suggest that the autophagy flux in MVEC stimulated with characteristic PH triggers may be more likely to reach the threshold for autophagy-induced cell death (ACD) when compared to PAEC, and thus contribute to their propensity for apoptosis under hypoxia.

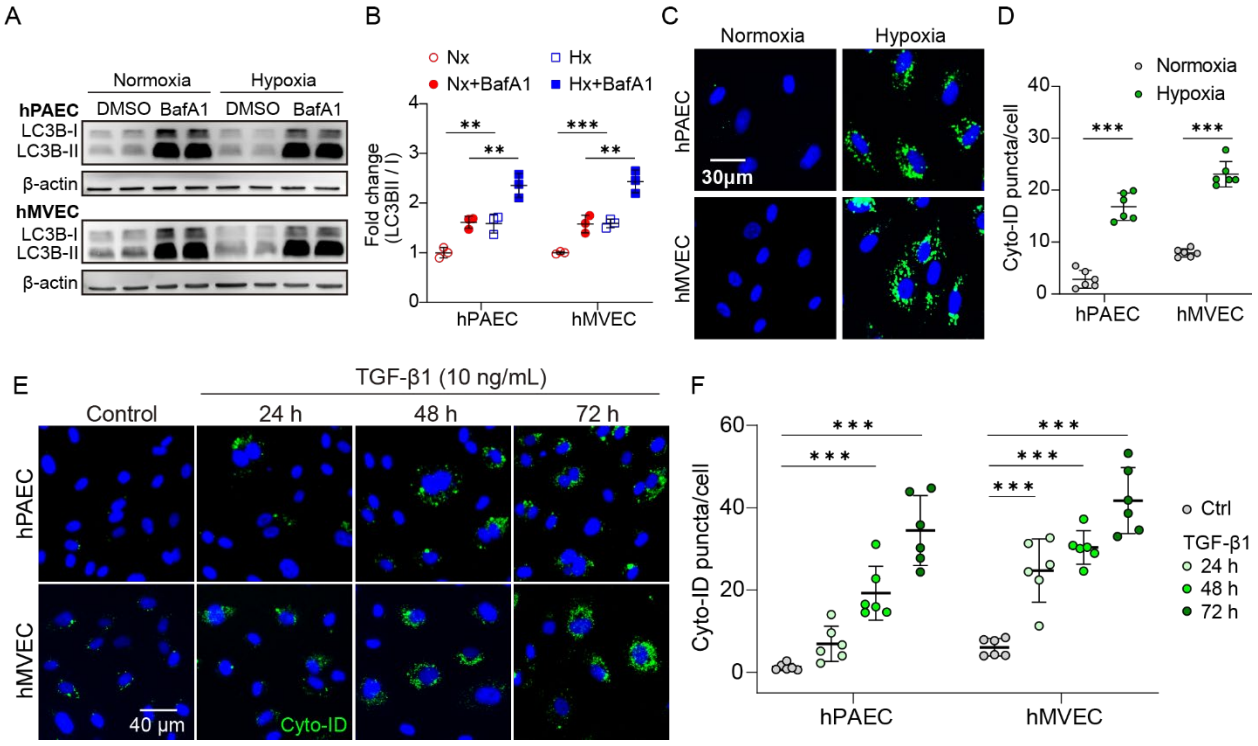

Figure 12. Hypoxia induces autophagy activation in PAEC and MVEC *in vitro* . Representative Western blots (**A**) and quantitative densitometric analysis (**B**) of LC3B expression in human PAEC (hPAEC) and MVEC (hMVEC) exposed to normoxia or hypoxia (1% O_2), with or without the autophagy inhibitor bafilomycin A1 (BafA1, 20 nMol/L) or vehicle (DMSO) for 24 h. The LC3B II/I ratio was used as an indicator of autophagy flux. Representative images (**C,E**) and quantitative analysis (**D,F**) of Cyto-ID staining for autophagic vacuoles (green; nuclei counterstained with DAPI) in hPAEC and hMVEC exposed to hypoxia for 24 h (**C,D**) or to TGFβ1 for 72 h (**E,F**), with comparison to their untreated controls. Data give GFP-positive puncta/cell. **A,B**: n=3 replicates each; **C-F**: n=6 replicates each; ** P ≤0.01, *** P ≤0.001.

3.4.2 Activation of endothelial autophagy *in vivo*

To validate autophagy activation of lung EC *in vivo*, we probed PAEC and MVEC for the characteristic double-membrane structure of autophagosomes by transmission electron microscopy (TEM). Consistently, TEM analysis revealed an increased abundance of autophagosomes in both PAEC and MVEC in the lungs of chronic hypoxic mice compared to normoxic mice (Fig. 13A). Furthermore, hypoxia-induced autophagy induction was also evident *in situ* in PCLS from GFP-LC3 homozygous mice where activated autophagy of lung EC was evident as an increased GFP signal. Upon exposure of PCLS to hypoxia for 24 h, we detected an increase in GFP fluorescence in both GS-IB4$^+$vWF$^+$ MVEC and GS-IB4$^-$vWF$^+$ PAEC, indicating enhanced autophagy activity compared to normoxic controls (Fig. 13B,C). In line with our *in vitro* findings, MVEC displayed a comparatively higher

level of autophagic vacuoles both at baseline and after 24 h of hypoxia compared to PAEC.

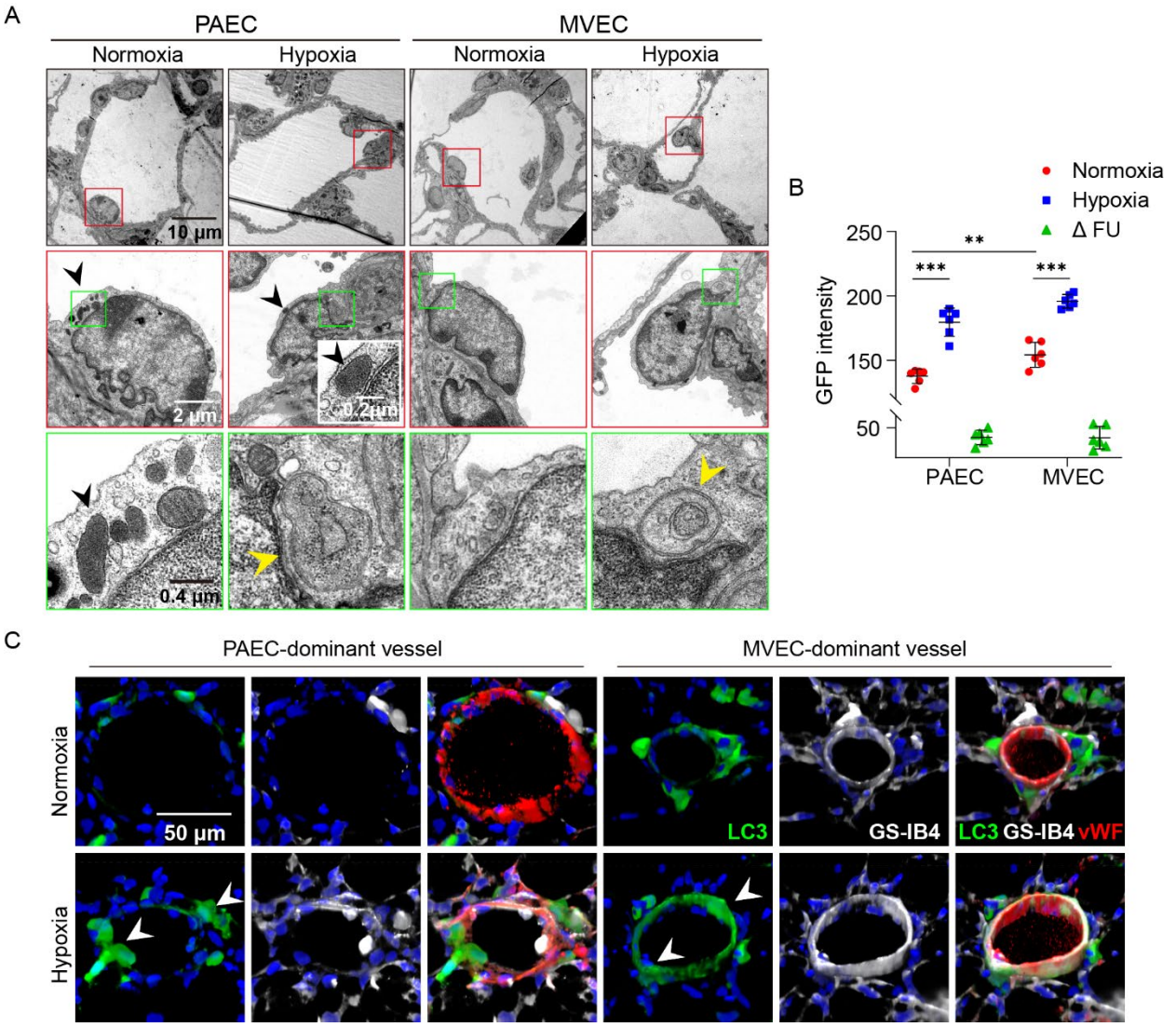

Figure 13. *In vivo/ex vivo* evidence shows autophagy activation in hypoxic PAEC and MVEC. (A) Representative transmission electron micrographs of pulmonary precapillary arterioles from chronic hypoxic or normoxic mice at (from top to bottom) increasing levels of magnification show autophagosomes in hypoxic PAEC and MVEC (highlighted by yellow arrowheads, with Weibel-Palade bodies in PAEC marked by black arrowheads). Quantitative analysis (**B**) and representative micrographs (**C**) show autophagic activation, assessed as GFP fluorescence (green; in fluorescence units, FU), in precision cut lung slices (PCLS) from GFP-LC3 mice exposed to hypoxia (1%) or normoxia for 24 h in the presence of 20 nMol/L bafilomycin A1. EC are identified by the pan-endothelial marker vWF (red), MVEC by positivity for *Griffonia simplicifolia* IB4 (GS-IB4; white), and PAEC by GS-IB4 negativity, respectively. White arrowheads mark GFP-positive PAEC and MVEC in hypoxic PCLS. Data give the mean GFP fluorescence intensity of GS-IB4$^-$vWF$^+$ PAEC and GS-IB4$^+$vWF$^+$ MVEC, as well as the difference in GFP fluorescence between hypoxic and normoxic PCLS from the same mouse lung (ΔFU). **A**: n=5 replicates each; **B,C**: n=6 replicates each. ** P ≤0.01, *** P ≤0.001.

3.4.3 Autophagy triggers differential responses in PAEC and MVEC *in vitro*

To investigate the impact of autophagy on PAEC and MVEC, we treated both cell types with TAT-Beclin-1, an autophagy inducer, for 24 h. Fig. 14A-B show that TAT-Beclin-1 treatment led to increased proliferation in hPAEC but decreased proliferation in MVEC, as assessed by Ki67 staining. Conversely, the induction of autophagy by Beclin-1 resulted in a significant increase in apoptosis specifically in hMVEC, as indicated by increased Cl-Cas3 staining (Fig. 14C-D). Based on the fact that a) both MVEC and PAEC increase autophagic activation in response to hypoxia, but b) autophagy activation results in opposing effects in terms of proliferation and apoptosis in these EC subsets, which mirror their differential response to hypoxia, we speculated that the differential response of PAEC and MVEC to hypoxia may be mediated by autophagy activation. To test this hypothesis, we silenced the key autophagy gene ATG7 by si*ATG7* transfection. Validation of *ATG7* knockdown by WB showed an approximately 40% reduction of ATG7 protein expression in hPAEC and a 50% reduction in hMVEC (Fig. 14E). The knockdown of *ATG7*, in contrast to the scrambled control siRNA, resulted in a reversal of hypoxia-induced proliferation in hPAEC and counteracted the suppressed proliferation in hMVEC, as demonstrated by BrdU assay (Fig. 14F). In parallel, silencing of *ATG7* attenuated apoptosis in MVEC, as evidenced by Annexin V staining (Fig. 14G-H). These findings identify a significant role for autophagy in mediating the differential responses of PAEC and MVEC to hypoxia.

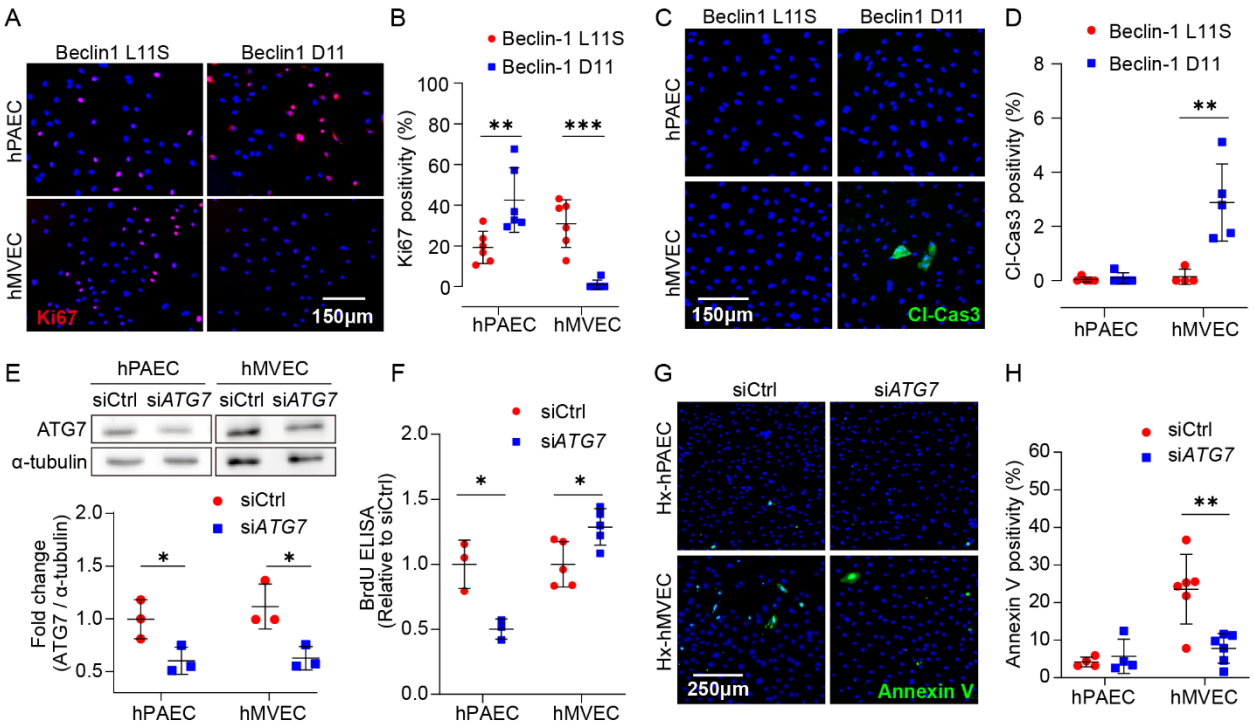

Figure 14. Differential responses of PAEC and MVEC to hypoxia are mediated by autophagy *in vitro*. Representative images (**A,C**) and quantitative analysis (**B,D**) of Ki67 (red) (**A,B**) and cleaved caspase 3 (Cl-Cas3, green) (**C,D**) staining in human PAEC (hPAEC) and MVEC (hMVEC) in response to the autophagy inducer Beclin-1 D11 (20 µMol/L, 24h) or the scrambled control L11S (20 µMol/L, 24h). Data are given as percentage of $Ki67^+$ (**B**) and $Cl\text{-}Cas3^+$ cells (**D**), respectively. (**E)** Representative immunoblotting images and quantitative analysis show knockdown of *ATG7* by siRNA (si*ATG7,* 100nMol/L, 48h) in human EC. BrdU assay (**F**) and staining for annexin V (green; nuclei counterstained with DAPI) (**G,H**) show proliferation and apoptosis, respectively, in hypoxic (Hx; 1% O_2, 24 h) hPAEC and hMVEC transfected with si*ATG7* or non-targeting control siRNA (siCtrl). Data give the percentage of Annexin V-positive cells (**H**). **A**,**B**: n=6 replicates each; **C,D**: n=4-5 replicates each; **E**: n=3 replicates each; **F**: n=3-5 replicates each; **G,H**: n=4-6 replicates each; * P ≤0.05, ** P ≤0.01, *** P ≤0.001.

3.4.4 Autophagy triggers differential responses in PAEC and MVEC *in vivo*

We next validated the findings in Section 3.4.3 by assessing the role of autophagy in lung endothelial responses to hypoxia *in vivo*. To this end, we measured proliferation and apoptosis in both EC subtypes in PCLS from chronic hypoxic *Atg7*$^{EN\text{-}KO}$ and corresponding wild-type *Atg7*$^{EN\text{-}WT}$ mice. ATG7 deficiency in EC was confirmed by ATG7 immunofluorescence staining, which showed no detectable ATG7 signal in EC in *Atg7*$^{EN\text{-}KO}$ mice (Fig. 15A). Ki67 staining revealed that the ratio of vessels containing at least one $Ki67^+$ PAEC (defined again as $GS\text{-}IB4^-CD31^+$ cells) was reduced in the transition zone in chronic hypoxic *Atg7*$^{EN\text{-}KO}$ mice when compared to chronic hypoxic *Atg7*$^{EN\text{-}WT}$ mice, while the proliferation of $GS\text{-}IB4^+CD31^+$ MVEC increased in chronic hypoxic *Atg7*$^{EN\text{-}KO}$ mice when compared to hypoxic *Atg7*$^{EN\text{-}WT}$ mice (Fig. 15B-E). Furthermore, Cl-Cas3 staining exhibited a reduced proportion of vessels containing apoptotic MVEC in chronic hypoxic *Atg7*$^{EN\text{-}KO}$ relative to chronic hypoxic *Atg7*$^{EN\text{-}WT}$ mice, while the level of apoptosis in PAEC remained low in both groups (Fig. 15F-G). Both PAEC and MVEC had a low level of proliferation and apoptosis in normoxia, with no significant differences between *Atg7*$^{EN\text{-}KO}$ mice and *Atg7*$^{EN\text{-}WT}$ mice (Fig. 15H-K). These findings further support the conclusion that autophagy plays a critical role in the differential responses of different EC subtypes to hypoxia, both *in vitro* and *in vivo*.

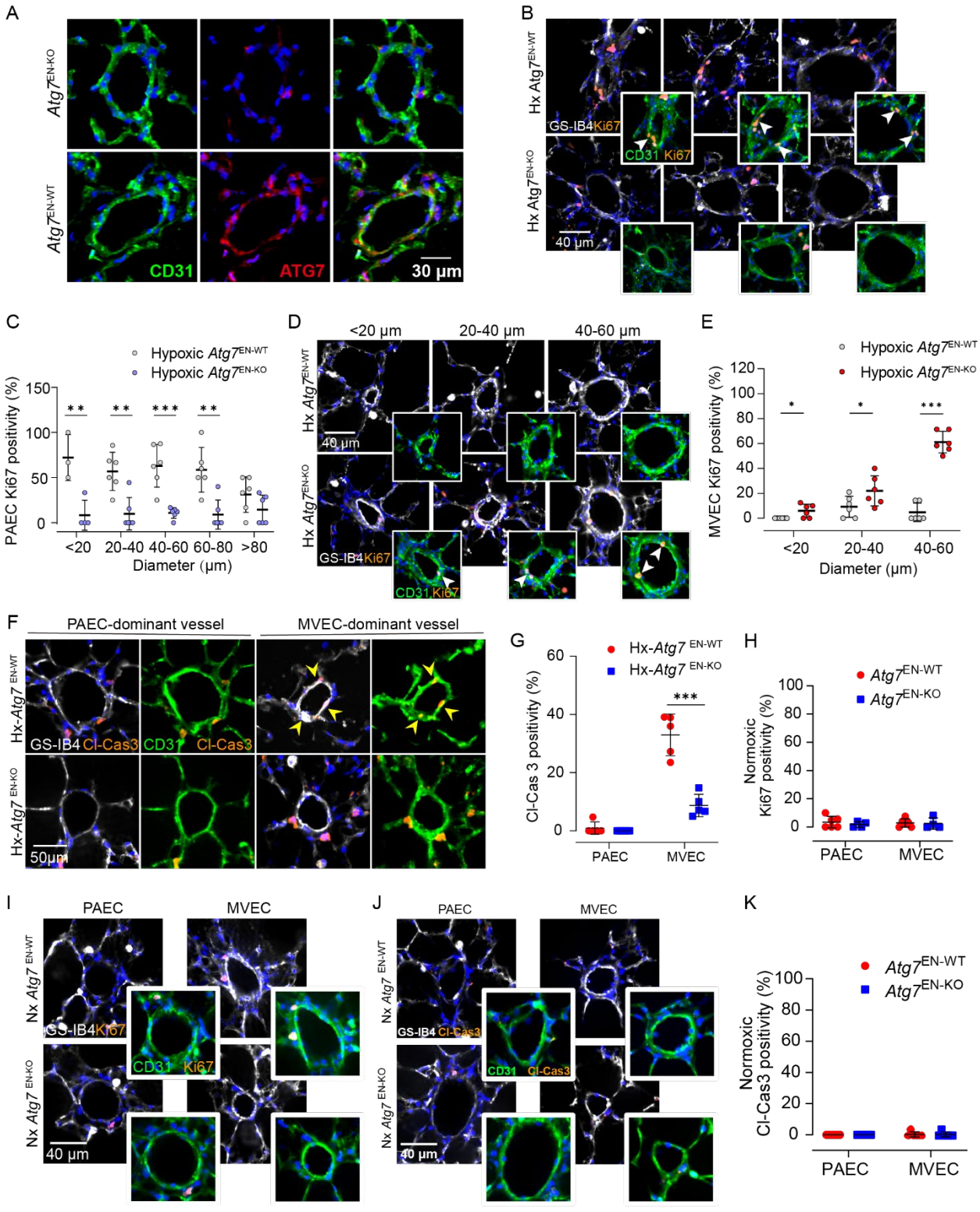

Figure 15. Differential responses of PAEC and MVEC to hypoxia are mediated by autophagy *in vivo*. **(A)** Representative images of ATG7 (red) staining in PCLS from normoxic endothelial *Atg7*-deficient (*Atg7*$^{EN\text{-}KO}$) and corresponding wild-type (*Atg7*$^{EN\text{-}WT}$) mice. ECs were identified by immunofluorescence staining for CD31 (green). Representative images (**B,D**) and quantitative analysis (**C,E**) of Ki67 (orange) staining in PAEC- (**B,C**) and MVEC- (**D,E**) dominant vessels in the transition zone in precision cut lung

slices (PCLS) from chronic (5 weeks) hypoxic (10% O_2) *Atg7*$^{EN-KO}$ and *Atg7*$^{EN-WT}$ mice. Representative images (**F**) and quantitative analysis (**G**) of Cl-Cas3 (orange) staining in PAEC- and MVEC-dominant vessels in PCLS from chronic (5 weeks) hypoxic (10% O_2) *Atg7*$^{EN-KO}$ and *Atg7*$^{EN-WT}$ mice. EC are identified by CD31 (green), MVEC by positivity for *Griffonia simplicifolia* IB4 (GS-IB4; white), and PAEC by GS-IB4 negativity, respectively. Proliferating GS-IB4$^-$CD31$^+$ PAEC (**B**) and apoptotic GS-IB4$^+$CD31$^+$ MVEC (**F**) in lungs of chronic hypoxic *Atg7*$^{EN-WT}$ mice, and proliferating GS-IB4$^+$CD31$^+$ MVEC (**D**) in lungs of chronic hypoxic *Atg7*$^{EN-KO}$ mice are highlighted by white arrowheads. Data are shown as percentage of vessels containing at least one Ki67 (**C,E**) or Cl-Cas3 (**G**) positive PAEC or MVEC, respectively. Representative images (**I**) and quantitative analysis (**H**) show very low levels of proliferating PAEC and MVEC in PCLS from normoxic *Atg7*$^{EN-WT}$ and *Atg7*$^{EN-KO}$ mice, as measured by Ki67 (orange) staining. Similarly, representative images (**J**) and quantitative analysis (**K**) of cleaved caspase-3 (Cl-Cas3, orange) staining show paucity of apoptotic PAEC and MVEC in PCLS from normoxic *Atg7*$^{EN-WT}$ and *Atg7*$^{EN-KO}$ mice. **A-E**: n=6 replicates each; **F-G**: n=5 replicates each; **H-K**: n≥4 replicates each; * P ≤0.05, ** P ≤0.01, *** P ≤0.001.

3.5 MVEC apoptosis promotes PAEC proliferation

In Section 3.4, we demonstrate that PAEC proliferation is stimulated by hypoxia-induced autophagy activation. Interestingly, the results from our Ki67 staining in the lungs of hypoxic mice indicate that the proliferation of PAEC was more prominent in the transition zone (20-60 µm in diameter), where both MVEC and PAEC coexist, as compared to the increased level of PAEC proliferation in vessels larger than 80 µm that are exclusively covered by PAEC (Fig. 16A,B). We hence speculated that in addition to their higher basal propensity to proliferate in response to hypoxia, PAEC proliferation may be further enhanced by cell death in neighboring MVEC. To substantiate this concept, we labeled hPAEC with CellTrace™ Oregon Green and evaluated their proliferative capacity using Ki67 staining under normoxic and hypoxic conditions, both in mono-culture and co-culture with CellTracker™ Blue-labeled hMVEC. As shown in Fig. 16C,D, hypoxia increased cell proliferation in mono-cultured hPAEC as compared to normoxic hPAEC, and this effect was further enhanced when hPAEC were co-cultured with hMVEC. Based on this finding, we hypothesized that autophagy-induced cell death of hMVEC could potentially promote hPAEC proliferation due to the loss of contact inhibition[70]. Contact inhibition is a regulatory process in which cells cease to divide when they come into contact with adjacent cells, preventing overgrowth. To test this notion, we silenced *ATG7* in hMVEC by siRNA before co-culturing them with hPAEC in normoxia or hypoxia. Subsequent Ki67 staining showed reduced hPAEC proliferation when PAEC were co-cultured with *ATG7*-knockdown hMVEC when compared to cells transfected with a scrambled siRNA (Fig. 16E,F).

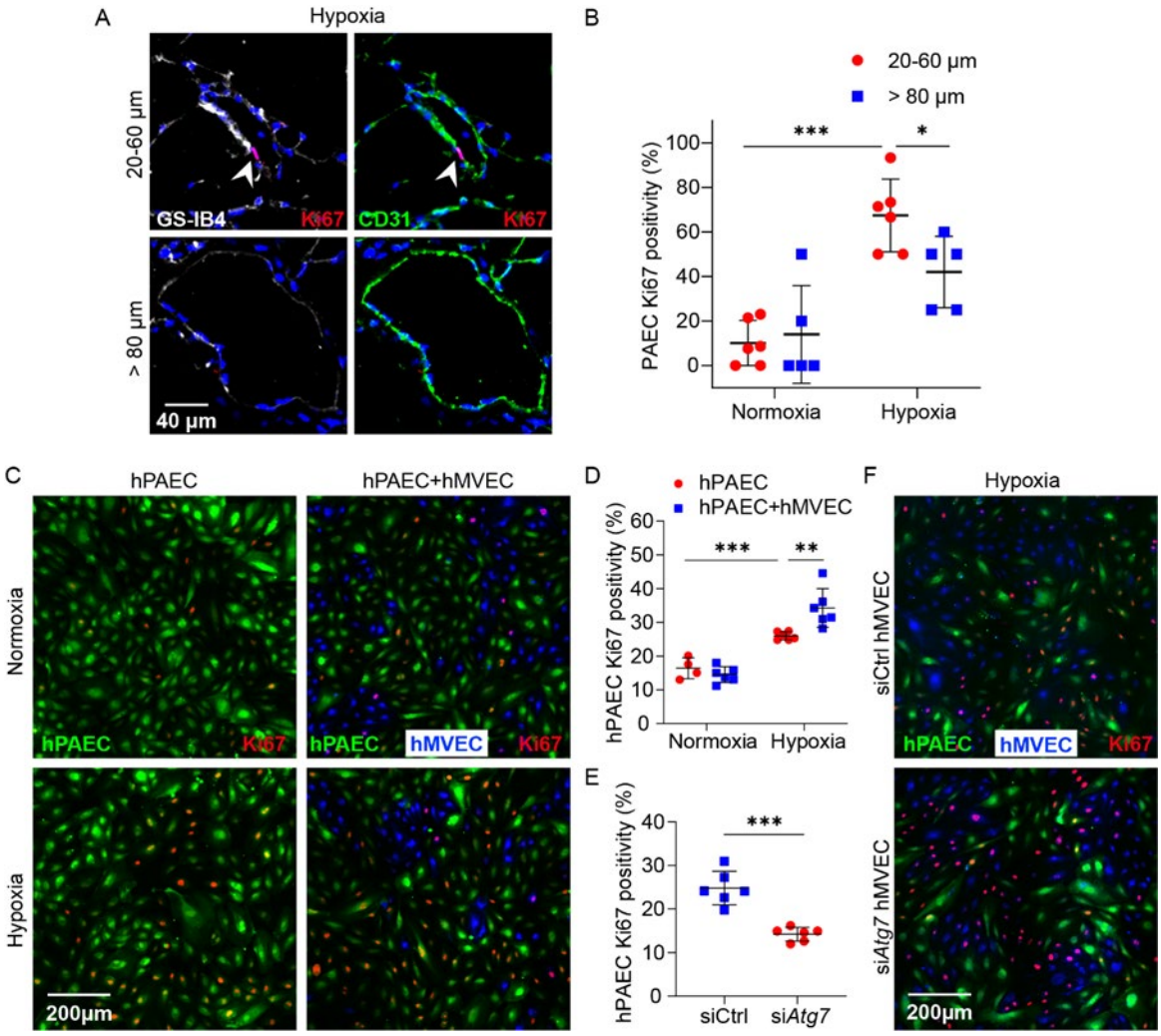

Figure 16. MVEC apoptosis promotes PAEC proliferation. Representative images (**A**) and quantitative analysis (**B**) of Ki67 (red) staining in two PAEC-dominant vessels, one in the transition zone (20-60µm) and the other > 80µm in diameter, in precision-cut lung slices (PCLS) from chronic (5 weeks) hypoxic mice. EC are identified by the pan-endothelial marker CD31 (green), MVEC by positivity for *Griffonia simplicifolia* IB4 (GS-IB4; white), and PAEC by GS-IB4 negativity, respectively. A proliferating GS-IB4$^-$CD31$^+$ PAEC neighboring GS-IB4$^+$CD31$^+$ MVEC is highlighted by a white arrowhead. Data are shown as percentage of vessels containing at least one Ki67$^+$ PAEC (**B**). Representative micrographs (**C**) and quantitative analysis (**D**) show the proliferation of CellTrace™ Oregon Green-labeled human PAEC (hPAEC) in mono-culture (C, left panels) or in co-culture with CellTracker™ Blue-labeled human MVEC (hMVEC) (C, right panels) in response to 24 h of hypoxia (1% O_2) as detected by Ki67 staining (red). (**D**) Quantitative data are given as a percentage of Ki67$^+$ hPAEC. Representative micrographs (**F**) and quantitative analysis (**E**) show proliferation of CellTrace™ Oregon Green-labeled hPAEC cocultured with CellTracker™ Blue-labeled hMVEC transfected with si*ATG7* (100 nMol/L) or non-targeting control siRNA (siCtrl, 100 nMol/L) in response to 24 h of hypoxia as detected by Ki67 staining (red). **A-F**: n=4-6 replicates each; * P ≤0.05, ** P ≤ 0.01, *** P ≤ 0.001.

3.6 Autophagy drives PAEC replacement of MVEC in hypoxia

So far, we have demonstrated that hypoxia-induced autophagy induces differential responses in PAEC and MVEC, and that PAEC replace MVEC in distal arterioles of the transition zone in chronic hypoxic mice. To establish a causal mechanistic link between both findings, we next tested whether autophagy would regulate the replacement of MVEC by PAEC. To test this concept, we first co-cultured differentially labeled rPAEC and rMVEC in a 1:1 ratio. After 24 h exposure to hypoxia, we observed a significant expansion of the area occupied by rPAEC, which was approximately 40% larger than the respective area in normoxic conditions. However, this effect was completely reversed by the autophagy inhibitor BafA1 (Fig. 17A,B). Likewise, BafA1 inhibited the hypoxia-induced acceleration in hPAEC migration (that was notably absent in hMVEC) in a classic wound healing assay (Fig. 17C,D).

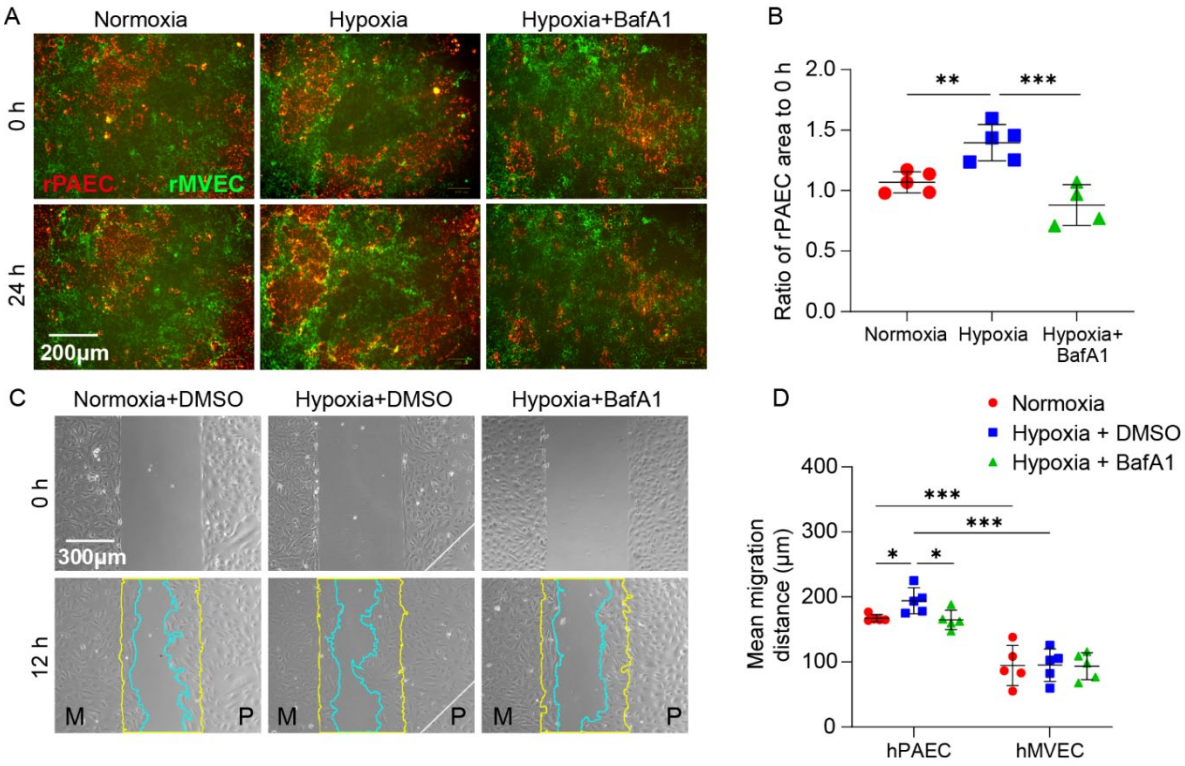

Figure 17. Autophagy drives PAEC replacement of MVEC in hypoxia *in vitro*. Representative images (**A**) and quantitative analysis (**B**) of PKH26 red-labeled rat PAEC (rPAEC) co-cultured with PKH67 green-labeled rat MVEC (rMVEC) in normoxia or in hypoxia (1% O_2 for 24 h) in the presence or absence of bafilomycin A1 (BafA1, 20 nMol/L). Hypoxia, yet not normoxia, causes progressive coverage of PAEC, as evidenced by an increase in total red (rPAEC-covered) area at 24 h relative to 0 h. BafA1 inhibited this effect. Representative images (**C**) and quantitative analysis (**D**) from a wound healing assay with hMVEC (M) and hPAEC (P) cultured on the left and right side of the wound, respectively. Yellow and cyan lines mark the margins of the wound gap captured at 0 (yellow) and 12 h (cyan) of normoxia or hypoxia in the

presence or absence of BafA1 (20nMol/L), respectively. Quantitative data give the average migration distance. A,B: n=4-5 replicates each, C,D: n=5 replicates each; * P ≤0.05, ** P ≤0.01, *** P ≤0.001.

To validate this finding *in vivo*, we stained endothelial cells with GS-IB4 and for vWF in PCLS from chronic *Atg7*$^{EN-KO}$ and *Atg7*$^{EN-WT}$ mice. As depicted in Fig. 18A,B, the absence of *Atg7* in EC inhibited the replacement of MVEC by PAEC in distal pulmonary arterioles, as evidenced by a lower percentage of PAEC-dominant vessels in the transition zone (20-60 µm in diameter) in lungs of chronic hypoxic *Atg7*$^{EN-KO}$ mice when compared to corresponding wild-type mice. Moreover, TEM showed a reduced coverage of WPb-positive PAEC in the transition zone in chronic *Atg7*$^{EN-KO}$ compared to *Atg7*$^{EN-WT}$ mice (Fig 18C,D). Collectively, these findings provide strong evidence supporting the hypothesis that hypoxia-induced replacement of MVEC by PAEC is driven by autophagy activation.

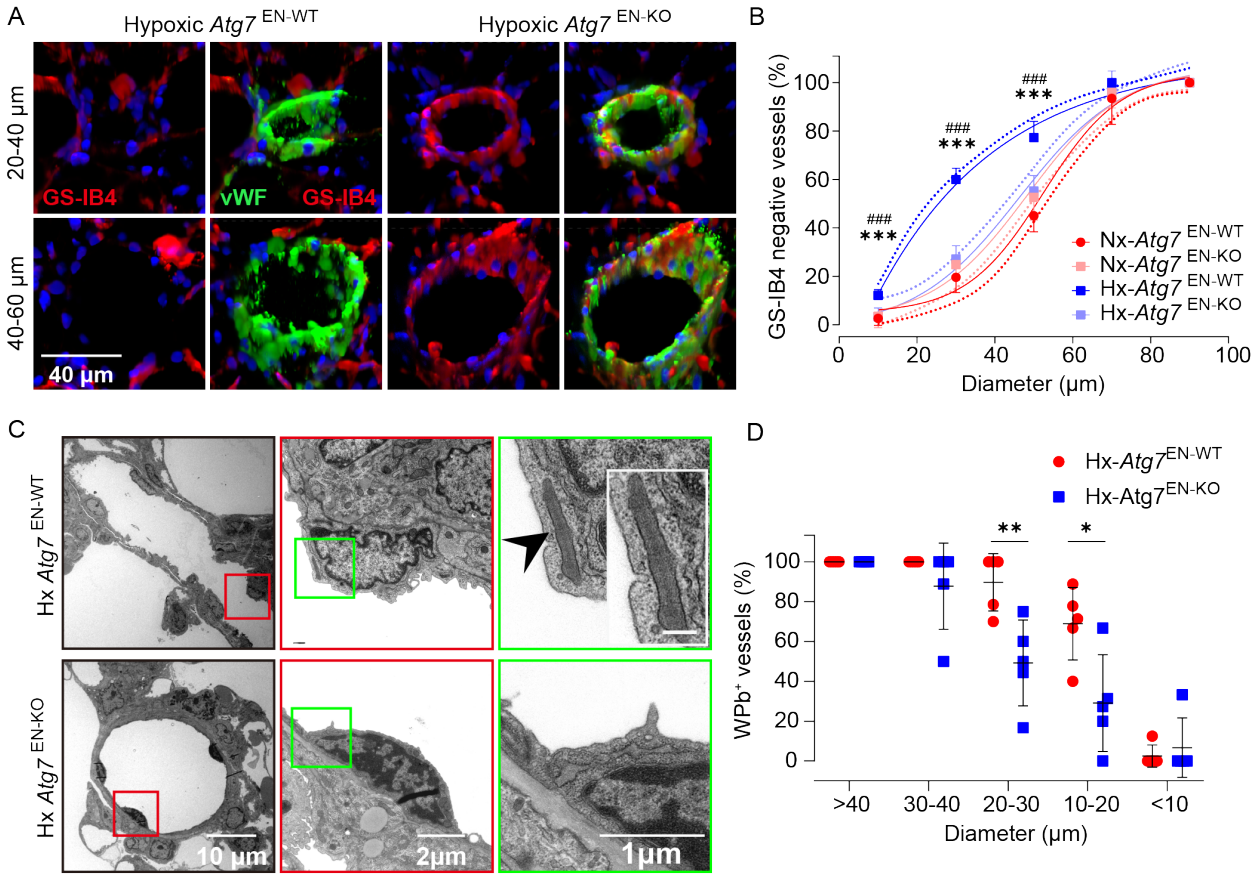

Figure 18. Autophagy drives PAEC replacement of MVEC in hypoxia *in vivo*. Representative micrographs (**A**) and quantitative analysis (**B**) demonstrate the abundance of MVEC and PAEC in precapillary arterioles of 20-60 µm diameter in precision cut lung slices (PCLS) from chronic (5 weeks) hypoxic (Hx, 10% O_2) endothelial cell-specific *Atg7*-deficient mice (*Atg7*$^{EN-KO}$) and corresponding wild-type mice (*Atg7*$^{EN-WT}$). EC are identified by the pan-endothelial marker von Willebrand factor (vWF; green), MVEC by positivity for *Griffonia simplicifolia* IB4 (GS-IB4; white), and PAEC by GS-IB4 negativity, respectively. Sigmoid curve fits

depict the correlation between vessel diameter and GS-IB4 negativity (i.e., PAEC-dominance). (**C)**: Representative transmission electron micrographs of pulmonary precapillary arterioles (diameters: 15-25 µm) from chronic hypoxic *Atg7*$^{EN-KO}$ and *Atg7*$^{EN-WT}$ mice at (from left to right) increasing levels of magnification show Weibel-Palade bodies (WPb), a PAEC-specific organelle (marked by arrowhead and shown enlarged as inserts (scalebar: 200 nm)). **(D)**: Corresponding quantitative analysis depicts the percentage of WPb^{+} (i.e., PAEC-containing) vessels, defined as vessels with at least one WPb detected in the endothelium, as a function of vessel diameter. **A,B**: n=6 replicates each, **C,D**: n=5 replicates each; **B**: *** P ≤ 0.001 vs. Nx-*Atg7*$^{EN-WT}$, ### P ≤ 0.001 vs. Hx-*Atg7*$^{EN-KO}$. **D**: * P ≤0.05, ** P ≤0.01.

3.7 EC- rather than SMC-specific autophagy promotes PH

To probe for the effects of these distinct autophagy-driven cellular responses in PAEC and MVEC on the progression of PH, we assessed right ventricular hemodynamics and vascular remodeling in chronic hypoxic *Atg7*$^{EN-WT}$ and *Atg7*$^{EN-KO}$ mice. After being exposed to hypoxia for 5 weeks, *Atg7*$^{EN-KO}$ mice exhibited a significant decrease in right ventricular systolic pressure (RVSP) and right ventricular hypertrophy, as measured by Fulton index (right ventricular weight/(septal + left ventricular weight)), compared to their corresponding wild-type counterparts (Fig 19A,B). Histological analysis revealed a noticeable decrease in vessel wall thickness in chronic hypoxic *Atg7*$^{EN-KO}$ mice when compared to hypoxic *Atg7*$^{EN-WT}$ mice (Fig. 19C-E). Furthermore, α-SMA staining revealed a decreased level of muscularization in distal arterioles in hypoxic *Atg7*$^{EN-KO}$ mice compared to *Atg7*$^{EN-WT}$ mice (Fig. 19F-G). These findings indicate that the autophagy-mediated replacement of MVEC by PAEC in distal pulmonary arterioles correlates with increased muscularization of these vessel segments, subsequently leading to the development of PH. To delve deeper into whether autophagy activation in PASMC is also associated with the PH progression, we performed the aforementioned experiments in chronic hypoxic *Atg7*$^{SMC-KO}$ and *Atg7*$^{SMC-WT}$ mice. There were no detectable differences in RVSP, right ventricular hypertrophy, and vessel wall thickness between chronic hypoxic *Atg7*$^{SMC-KO}$ mice and the WT counterparts (Fig 19A-C,E). These findings highlight the crucial role of autophagy in EC, but not in SMC in the development of pulmonary hypertension.

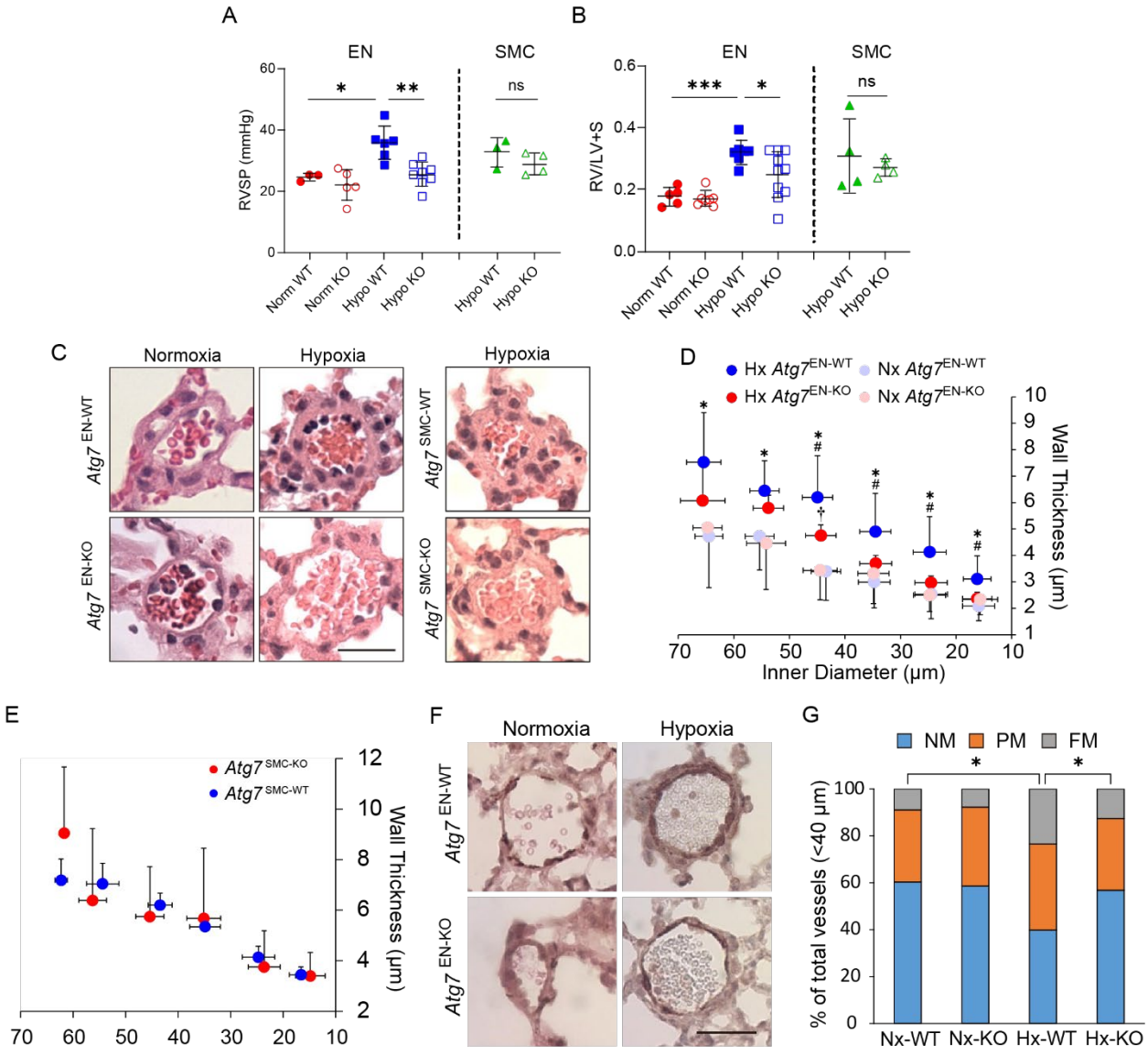

Figure 19. Role of autophagy in EC and SMC in chronic hypoxic PH. The development of chronic hypoxic PH was evaluated by measuring the right ventricular systolic pressure (RVSP) (**A**) and right ventricular hypertrophy using the Fulton Index (**B**) in mice with EC-specific Atg7 deficiency (*Atg7*$^{EN-KO}$) and SMC-specific *Atg7* deficiency (*Atg7*$^{SMC-KO}$) exposed to chronic hypoxia (Hx, 10% O_2) or normoxia (Nx), along with their corresponding wild-type mice. The Fulton Index was calculated as the right ventricular weight divided by the sum of the left ventricular weight and septum weight (RV/(LV+S)). Representative H&E images (**C**) and corresponding quantitative analysis (**D, E**) depict the vessel wall thickness in small pulmonary arterioles (≤40 µm diameter) of chronic hypoxic *Atg7*$^{EN-KO}$ and *Atg7*$^{SMC-KO}$ mice compared to their respective wild-type. Scale bar = 20 µm. Representative images of lung sections stained for smooth muscle actin (**F**) and quantitative analysis (**G**) show vascular muscularization of small pulmonary arterioles (≤40 µm diameter) in lungs of chronic hypoxic and normoxic *Atg7*$^{EN-WT}$ or *Atg7*$^{EN-KO}$ mice. Scale bar = 20 µm. FM, fully muscularized; PM, partially muscularized; NM, non-muscularized. **A**: n=3-8 replicates each; **B**: n=4-10 replicates each; **D, E**: n=220-380 vessels from n≥5 mice per group; **G**: n=187-421 vessels from n≥5

mice per group; **A,B,G**: * P ≤ 0.05, ** P ≤ 0.01, *** P ≤ 0.001. **D**: * P ≤ 0.05 vs normoxic *Atg7*$^{EN-WT}$, # P ≤ 0.05 vs. hypoxic *Atg7*$^{EN-KO}$, † P ≤ 0.05 vs. normoxic *Atg7*$^{EN-KO}$.

3.8 PAEC drive PASMC proliferation and migration in a PDGF-dependent manner

Based on the data accumulated so far, we reached two important conclusions: 1) Hypoxia triggers autophagy, which promotes the proliferation of PAEC and the apoptosis of MVEC, thus promoting the progressive replacement of MVEC by PAEC in distal small arterioles. 2) Activation of autophagy in EC drives the progression of PH, characterized by increased muscularization of small arterioles, elevated pulmonary arterial pressure, and right ventricular dysfunction. Viewed together, these findings raise the critical question of whether and how the autophagy-dependent replacement of MVEC by proliferating PAEC may contribute to the development and progression of PH. Previous studies have shown that EC can regulate the growth of SMC via paracrine signals, for instance TGF-β1[71,72] or IL-1β[73]. Therefore, we hypothesized that the presence of PAEC in small precapillary arterioles of chronic hypoxic lungs may provide a specific "macrovessel" context that drives SMC proliferation and migration into the distal arterioles, and as a result, promote small vessel muscularization. To probe this hypothesis, we collected CM from hPAEC or hMVEC cultured in hypoxia for 24 h and added the CM to hPASMC in a scratch assay. As shown in Fig. 20A,B, CM derived from hypoxic hPAEC accelerated wound recovery in hPASMC compared to CM from hypoxic MVEC. Furthermore, the CM from hypoxic hPAEC promoted hPASMC proliferation, as indicated by Ki67 staining, whereas the CM from hMVEC did not exhibit such an effect (Fig. 20C,D). These findings suggest that hypoxia stimulates PAEC to release a paracrine mediator that promotes PASMC migration and proliferation. scRNA-seq analysis performed in collaboration with Andrew H Baker from the Centre for Cardiovascular Science, University of Edinburgh, identified a significant upregulation of *Pdgfb* (a well-known regulator of PASMC proliferation and migration) in PAEC, yet not in capillary EC in hypoxic mice (data not shown), suggesting PDGF-BB as candidate paracrine mediator by which PAEC rather than MVEC may drive vessel muscularization in chronic hypoxia. Indeed, hypoxia led to a marked increase in the release of the high-affinity PDGF dimer PDGF-BB into the CM of hPAEC, while PDGF-BB was barely detectable in CM from hMVEC (Fig. 20E,F). To confirm the functional relevance of PDGF in this scenario, we treated PASMC with imatinib, a PDGF receptor inhibitor, in the presence of CM obtained from hypoxic hPAEC or hMVEC. Notably, imatinib

markedly inhibited PASMC migration and proliferation in response to CM from hypoxic hPAEC, while it had no effect on the response to CM from hypoxic hMVEC (Fig. 20A-D).

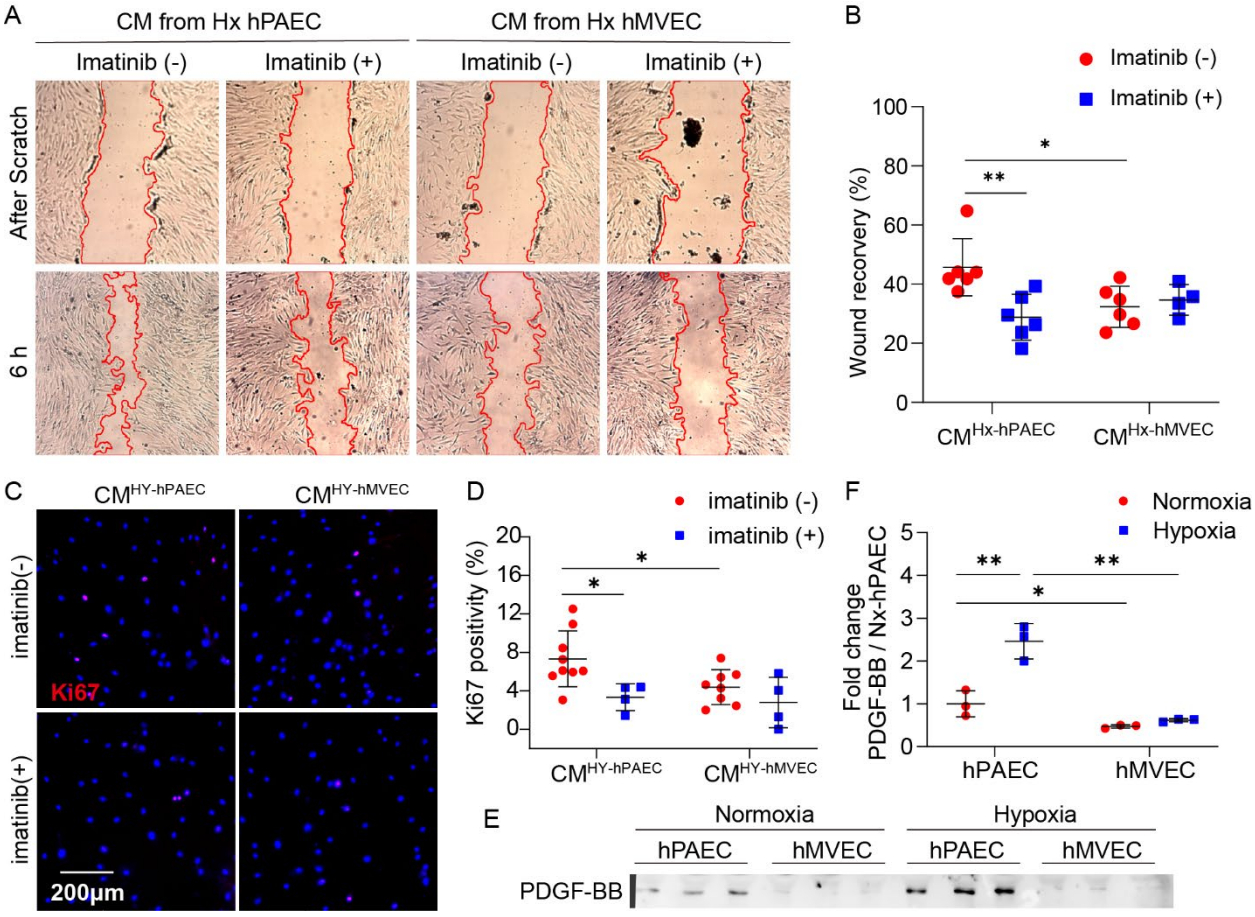

Figure 20. PAEC drive PASMC proliferation and migration in a PDGF-dependent manner. Representative images (**A**) and quantitative analysis (**B**) show results from a scratch assay of human pulmonary artery smooth muscle cells (hPASMC) cultured for 6h in conditioned media (CM) from hypoxic (1%, 24h) human PAEC ($CM^{Hx\text{-}hPAEC}$) and MVEC ($CM^{Hx\text{-}hMVEC}$), in the presence or absence of the PDGF receptor inhibitor imatinib (100 nMol/L). Data are given as area recovered at 6h as a percentage of the total scratch gap. Representative micrographs (**C**) and quantitative analysis (**D**) show proliferation of hPASMC cultured for 24h in $CM^{Hx\text{-}hPAEC}$ or $CM^{Hx\text{-}hMVEC}$ in the presence or absence of imatinib (100 nMol/L), as detected by Ki67 staining (red; nuclei counterstained with DAPI in blue). Representative Western blots (**E**) and quantitative densitometric analysis (**F**) show PDGF-BB expression in CM from hPAEC and hMVEC cultured for 24h in hypoxia and normoxia, respectively. PDGF-BB expression is normalized to data from normoxic hPAEC. **A-B**: n=4-6 replicates each; **C,D**: n=4-9 replicates each; **E,F**: n=3 replicates each. * $P \leq 0.05$. ** $P \leq 0.01$.

4. Discussion

In this study, we propose a novel mechanistic concept for small vessel muscularization in PH. We suggest that this process is primarily driven by the differential response of lung microvascular and macrovascular endothelial cells to autophagic stress, as illustrated in Figure 2. Specifically, we demonstrate that the activation of autophagy in response to hypoxia leads to the proliferation of PAEC, while simultaneously inducing apoptosis in MVEC. As a result, proliferating PAEC replace apoptotic MVEC, particularly in the transition zone, which refers to precapillary vessel segments ranging between 20 and 60 µm in diameter in mice that contain a mix of macro- and microvascular endothelial cells. PAEC, in turn, stimulate PASMC proliferation and migration towards distal arterioles – in part via the release of PDGF-BB – leading to small vessel muscularization and eventually promoting the development of PH. As such, the present study provides a paradigm shift in our understanding of the pathobiology of PH, as it delineates the critical role of endothelial cell heterogeneity in lung vascular health and disease.

4.1 Methodological considerations

To test the hypothesis, we developed and validated new methods, which are elaborated upon in the subsequent paragraphs.

The first methodological challenge involved distinguishing between different EC phenotypes, particularly PAEC and MVEC, which have impeded investigations into EC heterogeneity in acute and chronic lung disease in general, and in PH specifically. Importantly, canonical markers of macro- vs. microvascular endothelial cells established in the systemic circulation - such as connexin 40, which is selectively expressed in systemic arterial EC - cannot be readily applied to the pulmonary circulation, as, for example, connexin 40 is also expressed in pulmonary MVEC[74]. Furthermore, certain well-established arterial EC markers, which are normally absent in MVEC, can, however, be detected in MVEC under pathological conditions. For instance, Cytoplasmic tyrosine-protein kinase BMX (BMX)[75], typically expressed in arterial EC, can be upregulated in capillary EC in response to ischemia[76]. Similarly, SRY-Box Transcription Factor 17 (SOX17), known for its specific expression in arterial EC rather than MVEC[77,78], is also expressed in pulmonary MVEC in acute lung inflammation induced by lipopolysaccharide[79]. As such, EC subset-specific markers previously established for healthy systemic circulation cannot be unequivocally

applied to diseased pulmonary circulation, hampering their applicability for testing the role of EC heterogeneity in the present study.

In the current study, we utilized a lectin, i.e., GS-IB4, as a marker of MVEC, and a characteristic organelle, namely WPb, as a marker of PAEC. GS-IB4 has a high affinity for α-galactose, which is uniquely present on the MVEC surface but absent in PAEC. These two markers were optimized and validated for healthy pulmonary circulation in a series of prior studies by our collaborator Troy Stevens[29,56]. To validate marker specificity also under conditions of hypoxia, we performed a series of experiments in which we showed that rMVEC can again be labeled with GS-IB4 and do not express WPb in hypoxia. This finding confirms the usefulness of GS-IB4 as specific MVEC marker and also supports the absence of a phenotypic transition from MVEC to PAEC in hypoxia.

The second methodological consideration involves dynamically observing the process by which MVEC is replaced by PAEC in the lung. In this study, we propose the novel concept that MVEC are replaced by PAEC in distal arterioles, as evidenced by decreased GS-IB4 positivity and increased WPb positivity in the transition zone in chronic hypoxic mice. However, both techniques only provide the static snapshot of micrographs at a single time point, specifically at the endpoint of 5 weeks of hypoxia in mice in this study. The proof-of-principle would be even more compelling if PAEC replacement could be dynamically and directly visualized by microscopy, allowing for real-time monitoring of the process.

Intravital imaging provides unique insights into cellular functions and spatial interactions in intact tissue in real time. Previous studies have made significant advancements in pulmonary window techniques for the respective visualization of lung microvessels and tissue. In 1994, Kuebler and colleagues developed an intravital microscopic method by implanting a thoracic window on the right chest, enabling the visualization of pulmonary subpleural microvessels[80]. Tabuchi and coworkers further improved this technique allowing for the visualization of lungs in a closed thoracic cavity under physiological conditions[81]. In brief, they surgically removed the chest muscles and ribs without touching the lung tissue. Afterward, the window was covered with α-cyanoacrylate glue, and the air within the thoracic cavity was removed via an intrapleural catheter. Looney and coworkers developed an alternative approach by introducing a suction device, which enhanced the stability of the lung window during visualization[82]. This innovation allowed for stable imaging without interference from the respiratory cycle. However, this mechanical stabiliza-

tion of the lung surface may impact ventilation and circulation, potentially leading to inflammation and edema. Recently, Entenberg and colleagues introduced a novel window model called WHRIL (Window for High-Resolution Imaging of the Lung), enabling long-term observation of lungs in mice[83]. This window is inserted into the rib incision in the chest wall without affecting breathing. Fiducial marks on the windows facilitate the re-localization of specific lung areas for repeated imaging.

In our study, we applied a previously reported method using PCLS for live imaging to observe the dynamics of PAEC and MVEC in distal arterioles under hypoxia[84]. Images were captured at 5-minute intervals, allowing for the dynamic observation of cell kinetics. Over the time course of 24 - 48 hrs of hypoxia, several GS-IB4$^+$ MVEC were seen to detach from the wall of small arterioles primarily covered by GS-IB4$^+$ MVEC. This suggests that in hypoxia, MVEC are lost from the wall of precapillary arterioles, likely being replaced by GS-IB4$^-$ CD31$^+$ PAEC.

Compared to intravital microscopy, our approach using PCLS offers several clear advantages that are critical for the present study. First, live imaging of PCLS allows for frequent capture of images, with intervals typically in minutes, enabling precise tracking of individual cell dynamics for up to 3-4 days. In contrast, intravital microscopy requires animal anesthesia and immobilization, hindering continuous and long-term dynamic imaging. Second, *in vivo* labeling of EC presents challenges, particularly when specific transgenic models are not available. While GS-IB4 can be administered intravenously, its distribution in the lung is dependent on blood flow, resulting in uneven labeling. However, this issue is not encountered when staining PCLS. Our findings indicate that PAEC replacement occurs within 1-2 days after hypoxia, emphasizing the importance of short imaging intervals to avoid missing this phenomenon.

4.2 EC heterogeneity in the lung

Over the past decade, it has been recognized that not all EC are the same, and that this heterogeneity has fundamental functional implications. The recent advancements of scRNA-seq and the discovery of new EC subtypes have further advanced this understanding. Our findings highlight the importance of EC heterogeneity in the development of PH, in that PAEC become proliferative while MVEC undergo apoptosis in response to PH stimuli, resulting in the progressive replacement of MVEC by PAEC. This new concept diverges from previously proposed scenarios, which suggested that an initial wave of EC

apoptosis is followed by the subsequent emergence of apoptosis-resistant and hyperproliferative EC that propagate lung vascular remodeling. This prior hypothesis, however, failed to address important unresolved questions. Firstly, it remained unclear why some EC undergo apoptosis while others survive and then become hyperproliferative under the same pathological conditions. Secondly, if EC are viewed as a homogeneous population, it remained unclear why EC and SMC proliferation and muscularization predominantly occur in distal small arterioles rather than uniformly throughout the pulmonary circulation. In contrast, our new concept provides plausible explanations for these questions based on the recognition of the important role of EC heterogeneity, in that 1) different EC subtypes respond differentially to PH stimuli, and 2) this differential response becomes particularly relevant in the transition zone of distal arterioles as the predominant location of muscularization.

EC exhibit significant heterogeneity across different organs and vascular segments, including arterial, capillary, and venular regions. This heterogeneity is evident in their distinct morphologies, functions, and transcriptomes, as revealed by recent advancements in single-cell RNA sequencing (scRNA-seq)[85,86]. According to a recently published scRNA-seq study, EC in the lung were categorized into 6 EC subsets, namely lymphatic, arterial, general capillary (gCap) EC, aerocyte, pulmonary-venous EC, and systemic-venous EC[68]. Pulmonary-venous ECs are predominantly found in the lung parenchyma, while systemic-venous ECs are primarily localized in the airways and the visceral pleura. gCap and aerocyte represent newly distinguished capillary EC subtypes that are differentiated based on their morphology, localization, and function[27]. Specifically, aerocytes are a lung-specific cell type that plays a crucial role in gas exchange and facilitates the trafficking of leukocytes, while gCap have a distinct function in regulating vasomotor tone and endothelial repair.

In this study, we primarily focused on arterial EC and MVEC in the lung, which are essentially different EC phenotypes in terms of their origin, function, and surface marker expression[25]. While PAEC are derived from the pulmonary truncus through angiogenesis, MVEC originate from blood islands by vasculogenesis. PAEC and MVEC also differ in terms of their barrier function (with MVEC being more restrictive to protein and water flux when compared to PAEC), NO production (MVEC < PAEC), responses to mechanical stress, and their Ca^{2+} response to different stimuli [30-32,85]. Based on the recognition of these important functional differences, it becomes evident that lung EC probably cannot be regarded as a homogeneous cell population when we try to understand the role of EC

in the development and progression of lung diseases. This notion is supported by the findings by Niethamer and colleagues, who reported an increased proportion of *Car4*-high EC located in regenerating areas of the alveolus after influenza infection, suggesting that these cells were responsible for repairing damaged alveoli. The *Car4* gene encodes the enzyme Carbonic Anhydrase 4, which exhibits high expression levels in mouse MVEC. On the other hand, a population of proliferative ECs originates from multiple EC subsets, including *Vcam1*$^{+}$ macrovascular ECs, but not *Car4*-high ECs. This suggests that EC participating in proliferation and tissue repair are derived from distinct subtypes. These findings highlight the importance of EC heterogeneity in lung disease.

4.3 Autophagy in PH

Over the past decade, various studies have reported the activation of autophagy in the lungs of patients with PH and in various mouse models of PH[43,87-90]. Specifically, studies have shown that the expression of LC3B and its activation, assessed by the ratio of LC3B-II to LC3B-I, is elevated in the lungs of patients with IPAH. Immunostaining additionally revealed increased LC3 expression in the cells that form plexiform lesions, including EC and SMC[43]. Increased levels of autophagy were also detected in the lungs of chronic hypoxic mice[43,44] and in a rat model of monocrotaline-induced PH[91]. However, it is still unclear whether autophagy activation plays a detrimental or protective role in the development of PH. Some studies, however, indicate that autophagy plays a detrimental role in PH. Specifically, chloroquine, an inhibitor of autophagy, has been shown to attenuate the development of PH, right ventricular hypertrophy, and pulmonary vascular remodeling in monocrotaline-induced PH rats[91]. Consistently, overexpression of mTOR in chronic hypoxic mice inhibited autophagy, and this effect was associated with reduced right ventricular dysfunction and pulmonary artery remodeling[46]. In contrast, however, LC3B knockout mice had a worsened right ventricular dysfunction and vascular remodeling when compared to LC3B wild-type mice when exposed to chronic hypoxia, indicating autophagy as a protective mechanism that counteracts the development of PH[43]. We considered that these seemingly contradictory results may be attributed to differential roles of autophagy in different cell types involved in the pathobiology of PH, as neither pharmacological inhibition of autophagy nor global knockout of autophagy-related genes can specifically target a particular cell type. To overcome this limitation, we focused in the present study specifically on the role of autophagy in endothelial cells. By doing so, we

were able to show that *Atg7* knockout in EC alleviated hypoxia-induced PH, pulmonary arteriole muscularization, and right ventricular hypotrophy in a chronic hypoxia mouse model, while *Atg7* deficiency in SMC had no such beneficial effect.

It is important to note that autophagy is primarily a conserved physiological pathway that serves as a mechanism to prevent cell death under stress. Hypoxia is not only a stimulus for PH but also a common inducer of autophagy[92], suggesting that autophagy activation in chronic hypoxic lungs is likely to be not limited to EC but also prominent in SMC as well as other cell types where autophagy activation may be an important adaptive mechanism counteracting the development or progression of PH. As such, caution is warranted, in that the present identification of a detrimental role of EC autophagy in PH does not necessarily imply that global autophagy-targeted therapies would necessarily be beneficial in the treatment of clinical PH.

Notably, in our recent study, we illustrated that hypoxia-induced autophagy activation in EC results in PAEC proliferation, while MVEC undergoes apoptosis. The underlying reasons for these differential autophagic responses in the two EC subsets remain elusive. Although autophagy traditionally acts as a pro-survival mechanism, emerging evidence has highlighted its intricate relationship with cell death pathways[93-95]. Some autophagy-related proteins (Atgs) have been recognized as modulators of apoptosis. Atg5 is essential for autophagosome formation. However, when cleaved by calpain, its truncated form facilitates cell apoptosis[96]. Atg12 acts as a promoter of mitochondrial apoptosis by interacting with and neutralizing pro-survival members of the B cell lymphoma (Bcl)-2 family, such as Bcl-2 and Mcl-1[97]. P62 (or sequestosome 1, SQSTM1) is a cargo receptor facilitating the transport of ubiquitinated proteins and organelles to autophagosomes for degradation. Intriguingly, p62 is instrumental in activating caspase-8, a caspase family member integral to programmed cell death. Increased autophagy accelerates the degradation of p62, which in turn diminishes caspase-8 activation, ultimately inhibiting apoptosis[98]. Moreover, inefficient protein recycling via autophagy can deprive cells of essential resources, compromising survival. Tumor protein 53-induced nuclear protein 1 (TP53INP1) functions as a tumor suppressor and exhibits reduced expression across various organ-related cancers. Elevated levels of TP53INP1 can stimulate autophagy and competitively replace p62 within autophagosomes, resulting in insufficient protein recycling through autophagy, ultimately leading to cell death[99]. All of these mediators in autophagy may potentially be associated with the differential responses to autophagy in PAEC and MVEC.

However, we have not delved deeply into the causes of this heterogeneity. Future research is required to explore the origins of these differential alterations induced by autophagy in both EC subsets.

4.4 Limitations

While our findings shed light on the intricate role of EC autophagy in the development of PH, it is important to recognize the following limitations.

Firstly, we utilized GS-IB4 as a MVEC marker in mice. Unfortunately, GS-IB4 staining was effective only for murine MVEC and unfixed tissue samples, preventing its applicability in fixed human lung tissue samples. A recent human lung atlas study identified a series of marker genes uniquely expressed in PAEC, such as *BMX*, or in MVEC, notably *CA4* (Carbonic Anhydrase 4), in healthy donors.[100] Future studies should assess the specificity and consistent expression of these identified markers in human IPAH lung via immunofluorescence. This would pave the way for exploring EC subtype distribution in human lung samples, enhancing our understanding of EC heterogeneity in pulmonary hypertension.

Secondly, we performed live imaging on PCLS to observe the replacement of MVEC by PAEC. However, it is important to acknowledge that our method is not suitable for observing the effects of hypoxia over several weeks, and the *in vitro* cultivation of PCLS may not fully replicate the *in vivo* environment, potentially reducing the reliability of the results obtained. Therefore, further investigations into this pathological process in PH should consider the use of intravital microscopy as a complimentary approach to the imaging of PCLS.

Lastly, we did not differentiate between the two types of MVEC in this study, namely gCap and aerocyte. Therefore, we were unable to determine whether the capillary ECs in the transition zone were gCap or aerocyte. This aspect requires further validation and investigation in future studies.

5. Conclusions

In the present study, we have demonstrated the critical role of EC heterogeneity in the pathobiology of PH. Specifically, hypoxia-induced autophagy activation drives proliferation in PAEC, but apoptosis in MVEC. This divergent response to autophagy results in the replacement of MVEC by proliferating PAEC in distal arterioles, subsequently promoting SMC proliferation and migration, and ultimately driving distal vessel muscularization and the progression of PH (Fig. 2). With the advent of novel technologies able to dissect signaling pathways and cell dynamics at the single cell level, the heterogeneous responses of distinct cell populations are rapidly developing into a vibrant research field in organ homeostasis and disease, including PH. Recognition of this heterogeneity may not only advance pathophysiological concepts and insights, but also pave the way for novel cell subtype-specific therapies, ultimately allowing for exquisitely tailored and personalized medicine.

Reference list

1. Humbert M, Kovacs G, Hoeper MM, Badagliacca R, Berger RMF, Brida M, Carlsen J, Coats AJS, Escribano-Subias P, Ferrari P, Ferreira DS, Ghofrani HA, Giannakoulas G, Kiely DG, Mayer E, Meszaros G, Nagavci B, Olsson KM, Pepke-Zaba J, Quint JK, Rådegran G, Simonneau G, Sitbon O, Tonia T, Toshner M, Vachiery JL, Vonk Noordegraaf A, Delcroix M, Rosenkranz S, Schwerzmann M, Dinh-Xuan AT, Bush A, Abdelhamid M, Aboyans V, Arbustini E, Asteggiano R, Barberà JA, Beghetti M, Čelutkienė J, Cikes M, Condliffe R, De Man F, Falk V, Fauchier L, Gaine S, Galié N, Gin-Sing W, Granton J, Grünig E, Hassoun PM, Hellemons M, Jaarsma T, Kjellström B, Klok FA, Konradi A, Koskinas KC, Kotecha D, Lang I, Lewis BS, Linhart A, Lip GYH, Løchen ML, Mathioudakis AG, Mindham R, Moledina S, Naeije R, Nielsen JC, Olschewski H, Opitz I, Petersen SE, Prescott E, Rakisheva A, Reis A, Ristić AD, Roche N, Rodrigues R, Selton-Suty C, Souza R, Swift AJ, Touyz RM, Ulrich S, Wilkins MR, Wort SJ, Krim M, Hayrapetyan H, Lang I, Musayev O, Lazareva I, Sokolović Š, Velchev V, Cikes M, Michaloliakos I, Jansa P, Mellemkjær S, Hassan A, Anton L, Pentikäinen M, Meneveau N, Tsverava M, Lankeit M, Manginas A, Hizoh I, Maher V, Hirsch R, Galié N, Mukarov MA, Ibrahimi P, Talant S, Rudzitis A, Kiwan G, Gumbienė L, Codreanu A, Micallef J, Vataman E, Bulatovic N, Chraibi S, Post MC, Kostovska ES, Andreassen AK, Kurzyna M, Plácido R, Coman IM, Vasiltseva O, Zavatta M, Ristić AD, Šimkova I, Poglajen G, Salvador ML, Söderberg S, Ulrich S, Marjeh MYB, Ouarda F, Mutlu B, Sirenko Y, Coghlan JG, Abdullaev T. 2022 ESC/ERS Guidelines for the diagnosis and treatment of pulmonary hypertension. *European Heart Journal*. 2022. doi: 10.1093/eurheartj/ehac237
2. Gall H, Felix JF, Schneck FK, Milger K, Sommer N, Voswinckel R, Franco OH, Hofman A, Schermuly RT, Weissmann N, Grimminger F, Seeger W, Ghofrani HA. The Giessen Pulmonary Hypertension Registry: Survival in pulmonary hypertension subgroups. *The Journal of Heart and Lung Transplantation*. 2017;36:957-967. doi: 10.1016/j.healun.2017.02.016
3. Tuder RM. Pulmonary vascular remodeling in pulmonary hypertension. *Cell and Tissue Research*. 2017;367:643-649. doi: 10.1007/s00441-016-2539-y
4. Townsley MI. Structure and composition of pulmonary arteries, capillaries, and veins. *Compr Physiol*. 2012;2:675-709. doi: 10.1002/cphy.c100081
5. Jones R, Jacobson M, Steudel W. α -Smooth-Muscle Actin and Microvascular Precursor Smooth-Muscle Cells in Pulmonary Hypertension. *American Journal of Respiratory Cell and Molecular Biology*. 1999;20:582-594. doi: 10.1165/ajrcmb.20.4.3357
6. Sobin SS, Tremer HM, Hardy JD, Chiodi HP. Changes in arteriole in acute and chronic hypoxic pulmonary hypertension and recovery in rat. *J Appl Physiol Respir Environ Exerc Physiol*. 1983;55:1445-1455. doi: 10.1152/jappl.1983.55.5.1445
7. Kurakula K, Smolders VFED, Tura-Ceide O, Jukema JW, Quax PHA, Goumans M-J. Endothelial Dysfunction in Pulmonary Hypertension: Cause or Consequence? *Biomedicines*. 2021;9:57. doi: 10.3390/biomedicines9010057
8. Kuebler WM, Nicolls MR, Olschewski A, Abe K, Rabinovitch M, Stewart D, Chan SY, Morrell NW, Archer SL, Spiekerkoetter E. A pro-con debate: current controversies in PAH pathogenesis at the American Thoracic Society International Conference in 2017. *American Journal of Physiology-Lung Cellular and Molecular Physiology*. 2018;315:L502-L516. doi: 10.1152/ajplung.00150.2018

9. Jurasz P, Courtman D, Babaie S, Stewart DJ. Role of apoptosis in pulmonary hypertension: from experimental models to clinical trials. *Pharmacol Ther*. 2010;126:1-8. doi: 10.1016/j.pharmthera.2009.12.006
10. Sakao S, Taraseviciene‐Stewart L, Lee JD, Wood K, Cool CD, Voelkel NF. Initial apoptosis is followed by increased proliferation of apoptosis‐resistant endothelial cells. *The FASEB Journal*. 2005;19:1178-1180. doi: 10.1096/fj.04-3261fje
11. Taraseviciene‐Stewart L, Kasahara Y, Alger L, Hirth P, Mahon GM, Waltenberger J, Voelkel NF, Tuder RM. Inhibition of the VEGF receptor 2 combined with chronic hypoxia causes cell death‐dependent pulmonary endothelial cell proliferation and severe pulmonary hypertension. *The FASEB Journal*. 2001;15:427-438. doi: 10.1096/fj.00-0343com
12. Ciuclan L, Bonneau O, Hussey M, Duggan N, Holmes AM, Good R, Stringer R, Jones P, Morrell NW, Jarai G, Walker C, Westwick J, Thomas M. A Novel Murine Model of Severe Pulmonary Arterial Hypertension. *American journal of respiratory and critical care medicine*. 2011;184:1171-1182. doi: 10.1164/rccm.201103-0412oc
13. Goldthorpe H, Jiang J-Y, Taha M, Deng Y, Sinclair T, Ge CX, Jurasz P, Turksen K, Mei SHJ, Stewart DJ. Occlusive Lung Arterial Lesions in Endothelial-Targeted, Fas-Induced Apoptosis Transgenic Mice. *American Journal of Respiratory Cell and Molecular Biology*. 2015;53:712-718. doi: 10.1165/rcmb.2014-0311oc
14. Lee SD, Shroyer KR, Markham NE, Cool CD, Voelkel NF, Tuder RM. Monoclonal endothelial cell proliferation is present in primary but not secondary pulmonary hypertension. *Journal of Clinical Investigation*. 1998;101:927-934. doi: 10.1172/jci1910
15. Jonigk D, Golpon H, Bockmeyer CL, Maegel L, Hoeper MM, Gottlieb J, Nickel N, Hussein K, Maus U, Lehmann U, Janciauskiene S, Welte T, Haverich A, Rische J, Kreipe H, Laenger F. Plexiform lesions in pulmonary arterial hypertension composition, architecture, and microenvironment. *Am J Pathol*. 2011;179:167-179. doi: 10.1016/j.ajpath.2011.03.040
16. Masri FA, Xu W, Comhair SA, Asosingh K, Koo M, Vasanji A, Drazba J, Anand-Apte B, Erzurum SC. Hyperproliferative apoptosis-resistant endothelial cells in idiopathic pulmonary arterial hypertension. *Am J Physiol Lung Cell Mol Physiol*. 2007;293:L548-554. doi: 10.1152/ajplung.00428.2006
17. Levy M, Maurey C, Celermajer DS, Vouhe PR, Danel C, Bonnet D, Israel-Biet D. Impaired apoptosis of pulmonary endothelial cells is associated with intimal proliferation and irreversibility of pulmonary hypertension in congenital heart disease. *J Am Coll Cardiol*. 2007;49:803-810. doi: 10.1016/j.jacc.2006.09.049
18. Dabral S, Tian X, Kojonazarov B, Savai R, Ghofrani HA, Weissmann N, Florio M, Sun J, Jonigk D, Maegel L, Grimminger F, Seeger W, Savai Pullamsetti S, Schermuly RT. Notch1 signalling regulates endothelial proliferation and apoptosis in pulmonary arterial hypertension. *Eur Respir J*. 2016;48:1137-1149. doi: 10.1183/13993003.00773-2015
19. Sakao S, Tatsumi K, Voelkel NF. Endothelial cells and pulmonary arterial hypertension: apoptosis, proliferation, interaction and transdifferentiation. *Respiratory Research*. 2009;10:95. doi: 10.1186/1465-9921-10-95
20. Rodor J, Chen S-H, Scanlon JP, Monteiro JP, Caudrillier A, Sweta S, Stewart KR, Shmakova A, Dobie R, Henderson BEP, Stewart K, Hadoke PWF, Southwood M, Moore SD, Upton PD, Morrell NW, Li Z, Chan SY, Handen A, Lafyatis R, De Rooij LPMH, Henderson NC, Carmeliet P, Spiroski A-M, Brittan M, Baker AH. Single-

cell RNA-seq profiling of mouse endothelial cells in response to pulmonary arterial hypertension. *Cardiovascular Research*. 2021. doi: 10.1093/cvr/cvab296

21. Hong J, Arneson D, Umar S, Ruffenach G, Cunningham CM, Ahn IS, Diamante G, Bhetraratana M, Park JF, Said E, Huynh C, Le T, Medzikovic L, Humbert M, Soubrier F, Montani D, Girerd B, Tregouet DA, Channick R, Saggar R, Eghbali M, Yang X. Single-Cell Study of Two Rat Models of Pulmonary Arterial Hypertension Reveals Connections to Human Pathobiology and Drug Repositioning. *American journal of respiratory and critical care medicine*. 2021;203:1006-1022. doi: 10.1164/rccm.202006-2169OC
22. Saygin D, Tabib T, Bittar HET, Valenzi E, Sembrat J, Chan SY, Rojas M, Lafyatis R. Transcriptional profiling of lung cell populations in idiopathic pulmonary arterial hypertension. *Pulm Circ*. 2020;10. doi: 10.1177/2045894020908782
23. Potente M, Mäkinen T. Vascular heterogeneity and specialization in development and disease. *Nature Reviews Molecular Cell Biology*. 2017;18:477-494. doi: 10.1038/nrm.2017.36
24. Aird WC. Endothelial Cell Heterogeneity. *Cold Spring Harbor Perspectives in Medicine*. 2012;2:a006429-a006429. doi: 10.1101/cshperspect.a006429
25. Stevens T. Functional and molecular heterogeneity of pulmonary endothelial cells. *Proc Am Thorac Soc*. 2011;8:453-457. doi: 10.1513/pats.201101-004MW
26. Hennigs JK, Matuszcak C, Trepel M, Körbelin J. Vascular Endothelial Cells: Heterogeneity and Targeting Approaches. *Cells*. 2021;10:2712. doi: 10.3390/cells10102712
27. Gillich A, Zhang F, Farmer CG, Travaglini KJ, Tan SY, Gu M, Zhou B, Feinstein JA, Krasnow MA, Metzger RJ. Capillary cell-type specialization in the alveolus. *Nature*. 2020;586:785-789. doi: 10.1038/s41586-020-2822-7
28. Hopkins N, McLoughlin P. The structural basis of pulmonary hypertension in chronic lung disease: remodelling, rarefaction or angiogenesis? *Journal of Anatomy*. 2002;201:335-348. doi: 10.1046/j.1469-7580.2002.00096.x
29. Wu S, Zhou C, King JA, Stevens T. A unique pulmonary microvascular endothelial cell niche revealed by Weibel-Palade bodies and Griffonia simplicifolia. *Pulm Circ*. 2014;4:110-115. doi: 10.1086/674879
30. Stevens T, Phan S, Frid MG, Alvarez D, Herzog E, Stenmark KR. Lung vascular cell heterogeneity: endothelium, smooth muscle, and fibroblasts. *Proc Am Thorac Soc*. 2008;5:783-791. doi: 10.1513/pats.200803-027HR
31. Townsley MI. Permeability and calcium signaling in lung endothelium: unpack the box…. *Pulmonary Circulation*. 2018;8:204589321773821. doi: 10.1177/2045893217738218
32. Adkison JB, Miller GT, Weber DS, Miyahara T, Ballard ST, Frost JR, Parker JC. Differential responses of pulmonary endothelial phenotypes to cyclical stretch. *Microvasc Res*. 2006;71:175-184. doi: 10.1016/j.mvr.2006.02.007
33. Geiger M, Stone A, Mason SN, Oldham KT, Guice KS. Differential nitric oxide production by microvascular and macrovascular endothelial cells. *Am J Physiol*. 1997;273:L275-281. doi: 10.1152/ajplung.1997.273.1.L275
34. Fuchs A, Weibel ER. [Morphometric study of the distribution of a specific cytoplasmatic organoid in the rat's endothelial cells]. *Z Zellforsch Mikrosk Anat*. 1966;73:1-9.
35. Mizushima N, Komatsu M. Autophagy: renovation of cells and tissues. *Cell*. 2011;147:728-741. doi: 10.1016/j.cell.2011.10.026
36. Yu L, Chen Y, Tooze SA. Autophagy pathway: Cellular and molecular mechanisms. *Autophagy*. 2018;14:207-215. doi: 10.1080/15548627.2017.1378838

37. Ryter SW, Choi AM. Autophagy in lung disease pathogenesis and therapeutics. *Redox Biol*. 2015;4:215-225. doi: 10.1016/j.redox.2014.12.010
38. Kanzawa T, Kondo Y, Ito H, Kondo S, Germano I. Induction of autophagic cell death in malignant glioma cells by arsenic trioxide. *Cancer Res*. 2003;63:2103-2108.
39. Maiuri MC, Zalckvar E, Kimchi A, Kroemer G. Self-eating and self-killing: crosstalk between autophagy and apoptosis. *Nat Rev Mol Cell Biol*. 2007;8:741-752. doi: 10.1038/nrm2239
40. Li Y, Zhu H, Zeng X, Fan J, Qian X, Wang S, Wang Z, Sun Y, Wang X, Wang W, Ju D. Suppression of autophagy enhanced growth inhibition and apoptosis of interferon-beta in human glioma cells. *Mol Neurobiol*. 2013;47:1000-1010. doi: 10.1007/s12035-013-8403-0
41. Yazdani H, Huang H, Tsung A. Autophagy: Dual Response in the Development of Hepatocellular Carcinoma. *Cells*. 2019;8:91. doi: 10.3390/cells8020091
42. Long L, Yang X, Southwood M, Lu J, Marciniak SJ, Dunmore BJ, Morrell NW. Chloroquine prevents progression of experimental pulmonary hypertension via inhibition of autophagy and lysosomal bone morphogenetic protein type II receptor degradation. *Circ Res*. 2013;112:1159-1170. doi: 10.1161/CIRCRESAHA.111.300483
43. Lee SJ, Smith A, Guo L, Alastalo TP, Li M, Sawada H, Liu X, Chen ZH, Ifedigbo E, Jin Y, Feghali-Bostwick C, Ryter SW, Kim HP, Rabinovitch M, Choi AM. Autophagic protein LC3B confers resistance against hypoxia-induced pulmonary hypertension. *American journal of respiratory and critical care medicine*. 2011;183:649-658. doi: 10.1164/rccm.201005-0746OC
44. Mao M, Yu X, Ge X, Gu R, Li Q, Song S, Zheng X, Shen T, Li X, Fu Y, Li J, Zhu D. Acetylated cyclophilin A is a major mediator in hypoxia-induced autophagy and pulmonary vascular angiogenesis. *J Hypertens*. 2017;35:798-809. doi: 10.1097/HJH.0000000000001224
45. Orcholski ME, Khurshudyan A, Shamskhou EA, Yuan K, Chen IY, Kodani SD, Morisseau C, Hammock BD, Hong EM, Alexandrova L, Alastalo TP, Berry G, Zamanian RT, de Jesus Perez VA. Reduced carboxylesterase 1 is associated with endothelial injury in methamphetamine-induced pulmonary arterial hypertension. *Am J Physiol Lung Cell Mol Physiol*. 2017;313:L252-L266. doi: 10.1152/ajplung.00453.2016
46. Li L, Wang X, Wang L, Qu L, Zhu X, Li M, Dang X, Li P, Gao Y, Peng Z, Pan L, Wan L. Mammalian target of rapamycin overexpression antagonizes chronic hypoxia-triggered pulmonary arterial hypertension via the autophagic pathway. *International Journal of Molecular Medicine*. 2015;36:316-322. doi: 10.3892/ijmm.2015.2224
47. Torisu T, Torisu K, Lee IH, Liu J, Malide D, Combs CA, Wu XS, Rovira II, Fergusson MM, Weigert R, Connelly PS, Daniels MP, Komatsu M, Cao L, Finkel T. Autophagy regulates endothelial cell processing, maturation and secretion of von Willebrand factor. *Nature Medicine*. 2013;19:1281-1287. doi: 10.1038/nm.3288
48. Komatsu M, Waguri S, Ueno T, Iwata J, Murata S, Tanida I, Ezaki J, Mizushima N, Ohsumi Y, Uchiyama Y, Kominami E, Tanaka K, Chiba T. Impairment of starvation-induced and constitutive autophagy in Atg7-deficient mice. *Journal of Cell Biology*. 2005;169:425-434. doi: 10.1083/jcb.200412022

49. Alva JA, Zovein AC, Monvoisin A, Murphy T, Salazar A, Harvey NL, Carmeliet P, Iruela-Arispe ML. VE-Cadherin-Cre-recombinase transgenic mouse: A tool for lineage analysis and gene deletion in endothelial cells. *Developmental Dynamics*. 2006;235:759-767. doi: 10.1002/dvdy.20643
50. Zhang JCL, Kim S, Helmke BP, Yu WW, Du KL, Lu MM, Strobeck M, Yu Q-C, Parmacek MS. Analysis of SM22α-Deficient Mice Reveals Unanticipated Insights into Smooth Muscle Cell Differentiation and Function. *Molecular and Cellular Biology*. 2001;21:1336-1344. doi: 10.1128/mcb.2001.21.4.1336-1344.2001
51. Mizushima N, Kuma A. Autophagosomes in GFP-LC3 Transgenic Mice. In: Humana Press; 2008:119-124.
52. Ott C, Pappritz K, Hegemann N, John C, Jeuthe S, McAlpine CS, Iwamoto Y, Lauryn JH, Klages J, Klopfleisch R, Van Linthout S, Swirski F, Nahrendorf M, Kintscher U, Grune T, Kuebler WM, Grune J. Spontaneous Degenerative Aortic Valve Disease in New Zealand Obese Mice. *Journal of the American Heart Association*. 2021;10. doi: 10.1161/jaha.121.023131
53. Liu G, Betts C, Cunoosamy DM, Åberg PM, Hornberg JJ, Sivars KB, Cohen TS. Use of precision cut lung slices as a translational model for the study of lung biology. *Respiratory Research*. 2019;20. doi: 10.1186/s12931-019-1131-x
54. Held H-D, Martin C, Uhlig S. Characterization of airway and vascular responses in murine lungs. *British Journal of Pharmacology*. 1999;126:1191-1199. doi: 10.1038/sj.bjp.0702394
55. Grimmer B, Krauszman A, Hu X, Kabir G, Connelly KA, Li M, Grune J, Madry C, Isakson BE, Kuebler WM. Pannexin 1: a novel regulator of acute hypoxic pulmonary vasoconstriction. *Cardiovascular Research*. 2021. doi: 10.1093/cvr/cvab326
56. King J, Hamil T, Creighton J, Wu SW, Bhat P, McDonald F, Stevens T. Structural and functional characteristics of lung macro- and microvascular endothelial cell phenotypes. *Microvasc Res*. 2004;67:139-151. doi: 10.1016/j.mvr.2003.11.006
57. Hoffmann J, Yin J, Kukucka M, Yin N, Saarikko I, Sterner-Kock A, Fujii H, Leong-Poi H, Kuppe H, Schermuly RT, Kuebler WM. Mast cells promote lung vascular remodelling in pulmonary hypertension. *Eur Respir J*. 2011;37:1400-1410. doi: 10.1183/09031936.00043310
58. Hu Y, Zabini D, Gu W, Goldenberg NM, Breitling S, Kabir G, Connelly KA, Kuebler WM. The Role of the Human Immune System in Chronic Hypoxic Pulmonary Hypertension. *American journal of respiratory and critical care medicine*. 2018;198:528-531. doi: 10.1164/rccm.201711-2175LE
59. Reynolds ES. THE USE OF LEAD CITRATE AT HIGH pH AS AN ELECTRON-OPAQUE STAIN IN ELECTRON MICROSCOPY. *Journal of Cell Biology*. 1963;17:208-212. doi: 10.1083/jcb.17.1.208
60. Weibel ER. Fifty years of Weibel-Palade bodies: the discovery and early history of an enigmatic organelle of endothelial cells1. *Journal of Thrombosis and Haemostasis*. 2012;10:979-984. doi: 10.1111/j.1538-7836.2012.04718.x
61. Berriman JA, Li S, Hewlett LJ, Wasilewski S, Kiskin FN, Carter T, Hannah MJ, Rosenthal PB. Structural organization of Weibel-Palade bodies revealed by cryo-EM of vitrified endothelial cells. *Proc Natl Acad Sci U S A*. 2009;106:17407-17412. doi: 10.1073/pnas.0902977106
62. Maleszewski JJ, Lai CK, Nair V, Veinot JP. Anatomic considerations and examination of cardiovascular specimens (excluding devices). *Cardiovascular pathology*. 2022:27-84.

63. Zenner HL, Collinson LM, Michaux GG, Cutler DF. High-pressure freezing provides insights into Weibel-Palade body biogenesis. *Journal of Cell Science*. 2007;120:2117-2125. doi: 10.1242/jcs.007781
64. Yla-Anttila P, Vihinen H, Jokitalo E, Eskelinen EL. Monitoring autophagy by electron microscopy in Mammalian cells. *Methods Enzymol*. 2009;452:143-164. doi: 10.1016/S0076-6879(08)03610-0
65. Schott U, Solomon C, Fries D, Bentzer P. The endothelial glycocalyx and its disruption, protection and regeneration: a narrative review. *Scand J Trauma Resusc Emerg Med*. 2016;24:48. doi: 10.1186/s13049-016-0239-y
66. Gebb S, Stevens T. On lung endothelial cell heterogeneity. *Microvasc Res*. 2004;68:1-12. doi: 10.1016/j.mvr.2004.02.002
67. deMello DE, Reid LM. Embryonic and early fetal development of human lung vasculature and its functional implications. *Pediatr Dev Pathol*. 2000;3:439-449. doi: 10.1007/s100240010090
68. Schupp JC, Adams TS, Cosme C, Jr., Raredon MSB, Yuan Y, Omote N, Poli S, Chioccioli M, Rose KA, Manning EP, Sauler M, DeIuliis G, Ahangari F, Neumark N, Habermann AC, Gutierrez AJ, Bui LT, Lafyatis R, Pierce RW, Meyer KB, Nawijn MC, Teichmann SA, Banovich NE, Kropski JA, Niklason LE, Pe'er D, Yan X, Homer RJ, Rosas IO, Kaminski N. Integrated Single-Cell Atlas of Endothelial Cells of the Human Lung. *Circulation*. 2021;144:286-302. doi: 10.1161/CIRCULATIONAHA.120.052318
69. Schupp JC, Adams TS, Cosme C, Raredon MSB, Yuan Y, Omote N, Poli S, Chioccioli M, Rose K-A, Manning EP, Sauler M, Deiuliis G, Ahangari F, Neumark N, Habermann AC, Gutierrez AJ, Bui LT, Lafyatis R, Pierce RW, Meyer KB, Nawijn MC, Teichmann SA, Banovich NE, Kropski JA, Niklason LE, Pe'Er D, Yan X, Homer RJ, Rosas IO, Kaminski N. Integrated Single-Cell Atlas of Endothelial Cells of the Human Lung. *Circulation*. 2021;144:286-302. doi: 10.1161/circulationaha.120.052318
70. Lampugnani MG, Zanetti A, Corada M, Takahashi T, Balconi G, Breviario F, Orsenigo F, Cattelino A, Kemler R, Daniel TO, Dejana E. Contact inhibition of VEGF-induced proliferation requires vascular endothelial cadherin, β-catenin, and the phosphatase DEP-1/CD148. *Journal of Cell Biology*. 2003;161:793-804. doi: 10.1083/jcb.200209019
71. Hirschi KK, Rohovsky SA, D'Amore PA. PDGF, TGF-beta, and heterotypic cell-cell interactions mediate endothelial cell-induced recruitment of 10T1/2 cells and their differentiation to a smooth muscle fate. *J Cell Biol*. 1998;141:805-814. doi: 10.1083/jcb.141.3.805
72. Antonelli-Orlidge A, Saunders KB, Smith SR, D'Amore PA. An activated form of transforming growth factor beta is produced by cocultures of endothelial cells and pericytes. *Proc Natl Acad Sci U S A*. 1989;86:4544-4548. doi: 10.1073/pnas.86.12.4544
73. Asakawa H, Kobayashi T. The effect of coculture with human smooth muscle cells on the proliferation, the IL-1 beta secretion, the PDGF production and tube formation of human aortic endothelial cells. *Cell Biochem Funct*. 1999;17:123-130. doi: 10.1002/(SICI)1099-0844(199906)17:2<123::AID-CBF817>3.0.CO;2-3
74. Wang L, Yin J, Nickles HT, Ranke H, Tabuchi A, Hoffmann J, Tabeling C, Barbosa-Sicard E, Chanson M, Kwak BR, Shin H-S, Wu S, Isakson BE, Witzenrath M, De Wit C, Fleming I, Kuppe H, Kuebler WM. Hypoxic pulmonary vasoconstriction requires connexin 40–mediated endothelial signal conduction. *Journal of Clinical Investigation*. 2012;122:4218-4230. doi: 10.1172/jci59176

75. Ekman N, Lymboussaki A, Vastrik I, Sarvas K, Kaipainen A, Alitalo K. Bmx tyrosine kinase is specifically expressed in the endocardium and the endothelium of large arteries. *Circulation*. 1997;96:1729-1732. doi: 10.1161/01.cir.96.6.1729
76. He Y. Critical function of Bmx/Etk in ischemia-mediated arteriogenesis and angiogenesis. *Journal of Clinical Investigation*. 2006. doi: 10.1172/jci28123
77. Su T, Stanley G, Sinha R, D'Amato G, Das S, Rhee S, Chang AH, Poduri A, Raftrey B, Dinh TT, Roper WA, Li G, Quinn KE, Caron KM, Wu S, Miquerol L, Butcher EC, Weissman I, Quake S, Red-Horse K. Single-cell analysis of early progenitor cells that build coronary arteries. *Nature*. 2018;559:356-362. doi: 10.1038/s41586-018-0288-7
78. Corada M, Orsenigo F, Morini MF, Pitulescu ME, Bhat G, Nyqvist D, Breviario F, Conti V, Briot A, Iruela-Arispe ML, Adams RH, Dejana E. Sox17 is indispensable for acquisition and maintenance of arterial identity. *Nature Communications*. 2013;4. doi: 10.1038/ncomms3609
79. Liu M, Zhang L, Marsboom G, Jambusaria A, Xiong S, Toth PT, Benevolenskaya EV, Rehman J, Malik AB. Sox17 is required for endothelial regeneration following inflammation-induced vascular injury. *Nature Communications*. 2019;10. doi: 10.1038/s41467-019-10134-y
80. Kuebler WM, Kuhnle GE, Groh J, Goetz AE. Leukocyte kinetics in pulmonary microcirculation: intravital fluorescence microscopic study. *J Appl Physiol (1985)*. 1994;76:65-71. doi: 10.1152/jappl.1994.76.1.65
81. Tabuchi A, Mertens M, Kuppe H, Pries AR, Kuebler WM. Intravital microscopy of the murine pulmonary microcirculation. *J Appl Physiol (1985)*. 2008;104:338-346. doi: 10.1152/japplphysiol.00348.2007
82. Looney MR, Thornton EE, Sen D, Lamm WJ, Glenny RW, Krummel MF. Stabilized imaging of immune surveillance in the mouse lung. *Nat Methods*. 2011;8:91-96. doi: 10.1038/nmeth.1543
83. Entenberg D, Voiculescu S, Guo P, Borriello L, Wang Y, Karagiannis GS, Jones J, Baccay F, Oktay M, Condeelis J. A permanent window for the murine lung enables high-resolution imaging of cancer metastasis. *Nature Methods*. 2018;15:73-80. doi: 10.1038/nmeth.4511
84. Akram KM, Yates LL, Mongey R, Rothery S, Gaboriau DCA, Sanderson J, Hind M, Griffiths M, Dean CH. Live imaging of alveologenesis in precision-cut lung slices reveals dynamic epithelial cell behaviour. *Nature Communications*. 2019;10. doi: 10.1038/s41467-019-09067-3
85. Pries AR, Kuebler WM. Normal endothelium. *Handb Exp Pharmacol*. 2006:1-40. doi: 10.1007/3-540-32967-6_1
86. Kalucka J, De Rooij LPMH, Goveia J, Rohlenova K, Dumas SJ, Meta E, Conchinha NV, Taverna F, Teuwen L-A, Veys K, García-Caballero M, Khan S, Geldhof V, Sokol L, Chen R, Treps L, Borri M, De Zeeuw P, Dubois C, Karakach TK, Falkenberg KD, Parys M, Yin X, Vinckier S, Du Y, Fenton RA, Schoonjans L, Dewerchin M, Eelen G, Thienpont B, Lin L, Bolund L, Li X, Luo Y, Carmeliet P. Single-Cell Transcriptome Atlas of Murine Endothelial Cells. *Cell*. 2020;180:764-779.e720. doi: 10.1016/j.cell.2020.01.015
87. Lahm T, Petrache I. LC3 as a potential therapeutic target in hypoxia-induced pulmonary hypertension. *Autophagy*. 2012;8:1146-1147. doi: 10.4161/auto.20520
88. Teng RJ, Du J, Welak S, Guan T, Eis A, Shi Y, Konduri GG. Cross talk between NADPH oxidase and autophagy in pulmonary artery endothelial cells with intrauterine persistent pulmonary hypertension. *Am J Physiol Lung Cell Mol Physiol*. 2012;302:L651-663. doi: 10.1152/ajplung.00177.2011

89. Long L, Yang X, Southwood M, Lu J, Marciniak S, Dunmore B, Morrell N. Chloroquine prevents progression of experimental pulmonary hypertension via inhibition of autophagy and lysosomal bone morphogenetic protein type II receptor degradation. *CircRes*. 2013;112:1159-1170. doi: 10.1161/circresaha.111.300483
90. Rawat D, Alzoubi A, Gupte R, Chettimada S, Watanabe M, Kahn A, Okada T, McMurtry I, Gupte S. Increased reactive oxygen species, metabolic maladaptation, and autophagy contribute to pulmonary arterial hypertension-induced ventricular hypertrophy and diastolic heart failure. *Hypertension (Dallas, Tex : 1979)*. 2014;64:1266-1274. doi: 10.1161/hypertensionaha.114.03261
91. Long L, Yang X, Southwood M, Lu J, Marciniak SJ, Dunmore BJ, Morrell NW. Chloroquine Prevents Progression of Experimental Pulmonary Hypertension via Inhibition of Autophagy and Lysosomal Bone Morphogenetic Protein Type II Receptor Degradation. *CircRes*. 2013;112:1159-1170. doi: 10.1161/circresaha.111.300483
92. Mazure NM, Pouyssegur J. Hypoxia-induced autophagy: cell death or cell survival? *Curr Opin Cell Biol*. 2010;22:177-180. doi: 10.1016/j.ceb.2009.11.015
93. Galluzzi L, Green DR. Autophagy-Independent Functions of the Autophagy Machinery. *Cell*. 2019;177:1682-1699. doi: 10.1016/j.cell.2019.05.026
94. Green DR. The Coming Decade of Cell Death Research: Five Riddles. *Cell*. 2019;177:1094-1107. doi: 10.1016/j.cell.2019.04.024
95. Aits S, Jaattela M. Lysosomal cell death at a glance. *J Cell Sci*. 2013;126:1905-1912. doi: 10.1242/jcs.091181
96. Yousefi S, Perozzo R, Schmid I, Ziemiecki A, Schaffner T, Scapozza L, Brunner T, Simon HU. Calpain-mediated cleavage of Atg5 switches autophagy to apoptosis. *Nat Cell Biol*. 2006;8:1124-1132. doi: 10.1038/ncb1482
97. Rubinstein AD, Eisenstein M, Ber Y, Bialik S, Kimchi A. The autophagy protein Atg12 associates with antiapoptotic Bcl-2 family members to promote mitochondrial apoptosis. *Mol Cell*. 2011;44:698-709. doi: 10.1016/j.molcel.2011.10.014
98. Gump JM, Thorburn A. Autophagy and apoptosis: what is the connection? *Trends Cell Biol*. 2011;21:387-392. doi: 10.1016/j.tcb.2011.03.007
99. Seillier M, Peuget S, Gayet O, Gauthier C, N'Guessan P, Monte M, Carrier A, Iovanna JL, Dusetti NJ. TP53INP1, a tumor suppressor, interacts with LC3 and ATG8-family proteins through the LC3-interacting region (LIR) and promotes autophagy-dependent cell death. *Cell Death Differ*. 2012;19:1525-1535. doi: 10.1038/cdd.2012.30
100. Travaglini KJ, Nabhan AN, Penland L, Sinha R, Gillich A, Sit RV, Chang S, Conley SD, Mori Y, Seita J, Berry GJ, Shrager JB, Metzger RJ, Kuo CS, Neff N, Weissman IL, Quake SR, Krasnow MA. A molecular cell atlas of the human lung from single-cell RNA sequencing. *Nature*. 2020;587:619-625. doi: 10.1038/s41586-020-2922-4

Statutory Declaration

I, Zhang, Qi, by personally signing this document in lieu of an oath, hereby affirm that I prepared the submitted dissertation on the topic 'Endothelial heterogeneity in response to autophagy activation prompts distal vascular muscularization in pulmonary hypertension' (English) / 'Endothelheterogenität als Reaktion auf Autophagie-Aktivierung führt zu distaler vaskulärer Muskularisierung bei pulmonaler Hypertension' (German), independently and without the support of third parties, and that I used no other sources and aids than those stated.
All parts which are based on the publications or presentations of other authors, either in letter or in spirit, are specified as such in accordance with the citing guidelines. The sections on methodology (in particular regarding practical work, laboratory regulations, statistical processing) and results (in particular regarding figures, charts and tables) are exclusively my responsibility.

Furthermore, I declare that I have correctly marked all of the data, the analyses, and the conclusions generated from data obtained in collaboration with other persons, and that I have correctly marked my own contribution and the contributions of other persons (cf. declaration of contribution). I have correctly marked all texts or parts of texts that were generated in collaboration with other persons.

My contributions to any publications to this dissertation correspond to those stated in the below joint declaration made together with the supervisor. All publications created within the scope of the dissertation comply with the guidelines of the ICMJE (International Committee of Medical Journal Editors; http://www.icmje.org) on authorship. In addition, I declare that I shall comply with the regulations of Charité – Universitätsmedizin Berlin on ensuring good scientific practice.

I declare that I have not yet submitted this dissertation in identical or similar form to another Faculty.

The significance of this statutory declaration and the consequences of a false statutory declaration under criminal law (Sections 156, 161 of the German Criminal Code) are known to me.”

Date Signature

Curriculum Vitae

My curriculum vitae does not appear in the electronic version of my paper for reasons of data protection.

Publication list

Abstracts

Zhang, Q., Yaoita, N., Tabuchi, A., Finkel, T., Verma, S., Timm, S., Kuebler, W. M. (2022). Endothelial Heterogeneity in the Response to Autophagy Drives Vascular Muscularization in Pulmonary Hypertension. *Am J Respir Crit Care Med*, 205, 1.

Acknowledgments

I wish to begin by expressing profound gratitude to my country and its government for giving me the remarkable opportunity to pursue my studies abroad and for the generous financial support throughout my journey.

Foremost, my deepest appreciation goes to my supervisor, Prof. Dr. Wolfgang Kübler. His unwavering faith in my capabilities, coupled with his invaluable guidance, has been instrumental in my academic growth. I am indebted to him for fostering a nurturing environment within his esteemed team, consistently offering encouragement, sage advice, and unwavering trust in my endeavors.

I extend my sincere thanks to Dr. Jasmin Matuszak for her foundational experimental guidance during my initial year in Germany. My gratitude also extends to Dr. Nobuhiro Yaoita and Dr. Arata Tabuchi for their commendable preliminary work, which significantly facilitated my project's progression.

For their technical expertise with the TEM experiments, I am thankful to Prof. Dr. Matthias Ochs and Dr. Sara Timm. I am also grateful to Prof. Toren Finkel and Prof. Dr. Stefanie Dimmeler for providing transgenic mouse strains, and to Prof. Troy Stevens for his provision of rat PAEC, MVEC, and additional technical support.

I wish to acknowledge the invaluable contributions of my colleagues: Laura Michalick, Lasti Erfinanda, Mariya Kucherenko, Szandor Simmons, Sabrina Schulz, Pengchao Sang, Shaofei Liu, Qiuhua Li, Anna Bierögel, Paul-Lennard Perret, Philip Solymosi, and Niklas Hegemann. Their technical assistance, advice, and unwavering support have been pivotal to my project. I also extend my gratitude to all past and present members of the Institute of Physiology at Charité for fostering a collaborative and congenial laboratory environment.

A special note of appreciation goes to my fellow Chinese colleagues: Pengchao Sang, Mei Li, Shaofei Liu, Qiuhua Li, Caihong Li, Juquan Yao, and Donghai Tian. Amidst the challenges posed by the COVID-19 pandemic, which kept me away from home for three years, their camaraderie and empathy provided solace and mitigated my homesickness.

To my parents, Jianhe Zhang and Jinglian Hu, words cannot capture the depth of my gratitude. Their unwavering love, understanding, and encouragement have been the bedrock of my journey. Their sacrifices and teachings have shaped my character and aspirations.

Lastly, my heartfelt thanks go to WL Luo, whose steadfast love and belief in my potential have been my anchor during challenging times. Without this unwavering support, my journey would have been insurmountably difficult.

Statistician confirmation

CHARITÉ

CharitéCentrum für Human- und Gesundheitswissenschaften

Charité | Campus Charité Mitte | 10117 Berlin

Institut für Biometrie und klinische Epidemiologie (iBikE)

Direktor: Prof. Dr. Frank Konietschke

Postanschrift:
Charitéplatz 1 | 10117 Berlin
Besucheranschrift:
Reinhardtstr. 58 | 10117 Berlin

Tel. +49 (0)30 450 562171
frank.konietschke@charite.de
https://biometrie.charite.de/

Name, Vorname: Zhang, Qi
Email addresse: qi.zhang@charite.de
Matrikelnummer: 227520
PromotionsbetreuerIn: Wolfgang M. Kübler
Promotionsinstitution / Klinik: Institute of Physiology

Bescheinigung

Hiermit bescheinige ich, dass Herr *Qi Zhang* innerhalb der Service Unit Biometrie des Instituts für Biometrie und klinische Epidemiologie (iBikE) bei mir eine statistische Beratung zu einem Promotionsvorhaben wahrgenommen hat. Folgende Beratungstermine wurden wahrgenommen:

- Termin 1: 12.01.2023

Folgende wesentliche Ratschläge hinsichtlich einer sinnvollen Auswertung und Interpretation der Daten wurden während der Beratung erteilt:

- One-way und Two-way ANOVA
- Der t-Test für unabhängige Stichproben

Diese Bescheinigung garantiert nicht die richtige Umsetzung der in der Beratung gemachten Vorschläge, die korrekte Durchführung der empfohlenen statistischen Verfahren und die richtige Darstellung und Interpretation der Ergebnisse. Die Verantwortung hierfür obliegt allein dem Promovierenden. Das Institut für Biometrie und klinische Epidemiologie übernimmt hierfür keine Haftung.

Datum: 13.01.2023 Name der Beraterin: Pimrapat Gebert

[redacted]
Unterschrift BeraterIn, Institutsstempel

CHARITÉ
UNIVERSITÄTSMEDIZIN BERLIN
Institut für Biometrie und
Klinische Epidemiologie
Campus Charité Mitte
Charitéplatz 1 | D-10117 Berlin
Sitz: Reinhardtstr. 58